WL-TR-92-4071




# Thermomechanical Fatigue Behavior of a Silicon Carbide Fiber-Reinforced Calcium Aluminosilicate Glass-Ceramic Matrix Composite

L.M. Butkus, Captain, USAF
Air Force Institute of Technology (AFIT/CI)
Department of Mechanical Engineering and Applied Mechanics
The University of Michigan
Ann Arbor, MI 48109

in cooperation with:
Materials Behavior Branch (WL/MLLN)
Metals and Ceramics Divsion
Materials Directorate
Wright Laboratory
Wright-Patterson AFB, OH 45433-6533



August 1992

Final Report for Period August 1990 - December 1991

Approved for Public Release; Distribution is Unlimited.

MATERIALS DIRECTORATE
WRIGHT LABORATORY
AIR FORCE MATERIEL COMMAND
WRIGHT-PATTERSON AFB, OHIO 45433-6533

# NOTICE

When Government drawings, specifications, or other data are used for any purpose other than in connection with a definitely Government-related procurement, the United States Government incurs no responsibility nor any obligations whatsoever. The fact that the government may have formulated, or in any way supplied the said drawings, specifications, or other data, is not to be regarded by implication or otherwise in any manner construed, as licensing the holder of any other person or corporation, or as conveying any rights or permission to manufacture, use, or sell any patented invention that may in any way be related thereto.

This report is releasable to the National Technical Information Service (NTIS). At NTIS, it will be available to the general public, including foreign nations.

This technical report has been reviewed and is approved for publication.

Dr Theodore Nicholas
Research Director
Materials Behavior Branch

Katherine Williams
Technical Area Manager
Materials Behavior Branch

Allan Gunderson, Chief
Materials Behavior Branch

If your address has changed, if you wish to be removed from our mailing list, or if the addressee is no longer employed by your organization, please notify WL/MLLN, Wright-Patterson AFB, OH 45433-6533 to help us maintain a current mailing list.

Copies of this report should not be returned unless return is required by security considerations, contractual obligations, or notice on a specific document.

# REPORT DOCUMENTATION PAGE

Form Approved
OMB No. 0704-0188

| 1. AGENCY USE ONLY (Leave blank) | 2. REPORT DATE | 3. REPORT TYPE AND DATES COVERED |
|---|---|---|
| | August 1992 | Final Report - Aug 90 to Dec 91 |

4. TITLE AND SUBTITLE

**Thermomechanical Fatigue Behavior of a Silicon Carbide Fiber-Reinforced Calcium Aluminosilicate Glass-Ceramic Matrix Composite**

5. FUNDING NUMBERS

PE 61102F
PR 2302
TA P1
WU 01

6. AUTHOR(S)

**L.M. Butkus, Captain, USAF**

7. PERFORMING ORGANIZATION NAME(S) AND ADDRESS(ES)

**Materials Directorate**
**Wright Laboratory**
**Materials Behavior Branch (WL/MLLN)**
**Wright-Patterson AFB OH 45433-6533**

8. PERFORMING ORGANIZATION REPORT NUMBER

9. SPONSORING/MONITORING AGENCY NAME(S) AND ADDRESS(ES)

**Larry P. Zawada (513-255-1352)**
**Materials Directorate**
**Wright Laboratory**
**Materials Behavior Branch (WL/MLLN)**
**Wright-Patterson AFB OH 45433-6533**

10. SPONSORING/MONITORING AGENCY REPORT NUMBER

**WL-TR- 92-4071**

11. SUPPLEMENTARY NOTES

12a. DISTRIBUTION/AVAILABILITY STATEMENT

12b. DISTRIBUTION CODE

**Approved for Public Release; distribution is unlimited**

13. ABSTRACT (Maximum 200 words)

Isothermal fatigue and in-phase thermomechanical fatigue (TMF) tests were performed on a unidirectional, continuous-fiber, Nicalon - reinforced calcium aluminosilicate glass-ceramic composite ($[0]_{16}$, SiC/CAS-II). Monotonic tensile tests were performed at 1100°C and 100 MPa/sec to determine the material's ultimate strength and proportional limit. Isothermal fatigue tests at 100°C employed two loading profiles, a triangular waveform with ramp times of 60 seconds, and a similar profile with a superimposed 60 second hold time at maximum stress. All fatigue tests used a maximum stress of 100 MPa, R = 0.1. TMF loading profiles were identical to the isothermal loading profiles, but the temperature was cycled between 500 and 1100°C. All fatigued specimens reached run out (1000 cycles) and were tested in tension at 1100°C immediately following the fatigue tests. Residual modulus, residual strength, cyclic stress-strain modulus, and strain accumulation were all examined as possible damage indicators. Strain accumulation allowed for the greatest distinction to be made among the type of tests performed. Fiber and matrix stress analyses and creep data for this material suggest that matrix creep is the primary source of damage for the fatigue loading histories investigated.

| 14. SUBJECT TERMS | | 15. NUMBER OF PAGES |
|---|---|---|
| Ceramic Composites | High Temperature | 132 |
| Fatigue | Creep | 16. PRICE CODE |
| Thermomechanical Fatigue | Damage | |

| 17. SECURITY CLASSIFICATION OF REPORT | 18. SECURITY CLASSIFICATION OF THIS PAGE | 19. SECURITY CLASSIFICATION OF ABSTRACT | 20. LIMITATION OF ABSTRACT |
|---|---|---|---|
| Unclassified | Unclassified | Unclassified | UL |

NSN 7540-01-280-5500

Standard Form 298 (Rev. 2-89)
Prescribed by ANSI Std. Z39-18
298-102

## FOREWORD

This Technical Report was prepared by the author during his assignment to an Air Force Institute of Technology Civilian Institution Program (AFIT/CI) at the Department of Mechanical Engineering and Applied Mechanics at the University of Michigan. This report was prepared for Dr. Theodore Nicholas of the Materials Behavior Branch of the Metals and Ceramics Division, Materials Directorate (WL/MLLN) where the majority of the materials testing was performed. This report covers research sponsored by the Ceramic and Nonmetallic Structural Materials Branch of the Air Force Office of Scientific Research (AFOSR/NE) under a Grant No. 91-0106 to the University of Michigan. The report is essentially the thesis submitted by the author for his MS degree in Mechanical Engineering and covers his work during the period August 1990 through December 1991.

The author gratefully acknowledges the guidance provided by his thesis advisor, Dr. J.W. Holmes (University of Michigan) and the valuable discussions with his thesis committee, Dr. T. Nicholas (WL/MLLN), Dr. J.W. Jones and Dr. J.R. Barber (University of Michigan). The author also wishes to express his gratitude to Mr. L. Zawada of WL/MLLN for his insight during the research and his assistance in assembling this report. Mr. G. Hartman and Mr. K. Goecke of the University of Dayton Research Institute also deserve special recognition for their assistance and cooperation in designing and fabricating the testing equipment.

## TABLE OF CONTENTS

## TABLE OF CONTENTS (cont.)

## LIST OF FIGURES

**Figure**

## LIST OF FIGURES (cont.)

## LIST OF FIGURES (cont.)

## LIST OF FIGURES (cont.)

## LIST OF FIGURES (cont.)



## LIST OF TABLES

**Table**

# I: INTRODUCTION

Man-made composite materials have been in use for thousands of years. Pyramids were built with straw-reinforced clay bricks, hydroelectric dams, and highways have been constructed from concrete reinforced with steel bars, and speed brakes, tail sections, and access doors of aircraft are being constructed using carbon or glass fiber-reinforced epoxy resins. Presently, a new form of composite material, ceramic matrix composites (CMCs), is receiving a great deal of research emphasis. The attraction to ceramic composites is most evident in the aerospace industry where the use of CMCs promises weight savings and increased operating temperatures leading to greater efficiencies. In some engine applications, material performance limitations have prevented increases in maximum operating temperatures for over three decades.[1] The potential use of ceramic composites offers the chance to break these temperature barriers in the search for more efficient engines.

Ceramic matrix composites combine high specific strength and modulus with high temperature capabilities. Reinforcing carbon or silicon carbide fibers add toughness to the parent glass, glass-ceramic, or ceramic matrix material. The synergy between fibers and matrix gives CMCs unique properties which have propelled them to near the top of the list of enabling technologies for advanced turbine engines, hypersonic vehicles, and space applications.

Prior to being used to replace current metal superalloys and monolithic ceramics, the mechanical and thermal properties of CMCs must be extensively investigated. Research underway since the 1970s has examined many ceramic composites ranging from early versions of carbon fiber-

reinforced glasses to three-dimensionally braided silicon carbide fiber-reinforced silicon carbide (SiC/SiC) manufactured using the most advanced chemical vapor infiltration technology.

Of particular interest to engine designers are the fatigue and creep properties of these new materials. Although many investigations of the general mechanical properties of ceramic composites have been performed (see sources 2-10 for a brief sampling), the room temperature and elevated temperature fatigue properties of CMCs have been explored in a limited, though growing, number of studies.[11-17] A few works have also explored the thermal fatigue[18] and creep behavior[19,20] of ceramic matrix composites. Interest has been focused on the cyclic accumulation of damage within ceramic composites *en route* to the future life prediction models so desperately needed by turbine engine and structural design engineers. As the isothermal fatigue, thermal fatigue, and creep characteristics of these materials are investigated, however, further questions arise pertaining to their behavior under conditions of combined mechanical and thermal loading, often termed thermomechanical fatigue (TMF) conditions.

Thermomechanical fatigue most closely represents the environmental conditions experienced by turbine engine components and is, thus, a key area of research for high performance aerospace materials. This thesis will examine the behavior of one type of ceramic matrix composite, a 16-ply unidirectional silicon carbide fiber-reinforced calcium aluminosilicate glass-ceramic (SiC/CAS-II, $[0]_{16}$), under specific thermomechanical conditions. The SiC/CAS-II material, fabricated using established techniques, is considered a leading candidate for engine components operating in excess of 1000°C (1832°F).

Monotonic tensile, isothermal fatigue, and in-phase TMF tests were performed for this project. Tensile tests were performed at 1100°C and 100 MPa/sec to determine the ultimate material strength ($\sigma_{ult}$) and proportional limit ($\sigma_{pl}$). Isothermal fatigue tests conducted at 1100°C (2012°F) utilized two loading profiles: (1) a triangular profile consisting of ramp times of 60 seconds with a maximum stress of 100 MPa (40 percent of $\sigma_{pl}$), R = 0.1, and (2) an identical profile with a superimposed 60-second hold time at $\sigma_{max}$. Identical loading profiles were used for the thermomechanical fatigue tests. TMF test temperatures were cycled between 500 and 1100°C (932 and 2012°F), and were synchronized with the loading profiles. Fatigue stress levels and temperatures were chosen based upon (1) estimated maximum use temperatures for this material provided by the manufacturer, (2) creep performance of the SiC CAS-II composite, and (3) an estimated temperature profile of 500°C (932°F) to 1100°C (2012°F) which occurs in 4-10 seconds in current metallic turbine blades during operation.[21] Realizing that true TMF conditions for engine components are quite complex, simple profiles were chosen for this project to permit better test control and analysis.

The purpose of this project was threefold. The primary objective was to establish the capability of performing thermomechanical fatigue testing on CMCs. Based on an extensive literature review, it appears that the TMF tests conducted for this project are the first of their kind for ceramic matrix composites. The second objective was to investigate and compare the performance of the SiC/CAS-II material under isothermal and thermomechanical fatigue. The final objective was to acquire and analyze data to discover the indicators and extent of damage initiation and accumulation occurring during the specified profiles.

The results of the tests are presented and discussed in terms of the mechanical behavior of the composite and of its constituent fiber and matrix materials. Stress analyses of the fibers and matrix were performed and are used to suggest possible damage mechanisms under the test conditions investigated . To guide the future TMF research on ceramic matrix composites, this report also includes detailed descriptions of procedures, techniques, and problems encountered during testing.

The thermomechanical fatigue regime is extremely important to materials research because of its significance in aerospace, power-generation, and structural applications. Ceramic composites, as new materials proposed for use in hostile environments, must first be evaluated under extreme thermal and mechanical conditions prior to being approved for service. Though far from all-inclusive, this project has investigated the response of one type of ceramic matrix composite to a discrete set of thermomechanical fatigue parameters to bring laboratory research closer to the simulation of the environment in which the use of ceramic matrix composites is proposed.

## References — **CHAPTER I: INTRODUCTION**


1 Brahney, J.H., "Propulsion Systems for the '90s," *Aerospace Engineering*, Society of Automotive Engineers, Inc., Brimfield, OH, **10**, [8], August 1990, pp. 17-37.

2 Marshall, D.B. and Evans, A.G., "Failure Mechanisms in Ceramic Fiber/Ceramic Matrix Composites," *The Journal of the American Ceramic Society*, American Ceramic Society, Westerville, OH, **68**, [5], 1985, pp. 225-231.

3 Sbaizero, O. and Evans, A.G., "Tensile and Shear Properties of Laminated Ceramic Matrix Composites," *The Journal of the American Ceramic Society*, American Ceramic Society, Westerville, OH, **68**, [6], 1986. pp. 481-486.

4 Evans, A.G. and Dagleish, B.J., "Some Aspects of the High Temperature Performance of Ceramics and Ceramic Composites," in Advanced Materials for Severe Applications, Iida, K., and McEvily, A.J., eds., Elsevier Applied Science Publishers, London, England, 1986.

5 Marshall, D.B. and Cox, B.N., "Tensile Behavior of Brittle Matrix Composites: Influence of Fiber Strength," *Acta Metallurgica Et Materialia*, Pergamon Journals Ltd., Oxford, England, **35**, [11], 1987. pp. 2607-2619.

6 Hillig, W.B., "Strength and Toughness of Ceramic Matrix Composites," *Annual Review of Materials Science*, Vol. 17, 1987, pp. 341-383.

7 Thouless, M.D., and Evans, A.G., "Effects of Pull-Out on the Mechanical Properties of Ceramic Matrix Composites," *Acta Mettallurgica Et Materialia*, Pergamon Journals Ltd., Oxford, England, **36**, [3], 1988, pp. 517-522.

8 Sutco, M., "Statistical Fibre Failure and Single Crack Behavior in Uniaxially Reinforced Ceramic Composites," *Journal of Materials Science*, Chapman & Hall, Ltd., London, England, **23**, 1988, pp. 928-933.

9 Dryell, D.R. and Freeman, C.W., "Trends in Design in Turbines for Aero Engines," in Materials Development in Turbo-Machinery Design: 2nd Parsons International Turbine Conference, Taplin, D.M.R., Knot, J.F., and Lewis, M.H., eds. The Institute of Metals, Parsons Press, Dublin, Ireland, 1989, pg. 39.

10 Evans, A.G. and Marshall, D.B., "The Mechanical Behavior of Ceramic Matrix Composites," in Materials and Engineering Design: The Next Decade, Dysan, D.F., and Hayhurst, D.R., eds., The Institute of Metals, London, England, 1989. -AND- *Acta Metallurgica Et Materialia*, Pergamon Journals Ltd., Oxford, England, **37**, [10], 1989, pp. 2567-2583.

11 Prewo, Karl. M., "Fatigue and Stress Rupture of Silicon Carbide Fibre-Reinforced Glass-Ceramics," *Journal of Materials Science*, Chapman & Hall, Ltd., London, England, **22**, 1987, pp. 2695-2701.

12 Prewo, K.M., Johnson, B., and Starrett, S., "Silicon Carbide Fiber-Reinforced Glass Ceramic Composite Tensile Behavior at Elevated Temperature," *Journal of Materials Science*, Chapman & Hall, Ltd., London, England, **24**, 1989, pp. 1373-1379.

13 Holmes, J.W., Kotil, T., and Foulds, W.T., "High Temperature Fatigue of SiC Fiber Reinforced Si3N4 Ceramic Composites," in Symposium on High Temperature Composites, American Society for Composites, Technomic Publishing Co., Lancaster, PA, 1989, pp. 176-186.

[14] Rousseau, C.Q., "Monotonic and Cyclic Behavior of a Silicon Carbide/Calcium-Aluminosilicate Ceramic Composite," in Thermal and Mechanical Behavior of Metal Matrix and Ceramic Matrix Composites, ASTM STP 1080, Kennedy, J.M., Moeller, H.H., and Johnson, W.S., eds., American Society for Testing and Materials, Philadelphia, PA, 1990, pp. 136-151.

[15] Luh, E.Y., Dauskardt, R.H., and Ritchie, R.O., "Cyclic Fatigue Crack Behavior of Short Cracks in SiC-Reinforced Lithium Aluminosilicate Glass-Ceramic Composite," *Journal of Materials Science Letters*, Chapman & Hall, Ltd., London, England, **9**, [6], 1990, pp. 719-725.

[16] Holmes, John W., "Influence of Stress Ratio on the Elevated-Temperature Fatigue of a Silicon Carbide Fiber-Reinforced Silicon Nitride Composite," *Journal of the American Ceramic Society*, American Ceramic Society, Westerville, OH, **74**, [7], 1991, pp. 1639-1645.

[17] Zawada, L. P., Butkus, L.M., and Hartman, G.A., "Room Temperature Tensile and Fatigue Properties of Silicon Carbide Fiber-Reinforced Aluminosilicate Glass," *Journal of the American Ceramic Society*, American Ceramic Society, Westerville, OH, **74**, [11], 1991, pp. 2851-2858.

[18] Zawada, L.P. and Wetherhold, R.C., "The Effects of Thermal Fatigue on a SiC Fibre/Aluminosilcate Glass Composite," *Journal of Materials Science*, Chapman & Hall, Ltd., London, England, **26**, 1991, pp. 648-654.

[19] Abbe, F., Vincens, J., and Charmant, J.L., "Creep Behavior and Microstructural Characterization of a Ceramic Matrix Composite," *Journal of Materials Science Letters*, Chapman & Hall, Ltd., London, England, **8**, [9], 1989, pp. 1026-1028.

[20] Holmes, J.W., "Tensile Creep Behaviour of a Fiber-Reinforced SiC-$Si_3N_4$ Composite." *Journal of Materials Science*, Chapman & Hall, Ltd., London, England, **26**, [11], 1991, pp. 1808-1814.

[21] Holmes, J.W., McClintock, F.A., O'Hara, K.S., and Conners, M.E., "Thermal Fatigue Testing of Coated Monocrystalline Superalloys," in Low Cycle Fatigue, ASTM STP 942, Solomon, H.D., Halford, G.R., Kaisand, L.R., and Keis, B.N. , eds., American Society for Testing and Materials, Philadelphia, PA, 1985, pg. 672.

# II. BACKGROUND

Major research and development efforts are underway worldwide to formulate and tailor advanced aerospace materials for future turbine engines. Similar programs are investigating the use of advanced materials in hypersonic, industrial, and commercial applications. A trend toward using materials capable of operating at high temperatures, under severe stresses, and in oxidizing or otherwise hostile environments has sparked interest in a new class of materials called ceramic matrix composites. The family of fiber-reinforced ceramic matrix composites offers several advantages over current monolithic metal and ceramic technologies. However, further research concerning their mechanical and thermal properties and thermomechanical behavior is necessary prior to their widespread use.

## Current Aircraft Gas Turbine Engine Materials

Much of the relatively short history of fiber-reinforced ceramic matrix composites has been linked to the development of the aircraft gas turbine engine. For over 50 years, the development and adaptation of the turbine engine for aerospace use has created a need for high performance materials able to withstand ever-increasing temperatures. Because of their availability and a broad experience base, metals were and continue to be the choice of design engineers for use in the severe environments encountered in aircraft engines. Consideration of ceramics for use in turbine engines began during the late 1940s[1], but their lack of ductility and toughness, susceptibility to thermal shock, and poor reliability have prevented them from replacing traditional structural metals.

Current material usage in aircraft turbine engines is heavily comprised of nickel- and titanium-based superalloys which account for approximately 65 percent of the weight of a typical high performance jet engine.[2] Metals chosen most recently for turbine use are directionally-solidified single-crystal or eutectic[3] superalloys which have boosted engine operating temperatures into the 1100°C (2012°F) range.

## Future Aircraft Gas Turbine Engines

In the continuing search to extract greater performance from current aircraft powerplants, several large research programs have been undertaken in the U.S. and abroad. Most visible in the aerospace arena are the DoD/NASA-sponsored IHPTET (Integrated High Performance Turbine Engine Technology) and the NASA HITEMP (HIgh Temperature Engine Materials Program) projects. Both are multiyear, multibillion dollar, multicontractor programs aimed at taking the next leap rather than the next step in turbine engine development.

The IHPTET program has a set of aggressive goals[4] including doubling the thrust-to-weight ratio and reducing the fuel consumption by 40 percent for fighter aircraft engines by the year 2005. Equally ambitious performance targets have been set for cruise missile, helicopter, and (by the HITEMP program) civilian aircraft engines. The basic paths to achieving the high performance goals of these programs include increasing engine operating temperatures and reducing engine weight.

Increased operating temperatures are a necessity for future turbine engine improvements because of a low potential for further increases in geometry- or flow-dependent component efficiency.[5] The "trickle-down" benefits from increased temperatures have been outlined by several

authors,[6-12] and rest upon the fact that increased temperatures allow more oxygen to combine with fuel thereby increasing the production of energy in the form of hot, expanding gases. This effect provides greater thrust, and more importantly, greater thrust per unit of fuel consumed. Temperatures in the range of 1925-2200°C (3497-3992°F) are considered optimal because of the peak combustion efficiency attained at these levels.[13]

One method of increasing the turbine operating temperatures is the limitation of cooling airflow used for turbine components located aft of the combustor. Cooling air reduces the capability of the turbine to drive the compressor and mixes with the mainstream turbine air causing aerodynamic losses.[14] Thus, uncooled components, in addition to being less complex in design, could also permit greater efficiencies and thrusts.

Weight reduction is another strategy to achieve higher performance in turbine engines. Approximately half of the gross weight of an aircraft can be attributed to the propulsion system (engine+fuel).[15] It has also been estimated that every pound of engine weight added to an aircraft requires 7 pounds of airframe weight.[16] Furthermore, heavier rotating engine components demand more energy to begin and sustain their required motions.

## Limitations on Current Materials

Technological progress made to date in turbine engines has been primarily materials driven, and, therefore, materials limited.[17] Limitations on operating temperatures may prove insurmountable if alternatives to current monolithic metallic engine materials are not found.[18] Creep and oxidation effects limit the use temperature of polycrystalline and directionally-solidified nickel-based superalloys to 1090°C (1962°F), of gamma titanium aluminides (TiAl) to 1000°C (1832°F), and of conventional titanium alloys to 600°C

(1112°F).[19] Turbine airfoils fabricated from single-crystal nickel- and cobalt-based superalloys currently operate at 90-95 percent of the absolute melting temperature of these materials.[20] Plans for future engines call for even higher peak temperatures.[21] Efforts to improve the properties of metals continue and will certainly enable them to play a large future role in structural and propulsion applications. However, the need for new materials with improved properties is certainly recognized.

## Ceramic Matrix Composites

The attractive properties and advantages of ceramic matrix composites have recently generated much enthusiasm in the engine materials arena. Chief among these properties are their high temperature capabilities and high specific mechanical properties.

Ceramic composites, which are manufactured using glass, glass-ceramic, and ceramic matrices, owe their high temperature capability to their matrix materials. In general, monolithic ceramics possess a higher initial cracking strength than most ceramic matrix composites.[22] However, because of their reinforcing fibers, ceramic matrix composites are superior to monolithic ceramics in notch sensitivity, thermal shock resistance,[23] and fracture toughness.[24] Reinforcing fibers act to blunt or bridge cracks, making ceramic matrix composites less notch-sensitive and tougher than monolithic ceramics.[25-27] Optimal placement and direction of these high strength and high stiffness fibers will enable future CMCs to be tailored toward specific predicted stress patterns.

In an effort to improve upon the poor mechanical properties of high temperature monolithic ceramics, investigations of reinforced ceramics began in 1972 on carbon fiber-reinforced glass materials.[28,29] Carbon fibers,

however, proved limited by their oxidation characteristics to relatively low temperature processing and use. In response to a need for a more oxidation-resistant fiber, Yajima *et al.* [30,31] developed a silicon carbide fiber which is now commercially available from Nippon Carbon Co., Ltd. (Yokohama, Japan) under the name Nicalon®. A review of the literature shows that use of the Nicalon® fiber has increased dramatically with the recent emphasis on ceramic matrix composite research. The compatibility of this fiber with matrices of glass,[32] and glass-ceramic,[33] materials has been demonstrated. Currently, Nicalon® is the most popular silicon carbide fiber used in ceramic composites.

## Attractiveness of Ceramic Matrix Composites

Perhaps the greatest advantage of ceramic composites is their potential for use at temperatures above the use temperatures for metal alloys and equal to or nearly on par with those for monolithic glasses and ceramics. Projected temperature limits for ceramic matrix composites range to a high of 1650°C (3002°F) compared to 1150°C (2102°F) for uncooled superalloys.[34] Use of uncooled ceramic matrix composite components will increase engine efficiency and decrease part complexity.[35,36] Projected designs for uncooled turbine blades require no intricate internal cooling passages, an omission allowing production cost and time savings. Improved oxidation/corrosion resistance,[37] thermal shock and fatigue resistance, and thermal stability have also been cited as key temperature-related benefits of ceramic matrix composites.[38]

Engine components can also benefit from the lower densities of ceramic composites which average approximately 3.2 g/cm$^3$ (0.1 lb/in$^3$), opposed to the densities of superalloys which average near 7.9 g/cm$^3$ (0.3 lb/in$^3$).[39] Their lower density also permits CMCs to posses higher specific properties of strength and stiffness. This advantage is extremely well-defined at

temperatures above 800°C (1472°F) where a typical glass-ceramic matrix composite may have fourfold advantage in terms of specific strength and stiffness over a nickel-based superalloy.[40] The lower densities of ceramic composites have also permitted projections of increased component reliability, lifetime, and efficiency.[41]

Ceramic composites also hold an advantage over metals in the area of raw materials required for their production. The unique properties of high performance metals depend upon specific alloying elements, the supply of which is often considered "critical" or "strategic" due to mine locations and current world political situations. The U.S. is nearly entirely dependent upon foreign operations for many critical alloying elements. The U.S. supply of cobalt, used to impart high temperature strength and corrosion resistance to metals, is mined almost exclusively in Zaire. Niobium, an alloying element controlling fatigue and thermal shock resistance, is refined from Brazilian ores. Moreover, 80 percent of the U.S. supply of chromium, irreplaceable as an alloy for oxidation resistance, comes from South Africa. To further illustrate the importance of these materials, consider that each Pratt & Whitney F-100 turbofan engine requires 402 kg (885 lbs) of cobalt, 66 kg (145 lbs) of niobium, and 675 kg (1485 lbs) of chromium.[42]

Although most of the reinforcing fibers used in CMCs can be considered "strategic" owing to the dearth of domestic sources, many of the raw materials for these fibers and for the matrices of ceramic composites are relatively common: silicon, carbon, nitrogen. Furthermore, though unable to be fabricated from "beach sand and lamp black,"[43] CMCs show great promise for low-cost production based solely on considerations of the expense of their raw materials.

## Potential Uses of Ceramic Matrix Composites

Because of their unique qualities, ceramic matrix composites are being considered for use in aircraft turbine engine components and in applications in other technologies as well.

Ceramic composites are being investigated for use as turbine/compressor blade and vane materials.[44] Their high temperature capabilities and resistance to hostile environments have made them leading candidates for combustor liners, flameholders, and exhaust path components.[45] Ceramic composite (SiC/SiC) exhaust nozzle vanes, fabricated by France's Societe Europeene Propulsion (SEP), were recently installed on a French Mirage fighter aircraft and exhibited at the 1990 Paris Air Show.[46]

Many large national research projects in the field of hypersonics have identified several potential applications for CMCs. The U.S.'s National Aero-Space Plane (NASP) may use ceramic matrix composites on surfaces adjacent to the nose cone and in engine components.[47] Britain's Horizontal Takeoff and Land (HOTOL) project is considering the use of CMCs on lower aeroshell panels, air intake leading edges, and the nose cone where temperatures may climb to 900-1500°C.[48] NASA has proposed the use of CMCs in the engines of their High Speed Civil Transport (HSCT) to allow for increased engine temperatures leading to reduced emissions of ozone-depleting nitrous oxide.[49]

In an effort to reduce nitrous oxide ($NO_x$) emissions, ceramic composites are also being considered for applications in hostile power-generation and industrial environments. Here, the use of CMCs is also promising because of their oxidation and corrosion resistance. The U.S. Department of Energy has estimated that the use of CMCs in these areas could reduce $NO_x$ emissions by 0.6 million tons/year[50] and save 0.7 quadrillion ($0.7 \times 10^{15}$) Btu/year in energy.[51]

Ceramic composites may also find use in automotive applications. Monolithic ceramics are currently featured in high performance automobile engines as turbocharger rotors (Nissan/NTK) and valve arm rocker pads (Kyocera/Isuzu, Nissan/NTK, and Bosch).[52] The use of CMCs in such applications is a logical extension of the use of monolithic ceramics.

In addition, ceramic composites are being considered for such diverse applications as biomedical implants, lightweight armor, spacecraft protection,[53] trash incinerators,[54] and tool holders.[55]

## Barriers to CMC Usage

Despite the high level of enthusiasm surrounding the their potential use in turbine engines and other applications, ceramic matrix composites still have many barriers to overcome.

*Fabrication technology is a dilemma for the production of ceramic matrix composites.*[56,57] Research continues to seek low-cost, reproducible methods of incorporating fibers into the parent matrix material. These methods must avoid damaging the fibers while simultaneously producing the important subtle characteristics required of an effective fiber-matrix interface.

The constituent materials of ceramic composites must also be improved.[58,59] In extremely high temperature (above 1200°C [2192°F]), long duration operations, environmental degradation of the relatively oxidation-resistant silicon carbide fibers and the carbon-rich fiber-matrix interface appears to be the mechanism which most severely limits strength and life. Further research is needed to develop optimized, matrix-compatible fibers and interfaces.

Final barriers are knowledge and experience. For CMCs to be used effectively, their properties must be studied and effective design techniques

must be developed and evaluated. Ceramic composites are well-suited to high-temperature, high-stress applications, but if designs utilizing this new class of materials are to be implemented, their behavior under static and cyclic loading at constant and varying temperatures must be understood. In addition, experience is required in forming CMCs into complex geometries and evaluating their performance in such geometries before they can be considered for many applications. With respect to turbine engine applications, a great need also exists for information regarding the behavior of ceramic matrix composites subjected to thermomechanical fatigue histories. The understanding of the interaction of mechanical and thermal stresses and strains, the evaluation of the effect of a high temperature oxidizing environment, and the characterization of thermomechanical fatigue damage evolution and accumulation in CMCs are key prerequisites for their widespread use in future engine and structural applications.

## Previous Work on Nicalon® -Reinforced Calcium Aluminosilicate

Interest in the Nicalon® fiber-reinforced calcium aluminosilicate (SiC/CAS) material began in the mid-1980s. Allaire, *et al.*,[60] performed room and elevated temperature (1250°C [2282°F]) flexure tests on an early unidirectional SiC/CAS system. These tests showed that the SiC/CAS system, although having lower room temperature strengths and proportional limits than other glass- and ceramic-matrix composites, had greater strength retention at high temperatures. Ultimate strengths for this material ranged from slightly over 300 MPa (44 ksi) at 1250°C (2282°F) to 752 MPa (109 ksi) at room temperature. Proportional limit stresses, the stress at which the stress-strain curve deviates from linearity, ranged from near 200 MPa (29 ksi) to 266 MPa (39 ksi) in the same temperature range.

Room and elevated temperature (1000°C [1832°F]) tension tests were conducted by Hartman, *et al.*,[61] using dogbone-shaped specimens. This work also illustrated the strength retention capabilities of the unidirectional SiC/CAS system at an elevated temperature. Problems were encountered during the high temperature tests because of failures which occurred in the radiused sections of the specimens.

Rousseau[62] investigated tension and fatigue behavior of a cross-plied $[0/90]_{2s}$ SiC/CAS-II composite at room and elevated temperatures (815°C [1500°F]). Tensile tests showed a distinctly nonlinear behavior of the material because of crack propagation along the fiber-matrix interface and cracking of the transverse plies at relatively low stresses. Again, this material exhibited good strength retention at elevated temperature. Fatigue testing revealed a pronounced loss of stiffness during initial fatigue cycles, and continuous strain accumulation. The author paralleled this behavior with damage initiation and accumulation using a critical element modeling approach.

Wang and Parvizi-Majidi[63] investigated the room temperature behavior of unidirectional and cross-plied [0/90/0] SiC/CAS-II composites using tensile tests and fiber push-out tests. The authors determined the stress levels associated with interfacial shear, microcracking, proportional limit, and ultimate strength.

Room temperature tension and fatigue tests were also performed on this composite system by Butkus, *et al.*[64] These investigations examined the behavior of unidirectional $[0]_8$ and cross-plied $[0/90]_{2s}$ material and found behavior similar to that seen by Rousseau, and Wang and Parvizi-Majidi.

## References — **CHAPTER II: BACKGROUND**


1 Mason, J.L. and McLean, A.F., "Ceramics and Gas Turbine Engines," in Selection of Materials for Component Design, Boyer, H.E., ed., American Society for Metals, Metals Park, OH, 1986, pg. 93.

2 Newsam, S., "Aero Gas Turbines," in Research and Development of High Temperature Materials for Industry, Bullock, E., ed., Elsevier Science Publishers, Ltd., London, England, 1989, pg. 421.

3 Suo, M., "Turbine Cooling," in Aerothermodynamics of Aircraft Engine Components, Oates, G.C , ed., American Institute of Aeronautics and Astronautics, New York, NY, 1985, pg. 278.

4 Henderson, R.E., "Component Technology," in 1988 Turbine Engine Technology Symposium: A Focus on the Future, Turbine Engine Division, Aero-Propulsion Laboratory, Wright Research and Development Center, September 1988, pg. 12.

5 Dryell, D.R. and Freeman, C.W., "Trends in Design in Turbines for Aero Engines," in Materials Development in Turbo-Machinery Design: 2nd Parsons Int'l Conference, Taplin, D.M.R., Knot, J.F., and Lewis, M.H., eds., The Institute of Metals, Parsons Press, Trinity College. Dublin, 1989, pg. 39.

6 Lines, D.J., "Ceramic Materials For Gas Turbine Components," in High Temperature Materials in Gas Turbines, *Sham, P.R. and Speidel*, M.O., eds., Elsevier Scientific Publishing Company, Amsterdam, Netherlands, 1974, pp. 155-173.

7 Kirk, G.E., "The Composite Aeroengine," in Fibre Reinforced Composites '88 - Extending the Limits, The Plastics and Rubber Institute, London, England, 1988, pp. K1/1-K1/15.

8 Newsam, *op. cit.*, pp. 405-421.

9 Brown, S.F., "21st Century Hot Jet Engines," *Popular Science*, June 1990, pp. 83-89.

10 Stephens, J.R., "Intermetallic and Ceramic Matrix Composites for 815 to 1370°C (1500 to 2500°F) Gas Turbine Engine Applications," in Metal & Ceramic Matrix Composites: Processing, Modeling & Mechanical Behavior, Bhagat, R.B., Clauer, A.H., Kumae, P., and Ritter, A.M., eds., The Minerals, Metals, & Materials Society, Warrendale, PA, 1990, pp. 3-11.

11 Brahney, J.H., "Propulsion Systems for the '90s," *Aerospace Engineering*, Society of Automotive Engineers, Inc., Brimfield, OH, **10**, [8], August 1990, pp. 17-37.

12 Simmons, W.F., Current and Future Materials Usage in Aircraft Gas Turbine Engines - MCIC Report #73-14, Metals and Ceramics Information Analysis Center, Columbus, OH, 1973.

13 "Forecast '91: Ceramics," *Advanced Materials & Processes*, ASM International, Metals Park, OH, **139**, [1], January 1991, pg. 46.

14 Suo, *op. cit.*, pg. 278.

15 Dix, D., "Keynote Address," 1988 Turbine Engine Technology Symposium: A Focus on the Future, Turbine Engine Division, Aero-Propulsion Laboratory, Wright Research and Development Center, September 1988, pg. 6.

16 Henderson, *op. cit.*, pg. 13. -AND- Dr. James Petty (Acting Deputy for Technology Wright Research and Development Center, Wright-Patterson AFB, OH) quoted in Brown, *op. cit.*, pg. 89.

17 Brahney, *op. cit.*, pg. 23, Simmons, *op. cit.*, pg. 1, -AND- Van de Voorde, M.H., "Advanced High Temperature Materials," in Research and Development of High Temperature Materials for Industry, Bullock, E., ed., Elsevier Science Publishers, Ltd., London, England, 1989, pg. 2.

18 Materials Laboratory, "Research Plan: Damage Mechanisms, Failure Prediction and Durability of Advanced High Temperature Ceramic Composites," Materials Laboratory, Metals Behavior Branch AFWAL/MLLN, Wright-Patterson AFB, OH, August 1988, pg. 1.

19 Brown, A.S., "Titanium is Hot, But Can It Stand the Heat?", *Aerospace America*, American Institute of Aeronautics and Astronautics, Washington, DC, June, 1991, pg. 40.

20 Sprague, R.A., "Future Aerospace - Materials Directions," *Advanced Materials & Processes*, ASM International, Metals Park, OH, **133**, [1], January 1988, pg. 67.

21 Dryell, *op. cit.*, pg. 39.

22 Evans, A.G., "Engineering Property Requirements for High Performance Ceramics," *Materials Science and Engineering*, Elsevier Sequoia, Lausanne, Switzerland, **71**, 1985, pg. 15.

23 Donald, I.W., and McMillan, P.W., "Review: Ceramic Matrix Composites," *Journal of Materials Science*, Chapman & Hall, Ltd., London, England, **11**, [5], 1976, pg. 949.

24 Larsen, D.C., Stuchly, S.L., and Adams, J.W., Evaluation of Ceramics and Ceramic Composites for Turbine Engine Applications: AFWAL Technical Report AFWAL-TR-88-4202, Materials Laboratory, Air Force Wright Aeronautical Laboratories, Wright-Patterson AFB, OH, December 1988, pg. 1.

25 DiCarlo, J.A., "CMCs For The Long Run," *Advanced Materials & Processes*, ASM International, Metals Park, OH, **135**, [6], June 1989, pg. 41.

26 Prewo, K.M., "Glass and Ceramic Matrix Composites: Present and Future," in High Temperature/High Performance Composites: Materials Research Society Symposium Proceedings, Vol. 120, Lemkey, F.D., Fishman, S.G., Evans, A.G., and Strife, J.R., eds., Materials Research Society, Pittsburgh, PA, 1988, pg. 145.

27 Ronald, T.F., "Advanced Materials to Fly High in NASP," *Advanced Materials & Processes*, ASM International, Metals Park, OH, **135**, [5], May 1989, pg. 24.

28 Sambell, R.A.J., Briggs, A., Phillips, D., and Bowen, D., "Carbon Fiber Composites with Ceramic and Glass Matrices," *Journal of Materials Science*, Chapman & Hall, Ltd., London, England, **7**, 1972, pp. 676-681.

[29] Phillips, D., "The Fracture Energy of Carbon Fiber Reinforced Glass," *Journal of Materials Science*, Chapman & Hall, Ltd., London, England, **7**, 1972, pp. 1175-1191.

[30] Yajima, S., Hayashi, J., Omori, M., and Okamura, K., "Development of a Silicon Carbide Fiber with High Tensile Strength," *Nature*, **261**, 1976, pg. 683.

[31] Yajima, S., Hasegawa, Y., Hayashi, J., and Iimura, M., "Synthesis of Continuous Silicon Carbide Fibre with High Tensile Strength and High Young's Modulus," *Journal of Materials Science*, Chapman & Hall, Ltd., London, England, **13**, 1978, pp. 2569-2576.

[32] Prewo, K.M. and Brennan, J.J., "High Strength Silicon Carbide Fibre-Reinforced Glass Matrix Composites," *Journal of Materials Science*, Chapman & Hall, Ltd., London, England, **15**, 1980, pp. 463-468.

[33] Brennan, J.J. & Prewo, K.M., "Silicon Carbide Fibre Reinforced Glass-Ceramic Matrix Composites Exhibiting High Strength and Toughness," *Journal of Materials Science*, Chapman & Hall, Ltd., London, England, **17**, 1982, pp. 2371-2383.

[34] Sprague, *op. cit.*, pg. 68.

[35] Newsam, *op. cit.*, pg. 409.

[36] Larsen, *ibid.*

[37] Lines, *op. cit.*, pg. 158.

[38] Donald and McMillan, *op. cit.*, pg. 970.

[39] Newsam, *op. cit.*, pg. 417.

[40] Kirk, *op. cit.*, pg. K1/14.

[41] Hyde. A.R., "Ceramic Matrix Composites," *Materials and Design*, Pergamon Press, Ltd., Oxford, England, **11**, [1], February 1990, pg. 30.

[42] Anderson, E.W., Strategic Minerals: The Geopolitical Problems for the United States, Preager Publishers, New York, NY, 1988, pp. 26-44.

[43] Sims, C.T., "Non-Metallic Materials for Gas Turbine Engines: Are They Real?", *Advanced Materials & Processes*, ASM International, Metals Park, OH, **139**, [6], June 1991, pg. 39.

[44] Dryell, *op. cit.*, pp. 40-45.

[45] Newsam, *op. cit.*, pp. 418-420.

[46] Grisaffe, S.J, "Ceramic Matrix Composites," *Advanced Materials & Processes*, ASM International, Metals Park, OH, **137**, [1], January 1990, pg. 44.

[47] Ronald, *op. cit.*, pg. 34.

[48] Barker, N.H., Walmsley, S. and Wilson, J., "Materials Challenge for HOTOL - A Reusable Space Vehicle," in Fibre Reinforced Composites '88 - Extending the Limits, The Plastics and Rubber Institute, London, England, 1988, pg. 37.

[49] Piellisch, Richard, J., "Composites Move Into Jet Engine Design," *Aerospace America*, American Institute of Aeronautics and Astronautics, Washington, DC, July 1991, pg. 29.

[50] Karnitz, M.A., Craig, D.F., and Richlen, S.L., "Continuous Fiber Ceramic Composite Program," *American Ceramic Society Bulletin*, American Ceramic Society, Westerville, OH, **70**, [3], 1991, pg. 432.

[51] Richlen, S.L., "Continuous Fiber Ceramic Composites," *ASTM Standardization News*, American Society for Testing and Materials, Philadelphia, PA, **18**, [9], September 1990, pg. 66.

[52] Lewis, *op. cit.*, pg. 251.

[53] Donald and McMillan, *op. cit.*, pg. 970.

[54] Richlen, *op. cit.*, pg. 64.

[55] Karnitz, *op. cit.*, pg. 431.

[56] Newsam, *op. cit.*, pg. 418.

[57] Charles River Associates, Inc., The International Trade Association, and the National Materials Advisory Board, Advanced Ceramic Materials: Technological and Economic Assessment, Noyes Publications, Park Ridge, NJ, 1985, pg 37.

[58] Ronald, *op. cit.*, pg. 34.

[59] Sims, *op. cit.*, pg. 37.

[60] Allaire, R.A., Janas, V.F., Stuchly, S., and Taylor, M.P., "Glass Matrix Composites for Higher Use Temperature Applications," *SAMPE Quarterly*, Society for the Advancement of Materials and Process Engineering, Lynchburg, VA, **19**, [1], October 1987, pp. 25-30.

[61] Hartman, G.A., Zawada, L.P., and Russ, S.M., "Techniques for Elevated Temperature Testing of Advanced Ceramic Composite Materials," in Fifth Annual Hostile Environments and High Temperature Measurements Conference Proceedings, Society for Experimental Mechanics, Inc., Englewood Cliffs, NJ, 1988, pp. 31-38.

[62] Rousseau, C.Q., "Monotonic and Cyclic Behavior of a Silicon Carbide/Calcium-Aluminosilicate Ceramic Composite," in Thermal and Mechanical Behavior of Metal Matrix and Ceramic Matrix Composites, ASTM STP 1080, Kennedy, J.M., Moeller, H.H., and Johnson, W.S., eds., American Society for Testing and Materials, Philadelphia, PA, 1990, pp. 136-151.

[63] Wang, S-W, and Parvizi-Majidi, A., "Mechanical Behavior of Nicalon Fiber Reinforced Calcium Aluminosilicate Matrix Composites," *Ceramic Engineering and Science Proceedings*, American Ceramic Society, Westerville, OH, **11**, [9-10], January 1989, pp. 1607-1616.

[64] Butkus, L.M., Zawada, L.P., and Hartman, G.A., "Room Temperature Tensile and Fatigue Behavior of Silicon Carbide Fiber-Reinforced Ceramic Matrix Composites," presented at *AeroMat '90*, ASM International, Long Beach, CA, May 1990.

# III. EXPERIMENTAL PROCEDURE

## Material

The material used in this project was a Nicalon® fiber-reinforced calcium aluminosilicate glass-ceramic composite designated SiC/CAS-II by its manufacturer, Corning Glass Works (Corning, NY). The composite was supplied in 16-ply, unidirectionally reinforced ($[0]_{16}$) panels, measuring 152.4 cm x 152.4 cm (6 in x 6 in).

Reported properties of the fibers and matrix are shown in Table 3-1.

**Table 3-1. Selected Fiber, Matrix, and Composite Properties**

| Property [a,b] | Fiber<br>Nicalon® NL-202 | Matrix<br>CAS-II | Composite<br>SiC/CAS-II, $[0]_{16}$ [d] |
|---|---|---|---|
| Density | 2.55 g/cm$^3$<br>(0.0092 lb/in$^3$) | 2.80 g/cm$^3$<br>(0.0101 lb/in$^3$) | 2.70 g/cm$^3$<br>(0.0098 lb/in$^3$) |
| CTE (25 to 1000°C)<br>(77 to 1832°F) | 4.0 x 10$^{-6}$/°C<br>(7.2 x 10$^{-6}$/°F) | 5.01 x 10$^{-6}$/°C<br>(9.02 x 10$^{-6}$/°F) | 4.6 x 10$^{-6}$ /°C<br>(8.3 x 10$^{-6}$/°F) |
| Elastic Modulus | 193 GPa<br>(28 Msi) | 98 GPa<br>(14 Msi) | 131-138 GPa<br>(19-20 Msi) |
| Poisson's Ratio | 0.2 | 0.26 | 0.25 |
| Tensile Strength | 2520-3290 MPa [c]<br>(365-477 ksi) | | 448-597 MPa<br>(64-87 ksi) |
| 4-Point Flex Strength | | 133 MPa<br>(193 ksi) | |

[a] At 25°C unless noted
[b] Data supplied by Corning unless noted
[c] Mah, T., Mendriatta, M.G., Katz, A.P., and Mazdiyasni, K.S., "Recent Developments in Fiber-Reinforced High Temperature Ceramic Composites," *American Ceramic Society Bulletin*, American Ceramic Society, Westerville, OH, **66**, [2], 1987, pg. 304.
[d] Data for SiC/CAS-II with 35% fiber volume

The NL-202 (ceramic-grade) Nicalon® fiber used in the SiC/CAS-II material is produced by Nippon Carbon Co., Ltd., from an organometallic polycarbosilane precursor. This precursor is melt-spun prior to being subjected to vacuum pyrolysis at 1500°C (2732°F).[1] The resulting coreless fiber consists of polycrystalline beta-phase silicon carbide containing 59 percent silicon, 31 percent carbon, and 10 percent oxygen (by weight).[2] The fibers are nominally circular in cross-section and approximately 10-15 μm (393-590 μin) in diameter, although variations may be seen in Figures 3-1 and 3-2. Several studies investigating the properties of various grades of Nicalon® fibers have indicated their susceptibility to grain growth, oxidation, decomposition, and creep at temperatures above 1000°C (1832°F).[3-15]

The CAS-II matrix material is comprised mainly of silica, and the oxides of aluminum, barium, calcium, and zirconium.[16] The "II" designation reflects Corning's refinement of an earlier calcium aluminosilicate formulation in an effort to promote more consistent crystallization in this material.[17] CAS-II has a strain point temperature† of 1260°C (2300°F) and a liquidus temperature†† of 1520-1540°C (2768-2804°F).[18] As a glass-ceramic, CAS-II is regarded as well-suited for use in composites because of its relatively low processing temperature, its ability to be tailored in composition to meet the need for specific properties,[19] and its superior high temperature performance.[20] Although CAS-II has the glass-like ability to flow around fibers while in the molten state (resulting in low porosity), it is semi-crystalline in its final state, having partially crystallized during heat treatment ("ceramming").[21]

† The strain point temperature is the temperature at which CAS-II has a viscosity of $10^{12}$ poise. Above this temperature (below this viscosity), the matrix loses its ability to retain stresses.

†† The liquidus temperature is that at which CAS-II begins to solidify from the melt upon cooling.

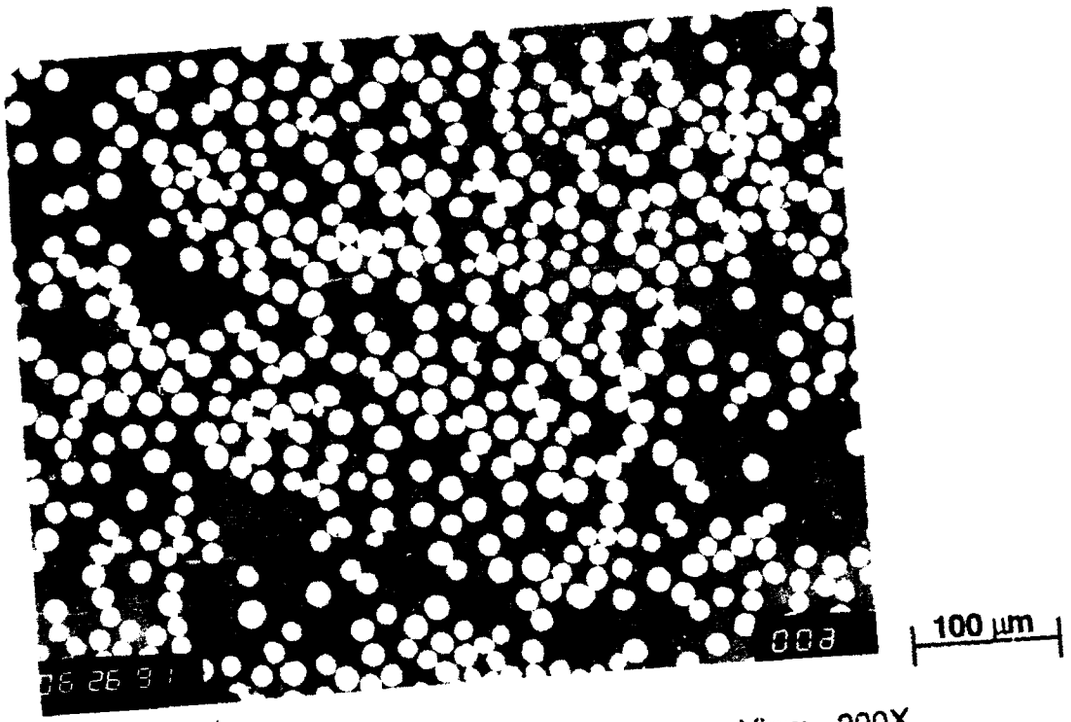


**Figure 3-1.** Microstructure of SiC/CAS-II, Transverse View. 200X


**Figure 3-2.** Microstructure of SiC/CAS-II, Longitudinal View. 200X

The composite material is produced by the hot-press method using prepregged unidirectional plies. The plies are approximately 0.56 mm (0.022 in.) thick and are fabricated using 500-count fiber tows. The hot-pressing temperature is approximately 1350°C (2462°F). The resulting composite contains approximately 40 percent fiber volume. The reaction between the matrix and fibers as the prepreg is hot-pressed and consolidated forms a carbon-rich fiber-matrix interface *in situ* as carbon is leached out of the Nicalon® fibers.[22] Temperatures above 800°C (1472°F) in air have been shown to cause embrittlement of Nicalon®-reinforced lithium aluminosilicate (LAS-III) and barium magnesium aluminosilicate (BMAS-III) glass-ceramics if prior matrix microcracking has exposed the fiber-matrix interface.[23]

Figures 3-1 and 3-2 show cross sections of the as-received material.

## Test System Overview

The task of accurately determining thermomechanical properties of ceramic matrix composites is challenging. Specimen design and gripping, load train alignment, and spatial temperature gradients are but a few of the several areas which must be addressed in developing a test station for the evaluation of ceramic composites. Mechanical testing for this project was carried out in the Materials Behavior Branch of the Materials Directorate, part of the U.S. Air Force's Wright Laboratory complex located at Wright-Patterson AFB, OH. During the past 5 years, engineers and technicians from the Materials Directorate and the University of Dayton Research Institute (UDRI) have developed test equipment which has proven successful in testing fiber-reinforced ceramics.[24-26]

The test station used was a horizontal servohydraulic system (see Figures 3-3 through 3-6).

**Figure 3-3.** View of entire test system showing (from left to right) the load frame, central control console, and Zenith Z-248 PC for test control and data acquisition.

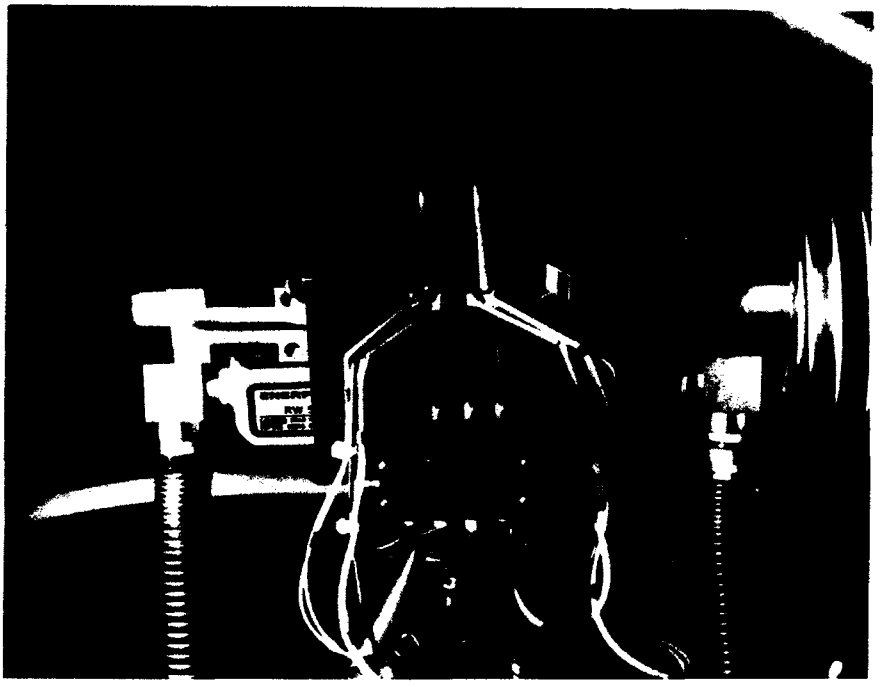

**Figure 3-4.** Close up of specimen in grips. Top lamp has been withdrawn to allow observation of extensometer (background) and thermocouples fixed to specimen with Cotronics® ceramic cement.

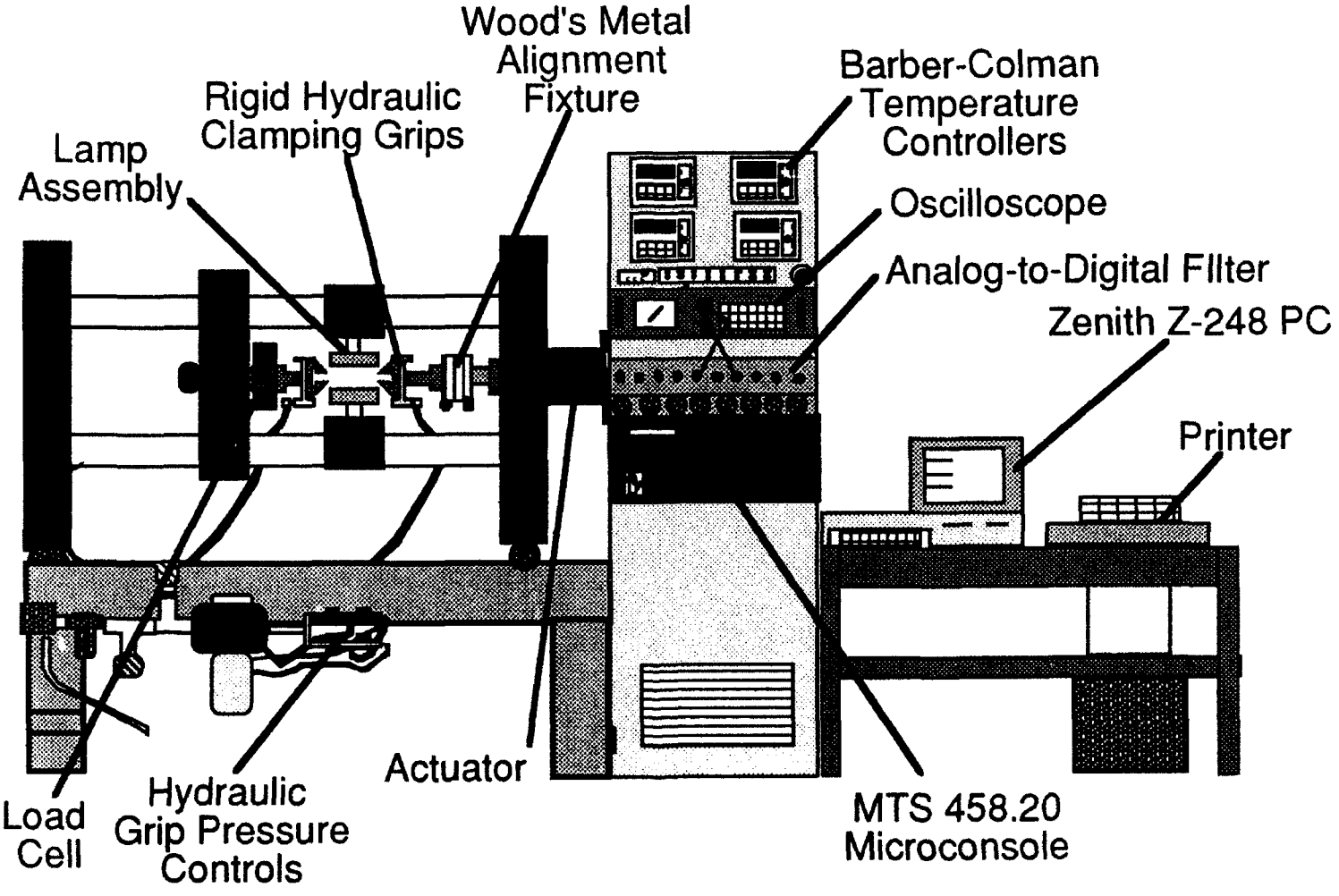


**Figure 3-5.** Servohydraulic Testing Machine located at the Materials Directorate, Wright-Patterson AFB, OH

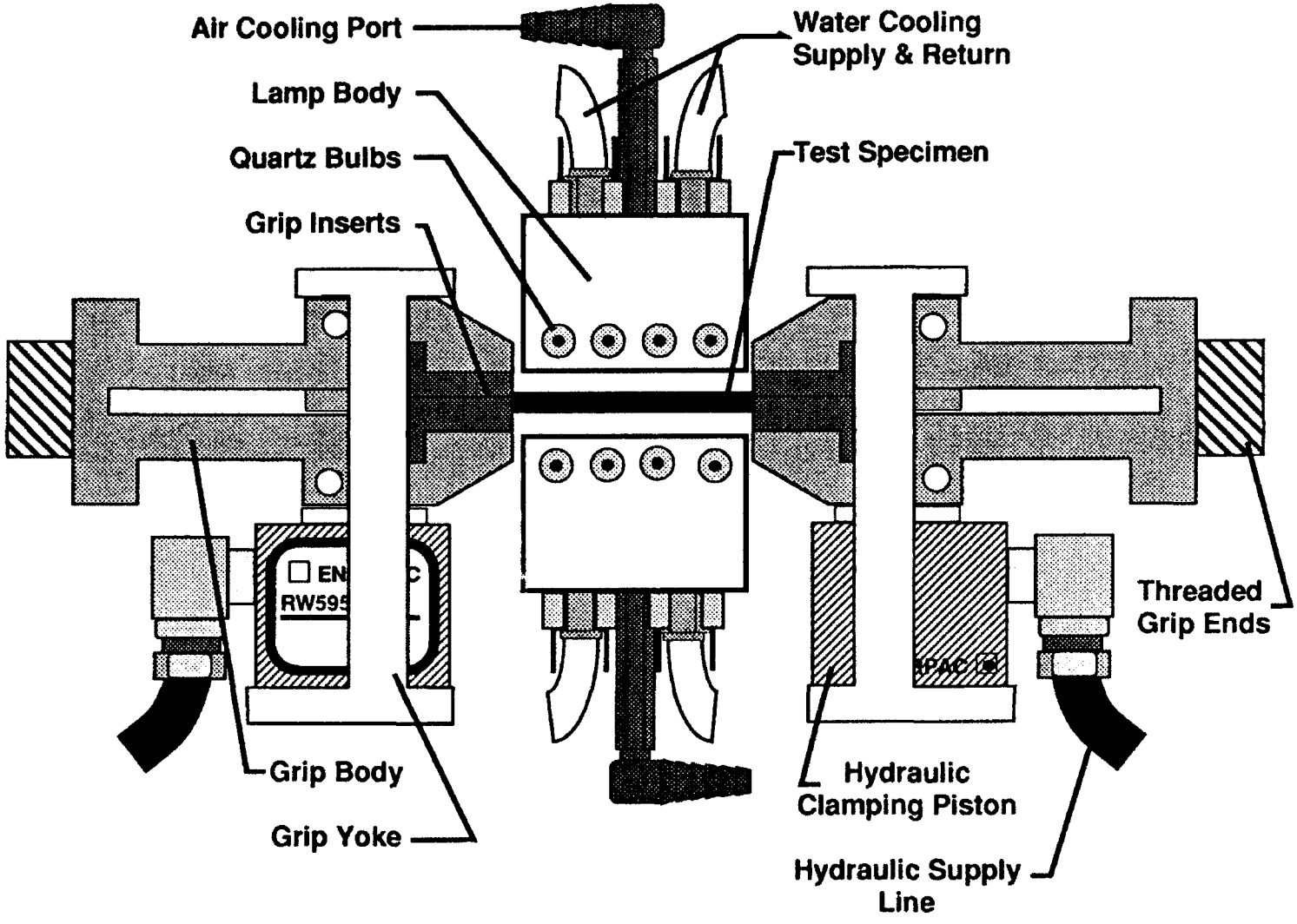


**Figure 3-6.** Detailed drawing of rigid grip system

The test station consists of:

1) Test Frame — built in-house at the Materials Directorate
2) 25kN load cell
3) 100kN actuator — manufactured by MTS (Mechanical Testing Systems) Corp., Minneapolis, MN; equipped with an antirotation device to prevent any rotation of the load train
4) Closed-Loop Controller - MTS Model #458.20
5) Extensometer — MTS Model #632.50B-01, high temperature, air-cooled, fitted with alumina rods
6) Radiant Heating and Temperature Control System — built in-house at the Materials Directorate
7) MATE (Materials Analysis and Test Environment) Automated Data-Acquisition and Test Control System Software — developed by UDRI and installed on an MS-DOS compatible personal computer[27]

Two main reasons exist for the unique horizontal positioning of the test frame. First, horizontal operation of the radiant heating technique employed with this system minimizes *nonuniform heating across* a test specimen. In contrast, vertical operation may allow conduction and convection to result in higher temperatures in the upper portions of a specimen and, thus, a larger temperature gradient along its length.

Second, horizontal positioning of the test frame permits a lower extensometer mounting force to be used. The extensometer used for strain measurements in this system is placed in contact with the specimen using spring tension. The reduction of this contact force minimizes the amount of nonaxial force applied to a specimen thereby reducing the potential for damage caused at the extensometer mounting points.

Test station development, use, and choice for this research addressed five critical technical concerns: (1) specimen design and gripping, (2) test frame and specimen alignment, (3) strain measurement, (4) heating technique, and (5) data acquisition.

## Specimen Design and Gripping

Tapered-end test specimens (Figure 3-7) were designed based upon geometry optimized by Kidder and Holmes.[28, 29] This geometry was designed for use with CMCs with low values of interfacial shear strength and can be used in either edge-loaded or face-loaded gripping systems. Edge-loading was used during this project. Specimens contained a 33-mm (1.3-in.) gage section and were machined from composite panels using precision diamond grinding machines holding dimensional tolerances of ±0.1-mm (±0.004-in) and angular tolerances of ±2'.[30] No machining was performed on the faces of the specimens; faces were left in the as-pressed condition of the parent panels.

A rigid grip system (Figures 3-4 and 3-6) is installed on the Materials Directorate test station. In this system, the grips are rigidly fixed to the actuator and load cell, and the test specimen is fixed between the grips by means of edge-loading or hydraulically activated face-loading. The grip bodies are capable of being water-cooled to maintain grip temperatures at approximately 40°C (104°F) throughout the course of a high temperature test. However, for this project the grip bodies were not actively cooled. The decision to test with uncooled grips was based upon experimental experience gathered at the University of Michigan's Ceramic Composites Research Laboratory which showed a greater percentage of gage section failures obtained by using uncooled, or heated grips.[31] It is postulated[32] that large thermal gradients produced by actively cooled grips can combine with the complex geometry of the specimen ends to produce severe stress concentrations outside of the specimen gage section thus causing undesirable failures. The absence of controlled cooling allowed grip temperatures to change with test temperature. Thermocouple readings indicated front-face grip temperatures (those on the face closest to the gage section) ranged from 165°C (330°F) with gage section

temperatures of 500°C (932°F), to 260°C (500°F) with gage section temperatures of 1100°C (2012°F). These readings give an indication of the relative temperature gradient between the gage section and gripped ends of each specimen. Back-face temperatures ranged from 60°C (140°F) to 65°C (150°F) for the same range of gage section temperatures.

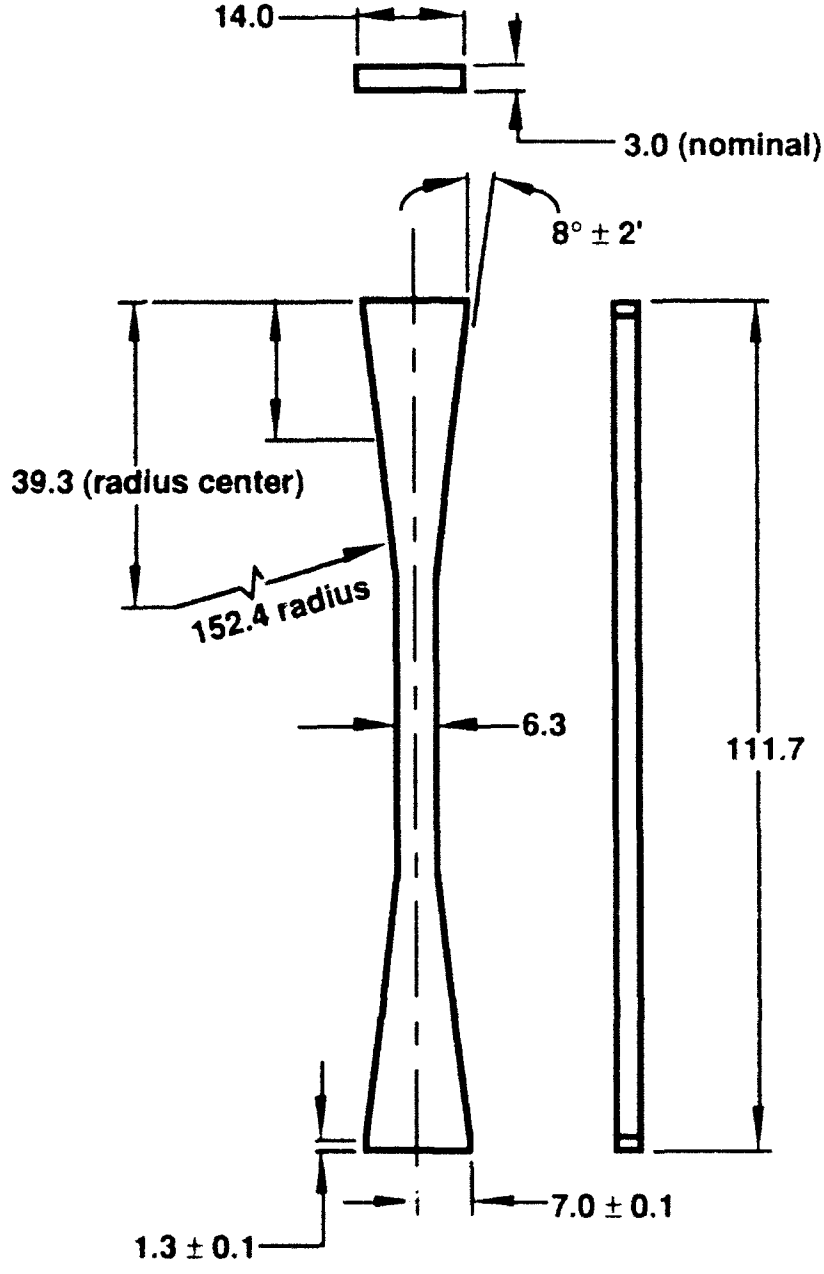


**Figure 3-7.** Edge-loaded test specimen geometry. All dimensions in mm.

To accommodate the specimen geometry, this project used edge-loading inserts (Figure 3-8) which mated to the grip cavities. The inserts and grip bodies were precision machined from a nickel-based superalloy (Inconel-100) to tolerances of ±0.025 mm (±0.001 in).

Each grip is independently activated by separate, adjustable hydraulic piston-and-yoke assemblies which provide gripping pressure required by face-loaded specimens. Since the specimens used for this project were edge-loaded, a minimal gripping force of less than 6.89 MPa (1 ksi) was necessary to minimize any transverse motion of the specimen and inserts. Load transfer to the specimens occurred through the step-like geometry of the inserts which effectively locked the inserts in place within the grip bodies.

## Test Frame and Specimen Alignment

Alignment of a test system designed to evaluate ceramic composites or other materials of limited ductility is crucial. The precision fabrication of the grip bodies on the system at the Materials Directorate allows for accurate alignment of the test frame. While the test frame is in a vertical position, one grip is fixed to the load cell, and a second grip is suspended from it using a special alignment fixture attached to the outside surfaces of both grips. Following this location procedure, the second (suspended) grip is placed in a cavity filled with molten Wood's metal.[33] As the Wood's metal solidifies, the second grip becomes fixed to the actuator, the load train becomes rigid, and alignment is preserved. The test frame is then rotated back to a horizontal operating position. Barring inordinate loading or crosshead movement, this alignment may be retained indefinitely. However, alignment is checked and verified periodically.

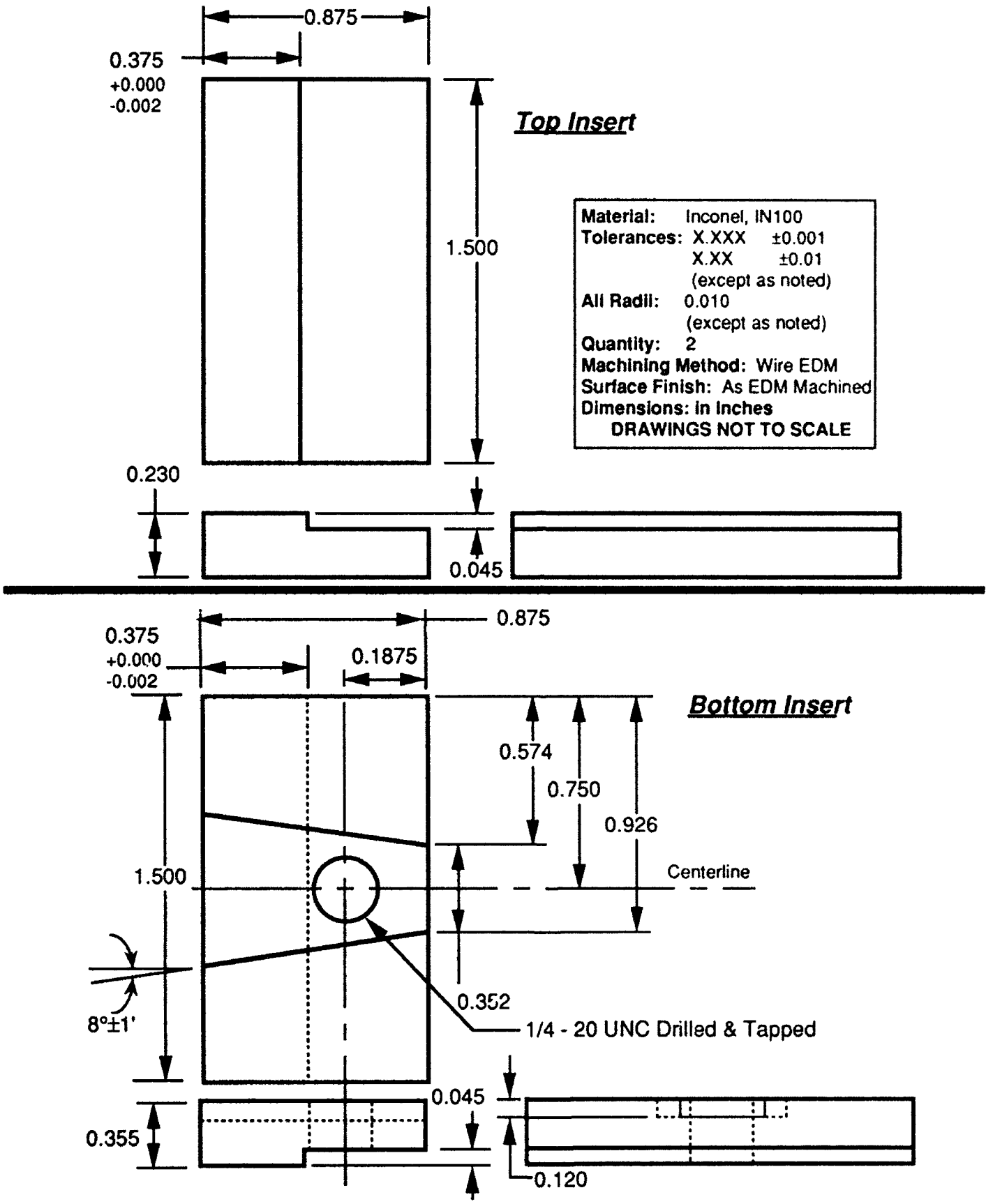


**Figure 3-8.** Edge-Loading Inserts

Alignment was checked using an Inconel-718 bar and a 25.4-mm (1.0-in) gage length clip-on extensometer. The extensometer was attached to a single side of the bar and a set of strain measurements was recorded as the bar was loaded to approximately 7.0 kN (1575 lbs) or 250 MPa (36.26 ksi) This procedure was repeated for each of the four sides of the bar. The readings were analyzed using the ASTM E1012-89 practice of determining bending within the bar.[34] Bending strains (Figure 3-9) were found to be less than 1 percent of the total strains at loads above 1.0 kN (225 lbs), indicating very good load train alignment.

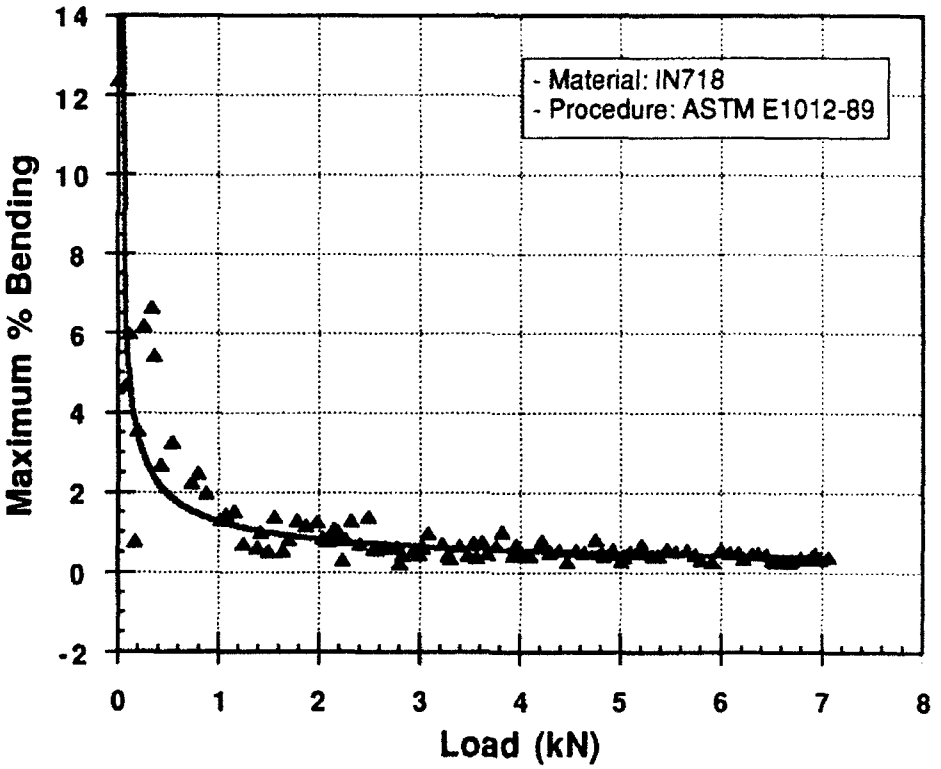


**Figure 3-9.** Bending strains on an Inconel specimen as a function of applied load.

Because of the horizontal orientation of the test frame, accurate positioning of a test specimen within the grips prior to testing is possible in the

absence of any axial loading force. For this project, specimen alignment was confirmed in three ways prior to beginning a test. First, the edge-loading inserts were placed in the grip bodies such that their sides were flush with the sides of the grip bodies. Because of the precise machining of the inserts and grip bodies, the alignment of a specimen's longitudinal axis with the loading axis of the test machine was thus ensured. A depth gage was then used to check the position of the specimen. Measurements were taken to determine the distance from the specimen edges to the sides of the grip bodies/inserts. Four identical measurements (one from each edge of the specimen to side of each grip) confirmed alignment. Finally, specimen alignment was rechecked using the same procedure following pressurization of the hydraulic piston-and-yoke assemblies.

## Strain Measurement

Strain was measured using a 25.4-mm (1.0-inch) gage length elevated temperature extensometer (MTS Model #632.50B-01). This air-cooled extensometer is equipped with 5-mm (0.197-in)-diameter alumina ($Al_2O_3$) rods with conical points. As stated previously, horizontal positioning of the test frame allows for a reduction in the forces necessary to hold the extensometer rods in contact with the specimen, thus decreasing the potential for damaging the specimen. Hold-down spring forces, set by the factory at 400 grams for vertical extensometer positioning, were reduced for this project to approximately 175 grams. Previous experience at the Materials Directorate has shown this force level to be adequate for horizontal positioning.

Modifications were performed on the strain range cards provided by MTS with the 458.20 controller. Because of the extremely small strains developed in this and in other forms of ceramic composites, it was necessary to

make changes to the internal electronics of the smallest (±5 percent) strain range card. The original 804 kΩ resistor was replaced with three 499 kΩ resistors. This converted the card to a ±4 percent range and permitted strain measurement sensitivity of approximately 5.91 x $10^{-5}$/volt.

## Heating Technique and Temperature Measurement

Specimen heating was accomplished using two banks of four high intensity (1000 watt) tungsten-filament quartz bulbs placed above and below the specimen and oriented perpendicular to the loading axis (Figures 3-4 and 3-10). Radiant energy is focused on a test specimen using reflectors which are

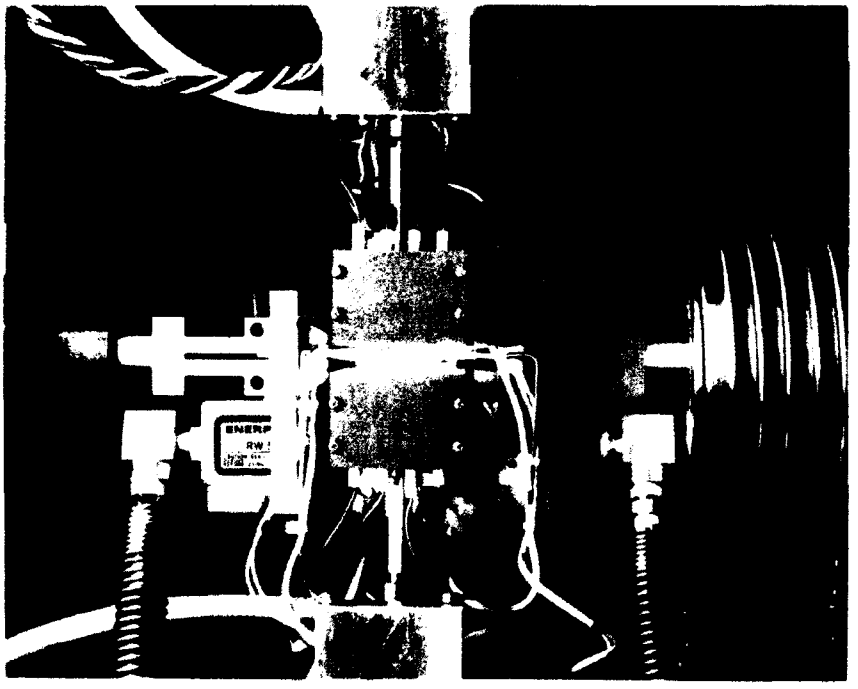

**Figure 3-10.** Lamps positioned in test configuration. Compare this view with that shown in Figure 3-4.

contained within the lamp bodies. The two compact units are air- and water-cooled and are mounted on adjustable stages. The stages permit the lamps to be positioned close to the specimen within the approximately 73-mm (2.87-in) gap present between the grip bodies during the testing of an edge-loaded specimen. The ability to place the lamps in close proximity to the specimen aids in temperature control and reduces thermal gradients within the gage section.

Using 50 percent power, these lamps are capable of achieving temperatures as high as 1500°C (2732°F) in a SiC/SiC composite specimen.[35] However, for this project's isothermal tests at 1100°C (2012°F), typical power outputs of the bulbs ranged from 40 to 60 percent. Thermal cycling, required by thermomechanical fatigue tests, often forced bulb outputs to exceed 85 percent for short periods of time.

Positioning of each lamp body 5 mm (0.2 in) from the centerline of the specimen appeared to provide the best temperature control.

The eight bulbs are paired into four groups of two, or "zones," for control purposes and to allow temperature control at four points along a specimen. A dedicated Barber-Colman Model #560 temperature controller and the MATE software provide temperature control for each of the four zones. The Barber-Colman controller is a PID-based (proportional/integral/derivative) system. Each zone requires independent control settings which vary based upon the desired temperature profile (see **Appendix A: Lessons Learned**).

Each of the four control zones was monitored by a beaded S-type (Platinum/Platinum-15 percent Rhodium) or K-type (Chromel/Alumel) thermocouple. S-type thermocouples were found to have better durability and accuracy for long-term tests and tests employing thermal cycles. K-type thermocouples exhibited time-dependent temperature readings and physical

failures which prevented their use in all but the short-duration isothermal tensile tests.

Each of the four thermocouples were affixed to the surface of the specimen using a twisted wire holder made from K-type thermocouple wire (Figure 3-11). To avoid causing erroneous readings, care was taken to prevent the attaching wires from contacting the thermocouple bead and from forming a junction between the two thermocouple lead wires. To provide more intimate contact between the thermocouples and the specimen and to prevent lamp radiation from influencing thermocouple readings, each thermocouple junction was also bonded to the specimen using Cotronics 903® water-based alumina ceramic adhesive.[36] Portions of the thermocouple leads located between the lamps were shielded by alumina tubes because of the inability of the factory-applied insulation to withstand test temperatures.

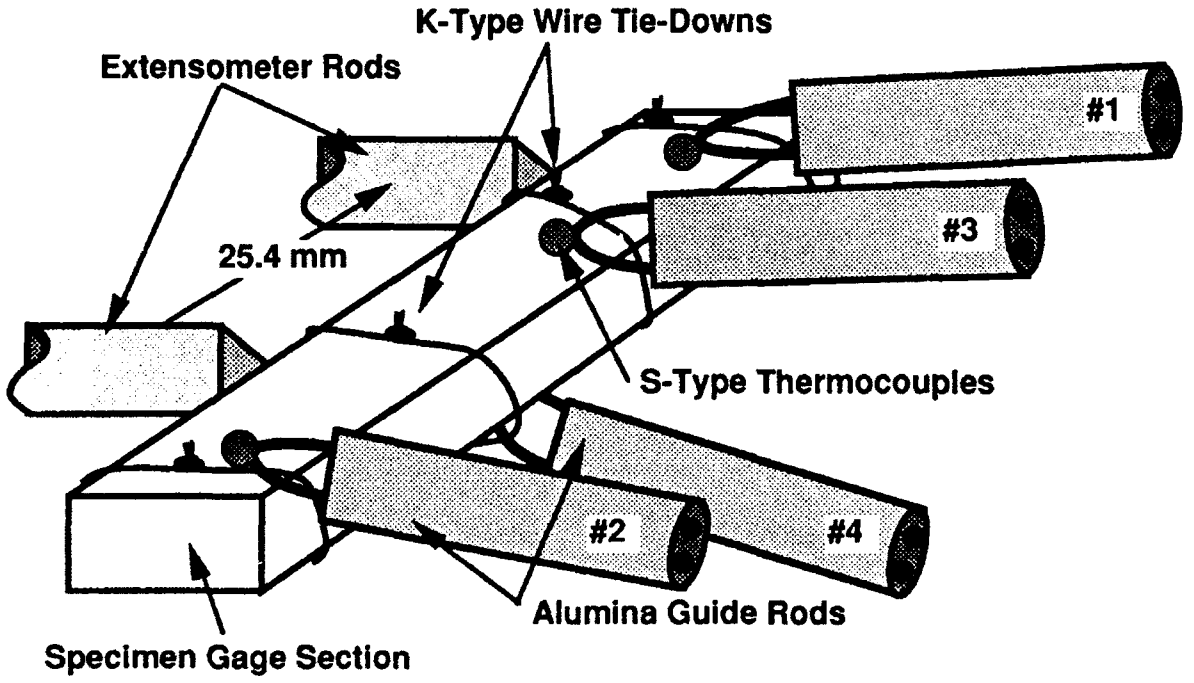


**Figure 3-11.** Schematic of thermocouple attachment to test specimen. Ceramic cement was applied over the wire tie-downs and thermocouple beads

Optimal thermocouple location (Figure 3-12) was determined through an iterative process using a specimen instrumented with thermocouples at seven locations across the gage section. Each of the four pairs of bulbs ("zones") was controlled by a separate thermocouple. Temperatures for several setpoints were monitored at each of the seven locations. The best location for each thermocouple was determined by temperature deviation from the setpoint and temperature uniformity between the seven locations. Deviation and uniformity across the gage section of ±4°C (±7°F) was confirmed using a specimen instrumented with thermocouples, coated with temperature-sensitive paint, and exposed to 1093°C (2000°F). Thermocouple readings during isothermal tensile tests yielded similar results.

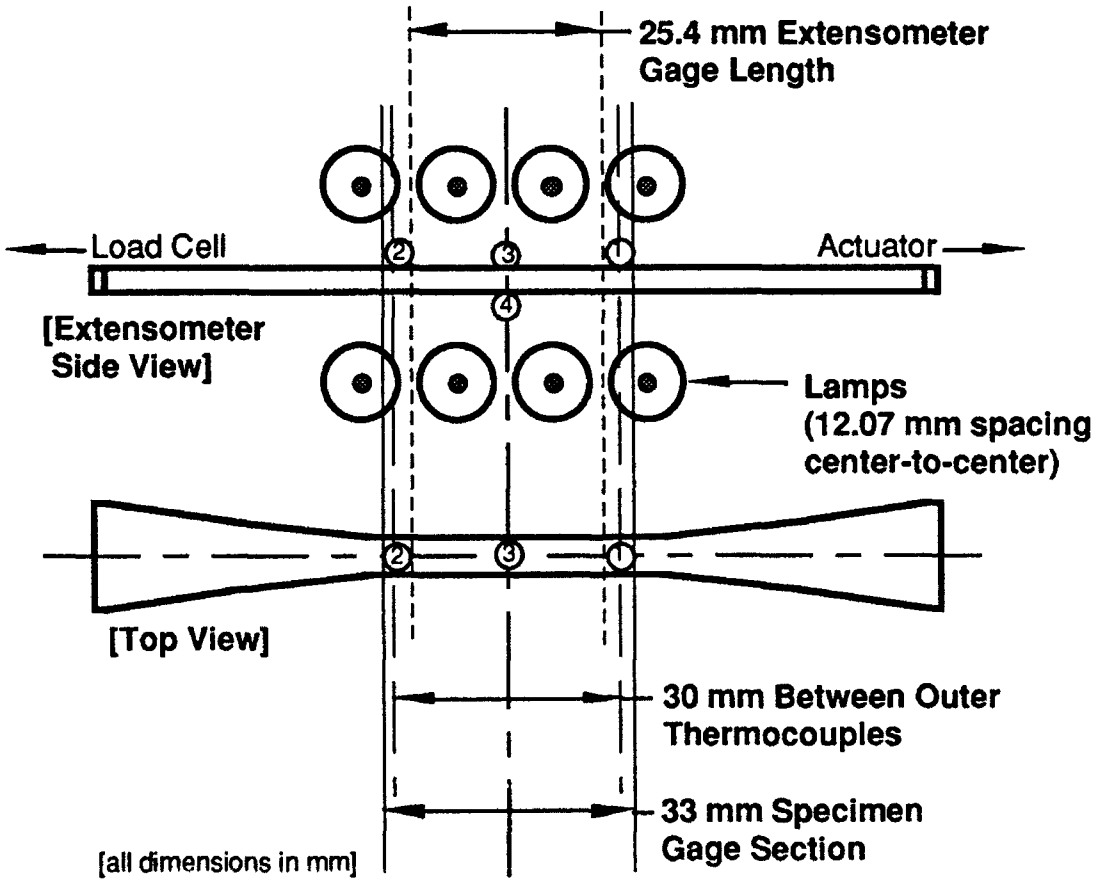


**Figure 3-12.** Thermocouple Positions. Numbers correspond to zones controlled by the numbered thermocouple.

## Data Acquisition and Test Control

Tests were controlled and data acquired using Version 3.60 of the MATE (Materials Analysis and Test Environment) system software. This software package is a 12-bit resolution, menu-based system designed for test control and data analysis of several types of mechanical tests ranging from room temperature tensile tests to thermomechanical fatigue. Real-time analysis and display of test information is also a feature of the MATE system. The software includes a function generator and the capability to monitor and adjust the control functions performed by the Barber-Colman temperature controllers.

MATE is installed on a Zenith Z-248 IBM-compatible personal computer which is linked to the test frame through an A/D (analog-to-digital) board. The computer is able to sample at a rate of 15 kHz, but true data acquisition speed is limited by the 200-Hz capacity of the MATE software. The Z-248 drives a printer to plot hard copies of information and graphical results of test data.

Long-term stability and repeatability of the data acquisition system has been demonstrated by Zawada, *et al.*[37] In this evaluation, the acquired modulus values of a steel specimen subjected to elastic range, sinusoidal loading for 1.25 million cycles varied by less than ±0.2 percent. This indicates a high degree of stability and repeatability offered by the MATE-based system.

The accuracy and resolution of the MATE system was checked during this project. Two specimens of Nicalon® fiber-reinforced barium magnesium aluminosilicate (SiC/BMAS) glass-ceramic, provided by the Materials Directorate, were tested in tension at 1000°C (1768°F). One test was performed in load control with a calculated stress rate of 100 MPa/sec (14.5 ksi/sec), and the other in stroke control with a stroke rate of 0.251 mm/sec ($9.88 \times 10^{-3}$ in/sec). Results acquired by the MATE system were compared with those acquired by a Macintosh-based, 16-bit GW Instruments data acquisition

system provided by Prof. J.W. Holmes of the University of Michigan's Ceramic Composites Research Laboratory. The validity and accuracy of data acquired by the GWI system was previously verified by Prof. Holmes. Although the MATE system stored an order of magnitude fewer data points than the GWI system, the MATE system results appeared free of noise acquired on the unfiltered load channel by the GWI system. Following filtering and 20-point smoothing of the GWI-acquired data, the test results from both systems apoeared identical (Figures 3-13 and 3-14).

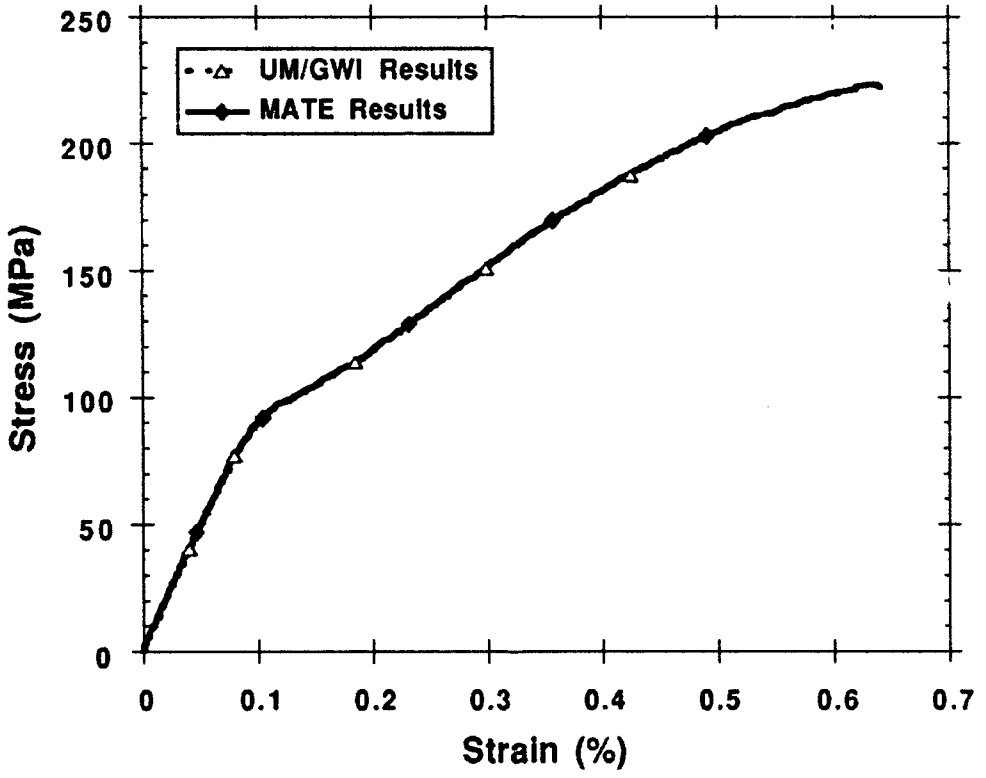


**Figure 3-13.** Comparison of MATE and GWI data acquisition systems for a load-controlled tensile test of SiC/BMAS [0/90] at room temperature.
Loading rate: 100 MPa/sec.
Data Acquisition Parameters: GWI - 1000 pts./sec, MATE - 100 pts./sec.

The agreement of the two data acquisition systems in this series of tests confirmed the adequacy of the accuracy and resolution offered by the MATE

test control and data acquisition system. Deviations in ultimate strength values were less than 0.12 percent (0.27 MPa [0.039 ksi]) for the load controlled test and less than 0.67 percent (1.46 MPa [0.212 ksi]) for the stroke controlled test. Deviations in initial modulus values were less than 1.6 percent (1.56 GPa [0.226 Msi]) for the load controlled test and less than 0.80 percent (0.84 GPa [0.122 Msi]) for the stroke controlled test.

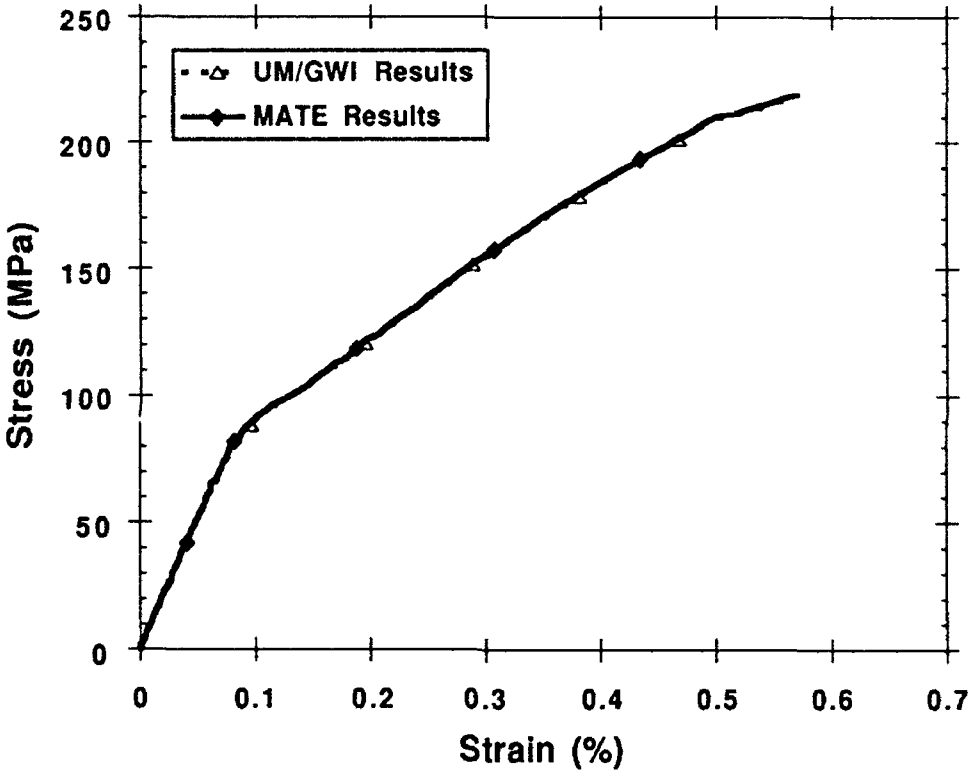


**Figure 3-14.** Comparison of MATE and GWI data acquisition systems for a stroke-controlled tensile test of SiC/BMAS [0/90] at room temperature.
Stroke rate: 100 MPa/sec.
Data Acquisition Parameters: GWI - 1000 pts./sec, MATE - 100 pts./sec.

## Test System Limitations

During the course of this project, the MATE system was continuously updated and improved. Most of the updates affected the accuracy and

timeliness of the real-time displays and the flexibility of the cycle specification and initiation procedures. **Chapter V: Conclusions and Recommendations** and **Appendix A: Lessons Learned** contain suggestions for optimal system operation and for system improvements. Four major issues which require further system improvements and perhaps a better understanding of material behavior are those of phase shift correction, initial system stability, noise, and gage section failures. Because of their importance in presenting the results of this project with the correct perspective, these issues are outlined in detail in the following paragraphs.

Because of the different response times of the heating system and servohydraulic load frame, a severe phase shift problem would have occurred in the thermomechanical fatigue tests had not corrective procedures been used. Without such corrections, the programming of identical, simultaneous temperature and load profiles would have resulted in a temperature lag because of the slower response time of the quartz-lamp heating system. Subsequent MATE versions now address this problem and permit automatic correction. However, for this project, the lag was corrected by manually programming the temperature to lead the load during thermomechanical tests. The combination of the programmed lead in the heating profile and the inherent lag in the lamp system permitted close agreement between the actual and desired load and temperature profiles (Figures 3-15 and 3-16). However, the temperature and load were never entirely synchronized, and this caused difficulties in analyzing hysteresis loops obtained from TMF tests (see the section entitled **Hysteresis Loops**).

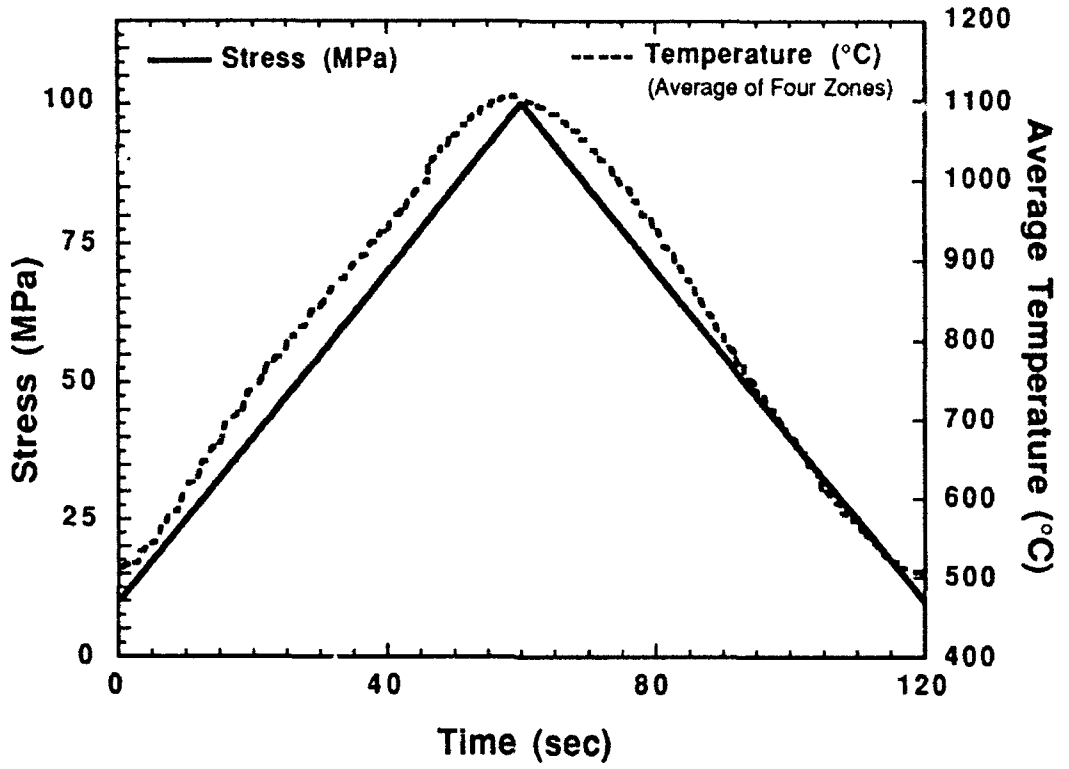


**Figure 3-15.** Typical stress and temperature profiles for thermomechanical fatigue tests without hold time. Temperature shown is the average temperature from the four control zones.

Thermomechanical fatigue tests also suffered from the inability to perform a correct first cycle. This problem occurred only with the temperature on these tests. Maximum and minimum temperatures attained during the initial portion of a thermomechanical fatigue test rarely matched the desired temperatures. Isolated deviations observed during the high temperature portions (1100°C [2012°F]) of the test cycles ranged from -20°C (-36°F) to +35°C (+63°F). Isolated deviations observed during the lower temperature portions (500°C [932°F]) of the test cycles were typically less than +35°C (+63°F). In some cases, the initial portion of a test consisted of the first five to

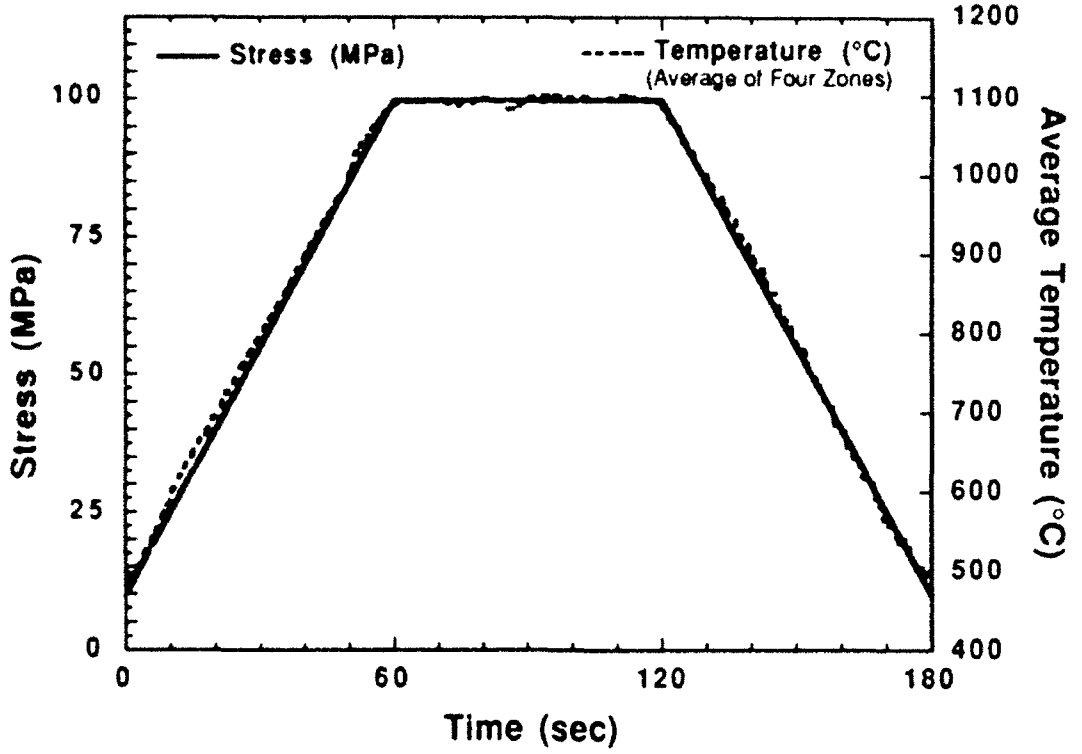


**Figure 3-16.** Typical stress and temperature profiles for thermomechanical fatigue tests with hold time at maximum stress and maximum temperature. Temperature shown is average temperature from the four control zones.

ten cycles, and sometimes recurred when the test was restarted after being put on hold. This problem was due, in part, to the aggressive temperature profile called for in the test matrix. A slower temperature ramp rate may permit improved temperature control on the initial cycles of future thermomechanical tests on CMCs. Experience with testing these materials and with the specific temperature controller settings will also aid in solving this problem.

Power surges required to boost the temperature to its maximum during thermomechanical fatigue tests and periodic power fluctuations necessary to stabilize the temperature during isothermal tests produced noise in the acquired strain signals. The source of the noise signal appeared to be in the

power control unit for the quartz lamps rather than in the lamp bodies, bulbs, or wiring. Deviations of up to ±0.0075 percent strain were observed during isothermal fatigue tests corresponding to a noise signal acquired by the extensometer of approximately ±0.25 volts. Noise also adversely affected attempts to monitor specimens using acoustic emission techniques. During the initial system assembly and checkout, noise was also found to affect the load signal. Repair of faulty cable shielding and adjustments to the gain on the MTS load range card suppressed these spurious signals. Several attempts were made to alleviate the noise problem in the strain readings, but all met with no success. A contributing factor to this problem may have been the extreme sensitivity of the strain range card used for the tests.

As noted earlier, it is speculated that the combination of specimen geometry and thermal gradients at the specimen ends results in stress states which promote failure outside of the 33-mm (1.3-in.) gage section of the specimen. Of the 11 specimens tested for this project, three failed entirely outside of the specimen gage section during tension testing. Failures of the remaining eight were at least partially contained in the specimen gage section. Only two of these eight failures occurred completely between the rods of the extensometer (i.e., in the 25.4-mm (1.0-in) extensometer gage section). See **Appendix C: Summary of Test Results** for further details. Recent work performed by Prof. J.W. Holmes at the University of Michigan[38] on specimens with a further optimized geometry has found that minimizing thermal gradient by using hot grips increases the number of gage section failures obtained. These results suggest the need for the use of an extensometer with a gage length to match the gage section of the specimen and a more thorough understanding of the effect of thermal gradients on the behavior of the material.

## Test Procedures

All testing for this project was conducted in air under load control.

Isothermal tensile tests were conducted on four specimens. Three were tested at 1100°C (2012°F), and one was tested at room temperature (23°C [73°F]). Specimens tested at elevated temperatures were brought to temperature in 10 minutes and allowed to "soak" at this temperature for 10 minutes before testing commenced. The loading rate used was equivalent to a stress rate of 100 MPa/sec (14.5 ksi/sec). This relatively high loading rate was chosen to prevent creep effects[39] and rate-dependent interfacial shear strength variations[40] from influencing the elevated temperature tensile behavior of the material .

Isothermal fatigue tests at 1100°C (2012°F) were conducted on three specimens using an R value of 0.1 (R is defined as the ratio of the minimum stress to the maximum stress). The maximum stress was arbitrarily chosen as 100 MPa (14.5 ksi) corresponding to 40 percent of the proportional limit at 1100°C (2012°F). One specimen was subjected to test conditions illustrated in Figure 3-17, a 60-second ramp from $\sigma_{min}$ to $\sigma_{max}$ with no hold time. Two specimens were subjected to a profile shown in Figure 3-18, a 60-second ramp from $\sigma_{min}$ to $\sigma_{max}$ with a superimposed 60-second hold time at $\sigma_{max}$.

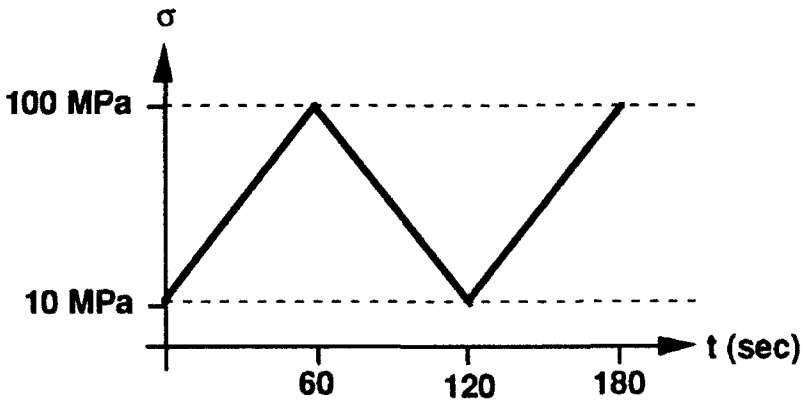


**Figure 3-17.** Isothermal fatigue profile with no hold.

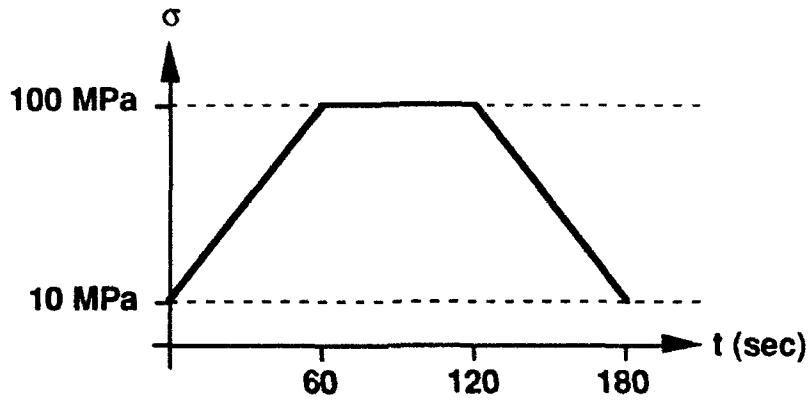


**Figure 3-18.** Isothermal fatigue profile with 60-sec hold at maximum stress and temperature.

Thermomechanical fatigue (TMF) tests were performed on five specimens using an R value of 0.1. Again, the maximum stress was arbitrarily chosen as 100 MPa (14.5 ksi) corresponding to 40 percent of the proportional limit at 1100°C (2012°F). Cycle temperatures ranged from a $T_{min}$ of 500°C (932°F) to a $T_{max}$ of 1100°C (2012°F) in an attempt to simulate actual turbine blade temperature conditions.[41] Three specimens were subjected to an in-phase cycle corresponding to the load/temperature profile illustrated in Figure 3-19, a 60-second ramp from $\sigma_{min}$, $T_{min}$ to $\sigma_{max}$,$T_{max}$. Two additional specimens were subjected to a simple test profile involving an in-phase cycle with a superimposed hold at maximum load and temperature. This cycle, illustrated in Figure 3-20, is comprised of a 60-second ramp from $\sigma_{min}$, $T_{min}$ to $\sigma_{max}$,$T_{max}$ with a 60-second hold time at $\sigma_{max}$, $T_{max}$ . These temperature ramps were chosen in an effort to perform the tests with the fastest cycle times possible while still maintaining adequate temperature control. Temperature excursions in actual turbine engines occur much faster than the cycle times used in this project.

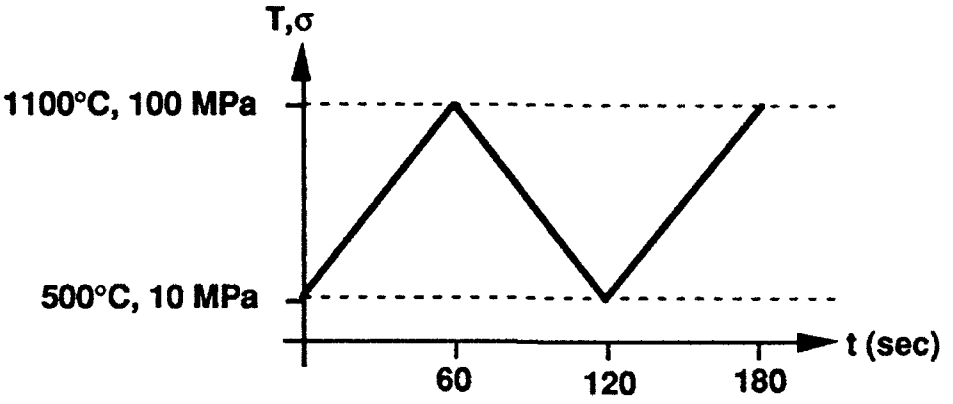


**Figure 3-19.** Thermomechanical fatigue profile with no hold.

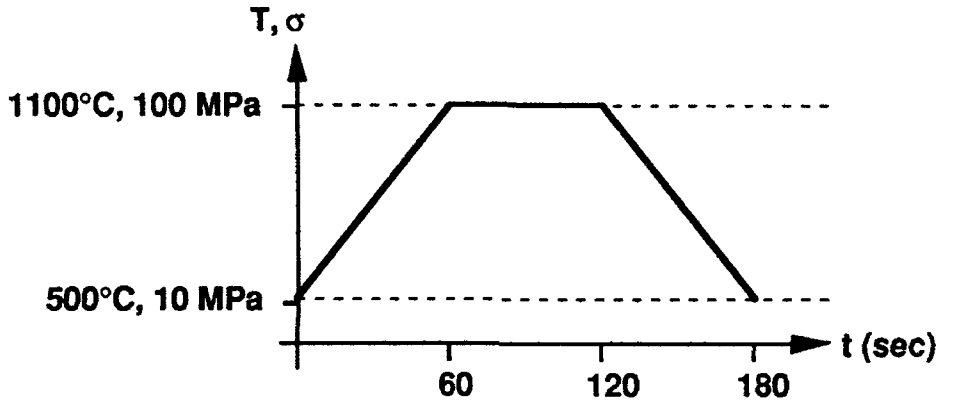


**Figure 3-20.** Thermomechanical fatigue profile with 60-sec hold at maximum stress and temperature.

Run out for the isothermal and thermomechanical fatigue tests was arbitrarily set at 1000 cycles. This corresponded to 33.3 continuous hours of testing using triangular fatigue profiles and 50 continuous hours of testing using profiles including the 60-second hold. Following 1000 cycles, the specimens were immediately subjected to tensile tests at 1100°C (2012°F) and 100 MPa/sec (14.5 ksi/sec).

For the isothermal and the thermomechanical fatigue tests, the initial start-up procedure used was governed by the capabilities of the MATE system. This test control system allows for a start-up procedure to consist only of a

separate loading and heating ramps. Temperature and load cannot be ramped simultaneously to the initial starting point from a room temperature, zero stress condition. The procedure used was to first ramp the temperature to the test's starting temperature followed by ramping the load. The ramp rate for each parameter was calculated to match the ramp rate used for that parameter during a thermomechanical fatigue test, i.e. 1.5 MPa/ sec (0.218 ksi/sec) and 10°C/sec (18°F/sec).

These ramp rates and ramp sequences were also followed when ramping to hold during the course of a test. The servohydraulic/MATE system allows a test to be put on hold manually, in preprogrammed intervals, when certain load, temperature, or stroke limits are engaged, or for safety reasons (such as a loss of cooling water to the machine). Hold loads and hold temperatures may be specified. For the purposes of this project, hold loads were programmed as those equivalent to $\sigma_{min}$ and hold temperatures as $T_{min}$. The only exceptions to these criteria came when maintenance was required on the lamps (thermocouple or bulb replacement, etc.) or when the test was left unattended. At these times, the hold temperature was specified as room temperature for safety considerations. The number of times a specimen was brought down to room temperature was limited in order to minimize any damage developed during cool down due to thermal residual stresses which are produced because of the mismatch of the coefficients of thermal expansion of the matrix and fibers.

## References — CHAPTER III: EXPERIMENTAL PROCEDURE


1 Bhaduri, S.B., and Froes, F.H., "The Science and Technology of Advanced Structural Ceramics," *Journal of Materials*, The Minerals, Metals, and Materials Society, Warrendale, PA, **43**, [5], May 1991, pg. 20.

2 Mah, T., Mendriatta, M.G., Katz, A.P., and Mazdiyasni, K.S., "Recent Developments in Fiber-Reinforced High Temperature Ceramic Composites," *American Ceramic Society Bulletin*, American Ceramic Society, Westerville, OH, **66**, [2], 1987, pg. 304.

3 Simon, G., and Bunsell, A.R., "The Creep of Silicon Carbide Fibers," *Journal of Materials Science Letters*, Chapman & Hall, Ltd., London, England, **2**, [9], 1983, pp. 80-82.

4 Simon, G., and Bunsell, A.R., "Creep Behavior and Structural Characterization at High Temperatures of Nicalon Silicon Carbide Fibres," *Jourr.al of Materials Science*, Chapman & Hall, Ltd., London, England, **19**, [11], 1984, pp. 3658-3670.

5 Simon, G., and Bunsell, A.R., "Mechanical and Structural Characterization of the Nicalon Silicon Carbide Fibre," *Journal of Materials Science*, Chapman & Hall, Ltd., London, England, **19**, [11], 1984, pp. 3649-3657.

6 Mah, T., Hecht, N.L., McCullum, D.E., Hoenigman, J.R., Kim, H.M., Katz, A.P., and Lipsitt, H.A., "Thermal Stability of SiC Fibres (Nicalon®)," *Journal of Materials Science*, Chapman & Hall, Ltd., London, England, **19**, 1984, pp. 1191-1201.

7 Clark, T.J., Arons, R.M., and Stamatoff, J.B., "Thermal Degradation of Nicalon SiC Fibers," *Ceramic Engineering and Science Proceedings*, American Ceramic Society, Westerville, OH, **6**, [7-8], 1985, pp. 576-588.

8 Sawyer, L.C., Arons, R., Haimbach, F., Jaffe, M., and Rappaport, K.D., "Characterization of Nicalon: Strength, Structure and Fractography," *Ceramic Engineering and Science Proceedings*, American Ceramic Society, Westerville, OH, **6**, [7-8], 1986, pp. 567-575.

9 Sawyer, L.C., Chen, R.T., Haimbach, F., Harget, P.J., Prack, E.R., and Jaffe, M., "Thermal Stability Characterization of SiC Ceramic Fibers, II: Fractography and Structure," *Ceramic Engineering and Science Proceedings*, American Ceramic Society, Westerville, OH, **7**, [7-8], 1986, pp. 914-930.

10 Clark, T.J., Jaffe, M., Rabe, J., and Langley, N.R., "Thermal Stability Characterization of SiC Ceramic Fibers, I: Mechanical Property and Chemical Structure Effects," *Ceramic Engineering and Science Proceedings*, American Ceramic Society, Westerville, OH, **7**, [7-8], 1986, pp. 901-913.

11 Fareed, A.S., Fang, P., Koczak, M.J., and Ko, F.M., "Thermomechanical Properties of SiC Yarn," *American Ceramic Society Bulletin*, American Ceramic Society, Westerville, OH, **66**, [2], 1987, pp. 353-358.

12 Clark, T.J., Prack, E.R., Haider, M.I., and Sawyer, L.C., "Oxidation of SiC Ceramic Fiber," *Ceramic Engineering and Science Proceedings*, American Ceramic Society, Westerville, OH, **8**, [7-8], 1987, pp. 717-731.

13 Pysher, D.J., Goretta, K.C., Hodder, R.S. Jr., and Tressler, R.E., "Strengths of Ceramic Fibers at Elevated Temperatures," *Journal of the American Ceramic Society*, American Ceramic Society, Westerville, OH, **72**, [2], 1989, pp. 284-288.

14 Rigdon, M.A., and Hong, W.S., "Comparison of High-Temperature Testing Results of Ceramic Fibers," in Thermal and Mechanical Behavior of Metal Matrix and Ceramic Matrix Composites, ASTM STP 1080, Kennedy, J.M., Moeller, H.H., and Johnson, W.S., eds. American Society for Testing and Materials, Philadelphia, PA, 1990, pp. 136-151.

15 Langley, N.R., LeGrow, G.E., and Lipowitz, J., "Chapter 3: Properties of Ceramic Fibers from Organosilicon Polymers." in Fiber Reinforced Ceramic Composites: Materials, Processing, and Technology, Mazdiyasni, K.S., ed., Noyes Publications, Park Ridge, NJ, 1990.

16 Corning Data Sheet, 1990.

17 Personal communication with R. Stewart, Corning Glass Works, 10 July 1991.

18 Personal communication with R. Stewart, Corning Glass Works, 1 October 1991.

19 Larsen, D.C., Stuchly, S.L., and Adams, J.W., Evaluation of Ceramics and Ceramic Composites for Turbine Engine Applications: AFWAL Technical Report AFWAL-TR-88-4202, Materials Laboratory, Air Force Wright Aeronautical Laboratories, Wright-Patterson AFB, OH, December 1988, pp. 7-8.

20 Allaire, R.A., Janas, V.F., Stuchly, S., and Taylor, M.P., "Glass Matrix Composites for Higher Use Temperature Applications," *SAMPE Quarterly*, Society for the Advancement of Materials and Process Engineering, Lynchburg, VA, **19**, [1], October 1987, pg. 29

21 Allaire, *et al.*, *op. cit.*, pg. 25.

22 Rousseau, C.Q., "Monotonic and Cyclic Behavior of a Silicon Carbide/Calcium-Aluminosilicate Ceramic Composite," in Thermal and Mechanical Behavior of Metal Matrix and Ceramic Matrix Composites, ASTM STP 1080, Kennedy, J.M., Moeller, H.H., and Johnson, W.S., eds. American Society for Testing and Materials, Philadelphia, PA, 1990, pg. 137.

23 Stewart, R.L., Chyung, K., Taylor, M.P., and Cooper, R.F., "Fracture of SiC Fiber/Glass-Ceramic Composites as a Function of Temperature," in Fracture Mechanics of Ceramics, Vol. 7: Composites, Impact Statistics and High-Temperature Phenomena, Bradt, R.C., Evans, A.G., Hasselman, D.P.H., and Lange, F.F., eds., Plenum Publishing Corp., New York, NY, 1985, pp. 33-51.

24 Hartman, G.A., Zawada, L.P., and Russ, S.M., "Techniques for Elevated Temperature Testing of Advanced Ceramic Composite Materials," in Fifth Annual Hostile Environments and High Temperature Measurements Conference Proceedings, Society for Experimental Mechanics, Inc., Englewood Cliffs, NJ, 1988, pp. 31-38.

25 Hartman, G.A., and Russ, S.M., "Techniques for Mechanical and Thermal Testing of Ti3Al/SCS-6 Metal Matrix Composites," in Metal Matrix Composites: Testing Analysis, and Failure Modes, ASTM STP 1032, Johnson, W.S., ed., American Society for Testing and Materials, Philadelphia, PA, 1989, pp. 43-53.

[26] Butkus, L.M., Zawada, L.P., and Hartman, G.A., "Fatigue Test Methodology and Results for Ceramic Matrix Composites at Room and Elevated Temperatures," Cyclic Deformation, Fracture, and Nondestructive Evaluation of Advanced Materials: ASTM STP 1157, Mitchel, M.R. and Buck, O., eds., American Society for Testing and Materials, Philadelphia, PA, 1992.

[27] Hartman, G.A., and Ashbaugh, N.E., "A Fracture Mechanics Test Automation System for a Basic Research Laboratory," in Applications of Automation Technology to Fatigue and Fracture Testing, ASTM STP 1092, Braun, A.A., Ashbaugh, N.E., and Smith, F.M., eds., American Society for Testing and Materials, Philadelphia, PA, 1990, pp. 95-110.

[28] Kidder, M., and Holmes, J.W., "Stress Analysis of an Edge-Loaded Ceramic Tensile Specimen," to be submitted to *Journal of the American Ceramic Society*, American Ceramic Society, Westerville, OH.

[29] Holmes, John W., "A Technique for Tensile Fatigue and Creep Testing of Fiber-Reinforced Ceramics," accepted for Publication in *Journal of Composite Materials*.

[30] Machining performed by BOMAS Machining, Somerville, MA.

[31] Personal Communication with Prof. J.W. Holmes, University of Michigan, 29 June 1991.

[32] Personal Communication with Prof. J.W. Holmes, University of Michigan, 13 June 1991.

[33] Wood's metal refers to a fusible alloy consisting of 12.5 % Sn, 50.0% Bi, 25.0% Pb, and 12.5% Cd. It is used in this application because of its low melting temperature (71°C, 160°F) and rigidity at room temperature. For further details see:
Mark's Standard Handbook for Mechanical Engineers, Eighth Edition, Baumeister, T., Avallone, E.A., and Baumeister, T. III, eds., McGraw-Hill Book Company, New York, NY, 1978, pg. 6-90.

[34] "ASTM E1012-89: Standard Practice for Verification of Specimen Alignment under Tensile Loading," 1990 Annual Book of ASTM Standards: Section 3, Metals Test Methods and Analytical Procedures, American Society for Testing and Materials, Philadelphia, PA, 1991, pp. 781-788.

[35] Butkus, Zawada, and Hartman, *ibid.*

[36] Cotronics Corp., Brooklyn, NY.

[37] Zawada, L.P., Butkus, L.M., and Hartman, G.A., "Room Temperature Tensile and Fatigue Properties of Silicon Carbide Fiber-Reinforced Aluminosilicate Glass," *Journal of the American Ceramic Society*, American Ceramic Society, Westerville, OH, **74**, [11], 1991, pp. 2851-2858.

[38] Personal Communication with Prof. J.W. Holmes, University of Michigan, 30 June 1991.

[39] Holmes, John W., "Influence of Stress Ratio on the Elevated-Temperature Fatigue of a Silicon Carbide Fiber-Reinforced Silicon Nitride Composite," *Journal of the American Ceramic Society*, American Ceramic Society, Westerville, OH, **74**, [7], 1991, pg. 1641.

40 Goettler, R.W. and Faber, K.T., "Interfacial Shear Stresses in SiC and $Al_2O_3$ Fiber-Reinforced Glasses," *Ceramic Engineering and Science Proceedings*, American Ceramic Society, Westerville, OH, **9**, [7-8], January 1988, pp. 864.

41 Holmes, J.W., McClintock, F.A., O'Hara, K.S., and Conners, M.E., "Thermal Fatigue Testing of Coated Monocrystalline Superalloys," in Low Cycle Fatigue, ASTM STP 942, Solomon, H.D., Halford, G.R., Kaisand, L.R., and Keis, B.N. , eds., American Society for Testing and Materials, Philadelphia, PA, 1985, p. 672.

# IV. RESULTS AND DISCUSSION

## Tensile Behavior

A single tensile test conducted at room temperature (23°C, 73°F) showed an initial material modulus, $E_i$, of 131 GPa (19 Msi) (Figure 4-1). This value agrees closely with modulus data supplied by Corning Glass Works (131 to 138 GPa [19 to 20 Msi]),[1] with that determined by Wang and Parvizi-Majidi (131.8 GPa [19.11 Msi]),[2] and with the value calculated using the "Rule of Mixtures" method (136 GPa [19.7 Msi], see **Appendix B: Modeling**). The observed ultimate strength, $\sigma_{ult}$, of 552 MPa (80 ksi) is also within the range reported by Corning (448 to 597 MPa [65.5 to 86.6 ksi]) as is the observed strain at failure, $e_{ult}$, of 1.05 percent (Corning's Data: 0.74 to 1.20 percent). The observed proportional limit, $\sigma_{pl}$, (the stress at which the stress-strain curve first deviates from linearity) occurred at 285 MPa (41 ksi), a higher level than that reported by Corning (173 to 217 MPa, 25.1 to 31.5 ksi).

Three SiC/CAS-II specimens were tested in tension at 1100°C (2012°F). A typical stress-strain curve is shown in Figure 4-2. Stress and strain values reported here represent the average of those attained during testing. The material tested in tension at 1100°C (2012°F) exhibited an initial modulus, $E_i$, of approximately 130 GPa (18.9 Msi), similar to that of the room temperature test. The average ultimate strength, $\sigma_{ult}$, of 361 MPa (52.4 ksi), average strain at failure, $e_{ult}$, of 0.58 percent, and proportional limit, $\sigma_{pl}$, of 249 MPa (36 ksi), are all lower than room temperature values. The observed modulus is surprisingly high given the reported reduced modulus values of the fiber[3,4] and matrix[5] at this temperature. A "Rule of Mixtures" calculation using a fiber modulus of 160 GPa (23.3 Msi) and a matrix modulus of 88.3 GPa (12.8 Msi)

yields a predicted modulus of only 117 GPa (17 Msi). A similar agreement in the modulus of the

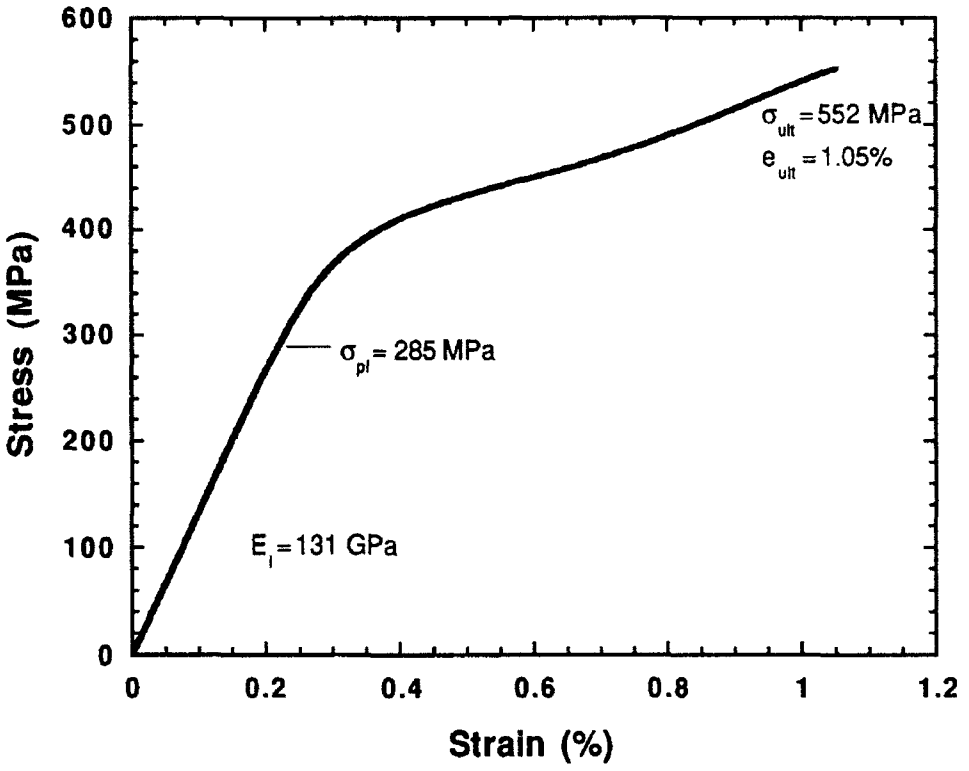


**Figure 4-1.** Room temperature tensile behavior of $[0]_{16}$ SiC/CAS-II. Test performed in air with a loading rate of 100 MPa/sec (14.5 ksi/sec).

SiC/CAS-II material tested at 20°C (68°F) and 815°C (1500°F) was reported by Rousseau.[6]

The distinctly nonlinear tensile behavior of the material can best be explained using the concepts of crack initiation and propagation.[7] Microcracks initiate in the matrix as the composite is strained to approximately 0.13 percent[8] at room temperature. At this point, the stress in the matrix is approximately 264 MPa (35.7 ksi); the sum of the stress applied to the composite, 160 MPa (23.2 ksi), and the processing-induced residual stress in the matrix, 86 MPa (12.5 ksi). At strains beyond this point, the microcracks propagate into the

composite in a direction perpendicular to the fibers. The majority of the cracks are deflected at the fiber-matrix interface and begin to travel along the interface. Some cracks may proceed through fibers.

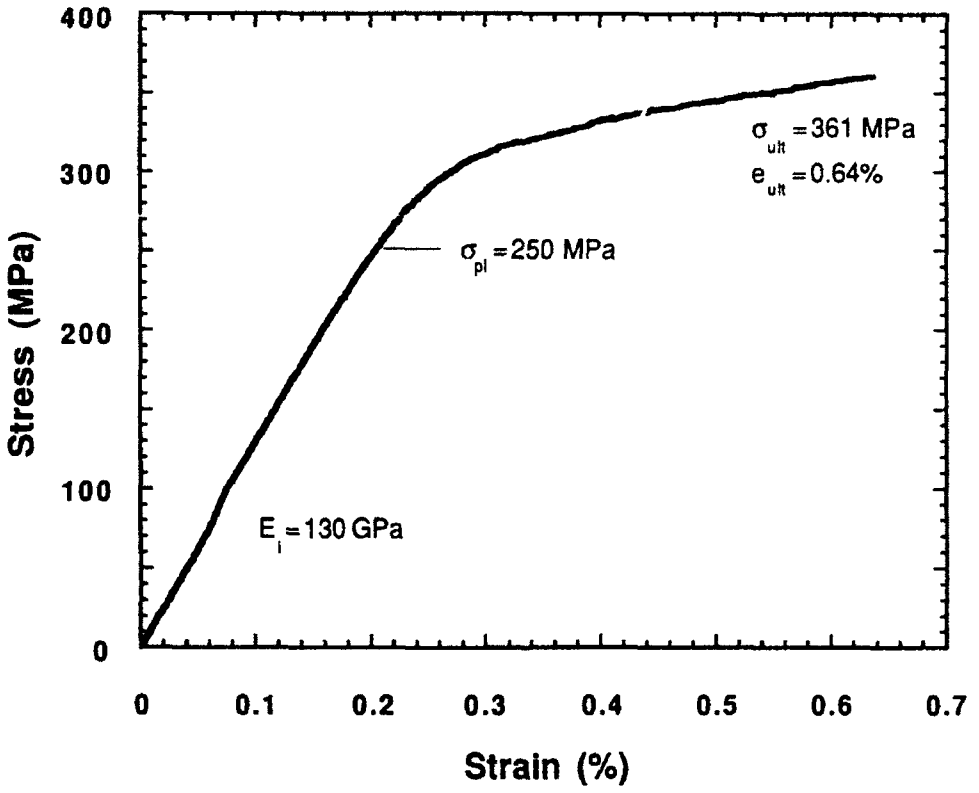


**Figure 4-2.** 1100°C (2012°F) tensile behavior of $[0]_{16}$ SiC/CAS-II. Test performed in air with a loading rate of 100 MPa/sec (14.5 ksi/sec).

Eventually, the interfacial cracking forms a network, effectively isolating some portions of the matrix and forcing the fibers to carry more load. This scenario gradually occurs near the "knee" of the tensile curve. The plateau that follows is caused by a combination of increasing stresses in the fiber and a decrease in the effective, load-carrying cross section of the composite due to the loss of the load-carrying capability of the now cracked matrix. The result is a relatively large extension with a very small increase in load. Recall, that

Figure 4-1 displays only the stresses calculated using the original cross-sectional area of the specimen. As the matrix cracks and ceases to carry load, the fiber stress increases until, near the end of the tensile test, the total loss of the load-carrying capability of the matrix forces the fibers to withstand stresses approximately 250 percent ($1/V_f$, $V_f$ = 40 percent) higher than those shown in Figure 4-1. As the fibers assume this higher stress, the observed tensile response of the composite begins to change (i.e., turns slightly upward) to depict the higher modulus of the fibers. The ultimate fiber stress is reached before this transition of the composite modulus to the fiber modulus is complete. Ostensibly, this proposed process occurs gradually rather than in discrete increments. The large residual compressive radial stress present in the fibers (see the section entitled **States of Stress in Fiber and Matrix**) may also contribute to the increase in modulus by producing sliding resistance as the fibers are pulled out of the matrix during failure. A high level of sliding resistance could result in an increase in stiffness which would, in turn, be evident in an increase in the modulus of the composite stress-strain curve near failure. Interactions caused by rate effects and debris formation may also play roles in governing the tensile behavior of this composite system.

In contrast, it is possible that the absence of a final increase in modulus and lower strain-to-failure values in the high temperature tensile behavior is caused by lower fiber strengths and the lower degree of residual compressive radial stress on the fibers present at elevated temperatures. (Studies[9,10] have shown that the strength of ceramic-grade Nicalon® decreases from approximately 2250 MPa (326 ksi) at 25°C (77°F) to 1400 MPa (203 ksi) at 1100 °C (2012°F)). Note that the initial modulus values for the room and elevated temperature tests are identical. A decrease in fiber strength, with a retention of modulus, would result in a lower ultimate strain for the fibers and

for the composite, since the behavior of the composite is fiber-dominated in the latter portion of the tensile test. Therefore, it is plausible that the ultimate strength and strain of the fibers is reached prior to the occurrence of any transition (i.e., upturn) of the composite modulus to the fiber modulus. In addition, a lower level of compressive radial stress upon the fibers could reduce the amount of sliding friction caused during pull-out, and thereby eliminate the increase in composite modulus which was observed in the room temperature tensile test.

Optical inspection of the fracture surfaces revealed that the specimens tested at 1100°C (2012°F) experienced a greater degree of fiber pull-out. The specimen tested at room temperature exhibited approximately 1.5 mm (0.059 in) of pull-out, whereas those tested at 1100°C (2012°F) exhibited approximately 10 mm (0.394 in) of fiber pull-out. These observations are in contrast to the phenomenon of decreasing fiber pull-out lengths with increasing temperature seen in other CMCs. This difference in behavior can be attributed to the temperature-dependent shear strength of the fiber-matrix bond. The strength of this bond is affected by two factors: the difference between the coefficients of thermal expansion of the fiber and matrix, and compositional changes of the interface and fibers at high temperatures.

Because of the difference between the coefficients of thermal expansion (CTE) of the fiber and the matrix, the matrix contracts more than the fibers upon cooling from the composite processing temperature. This CTE mismatch causes an increasingly compressive radial stress to be applied to the fiber during cool-down. Calculations performed using a plane-strain, two-dimensional concentric cylinder model[11] (see **Appendix B: Modeling**) indicate that the residual radial compressive stress rises to approximately 53 MPa (7.7 ksi) at room temperature. As the composite is reheated to testing

temperatures, this stress is relieved and falls to approximately 6 MPa (0.87 ksi) at 1100°C (2012°F). The stronger fiber-matrix mechanical bond at lower temperatures may permit some cracks to propagate from the matrix directly through the interface and into the fiber. This type of crack propagation results in less fiber pull-out. A direct correlation between fiber pull-out and CTE mismatch between the fiber and matrix has also been seen by Deshmukh, *et al.*[12]

Studies have indicated that exposure to elevated temperatures alters the composition and properties of some fiber-matrix interfaces and affects the amount of fiber pull-out observed in tensile tests.[13,14] At temperatures above 800°C (1472°F), carbon formed at the fiber-matrix interface during processing is replaced by an amorphous silicate, SiO.[15] This silicate strengthens and embrittles the interfacial bond.[16] which results in less fiber pull-out in material tested at elevated temperatures. Luh and Evans reported that a lithium aluminosilicate glass reinforced with Nicalon® (SiC/LAS) exhibited lower fiber pull-out lengths with increasing temperature.[17,18] Stewart, *et al.*, also reported a reduction in the fibrous appearance of the fracture surface of an SiC/LAS composite tested at 900°C (1652°F) in flexure as compared with a similar test at room temperature.[19] However, this type of behavior was not observed in tensile tests conducted during this project on the SiC/CAS-II material.

A possible explanation for the pull-out behavior observed in the tensile tests conducted for this thesis rests on the high loading rate used (100 MPa/sec [14.5 ksi/sec]). This loading rate may have reduced the length of time for which cracks in the composite were open to permit exposure of the fibers to the oxidizing test atmosphere. Such a limit in exposure time may account for the apparent dominance of the CTE mismatch effect over environmentally-governed compositional changes influencing the interfacial strength. Thus, the

material tested at 1100°C (2012°F) was less affected by a strong and embrittled interface than it was by reduced radial compressive stresses between the matrix and fiber. The strength gained by the interface due to exposure to elevated temperatures was offset by the reduction in radial compressive stresses on the fiber. Thus, in greater amounts of fiber pull-out occurred at the higher testing temperature.

## Creep Behavior

A limited number of creep tests were conducted in parallel with the tensile, isothermal, and thermomechanical tests outlined in the previous chapter. Tests performed at 1100°C (2012°F) at the University of Michigan's Ceramic Composites Research Laboratory revealed steady-state creep rates for the unidirectional SiC/CAS-II material of $4.4 \times 10^{-9}$/sec at 70 MPa (10.2 ksi) and $2.1 \times 10^{-8}$/sec at 120 MPa (17.4 ksi).[20]

There is a lack of literature addressing creep properties of the matrix material. However, a single creep test performed by Corning on a material similar to SiC/CAS-II at 1300°C (2372°F) and 5 MPa (725 psi) indicated a creep rate of $3.3 \times 10^{-7}$/sec.[21]

Simon and Bunsell conducted creep tests on two types of Nicalon® fibers.[22] One type, NLM-102, is similar to the NLM-202 Nicalon® fiber used in the SiC/CAS-II composite. They are both microcrystalline, an attribute contributing to the creep resistance of the fiber, according to the authors. The creep threshold stress for this fiber at 1100°C (2012°F) was reported as 600 MPa [87 ksi]). Estimated fiber stresses (see the section entitled **States of Stress in Fiber and Matrix**) are well below this stress level, suggesting that creep exhibited by the SiC/CAS-II material is due primarily to the creep behavior of the matrix material.

Average creep rates for isothermal and thermomechanical fatigue tests conducted for this thesis are discussed in the section entitled **Damage** and are included in Table 4-1 which summarizes the creep data discussed previously.

**Table 4-1. Selected Creep Rates for Nicalon®, CAS, and SiC/CAS-II $[0]_{16}$**

| Material | Test Condition | Effective $\sigma_{max}$ | Creep Rate |
|---|---|---|---|
| Nicalon® | creep 1100°C (2012°F) | ≤ 600 MPa (≤ 87 ksi) | negligible |
| CAS-like glass-ceramic | creep 1300°C (2372°F) | 5 MPa (0.725 ksi) | $3.3 \times 10^{-7}$/sec |
| SiC/CAS-II | creep 1100°C (2012°F) | 70 MPa (10.2 ksi) | $4.4 \times 10^{-9}$/sec |
| SiC/CAS-II | creep 1100°C (2012°F) | 120 MPa (17.4 ksi) | $2.1 \times 10^{-8}$/sec |
| SiC/CAS-II | isothermal fatigue, no hold 1100°C (2012°F) | 55 MPa (7.8 ksi) | $9.0 \times 10^{-9}$/sec |
| SiC/CAS-II | isothermal fatigue, 60-sec hold at $\sigma_{max}$ 1100°C (2012°F) | 70 MPa (10.2 ksi) | $7.0 \times 10^{-9}$/sec |
| SiC/CAS-II | TMF, no hold 500 - 1100°C (932 - 2012°F) | 55 MPa (7.8 ksi) | $2.0 \times 10^{-8}$/sec |
| SiC/CAS-II | TMF, 60-sec hold at $\sigma_{max}$ 500 - 1100°C (932 - 2012°F) | 70 MPa (10.2 ksi) | $2.0 \times 10^{-8}$/sec |

## Isothermal Fatigue Behavior

Figures 4-3 and 4-4 illustrate the typical cyclic strain response of unidirectional SiC/CAS-II under isothermal fatigue conditions at 1100°C (2012°F). Figure 4-3 shows the response of the material to a triangular

waveform. Figure 4-4 shows the response of the material to a waveform with identical ramp rates but with a superimposed 60-second hold at $\sigma_{max}$. The plots

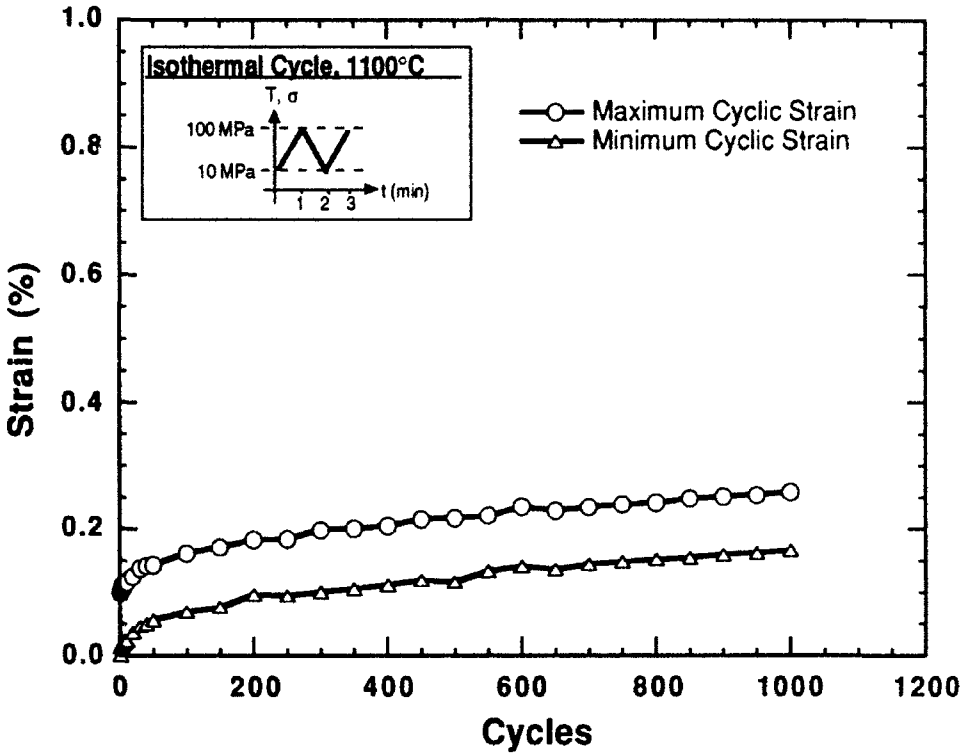


**Figure 4-3.** Cyclic strain response of $[0]_{16}$ SiC/CAS-II to an isothermal fatigue profile. $\sigma_{max}$ = 100 MPa (14.5 ksi), R = 0.1

show the minimum and maximum strains attained during cycles subjecting the specimens to a stress range of 10 to 100 MPa (1.45 to 14.5 ksi). Strains shown are expressed with respect to the initial state of the material at the beginning of each test (10 MPa at 1100°C). Therefore, Figures 4-3 and 4-4 illustrate the mechanical strain response of the material.

A slight difference was observed between the maximum attained strains for the two types of isothermal fatigue tests performed. Material subjected to the waveform including the 60-second hold time exhibited a maximum attained

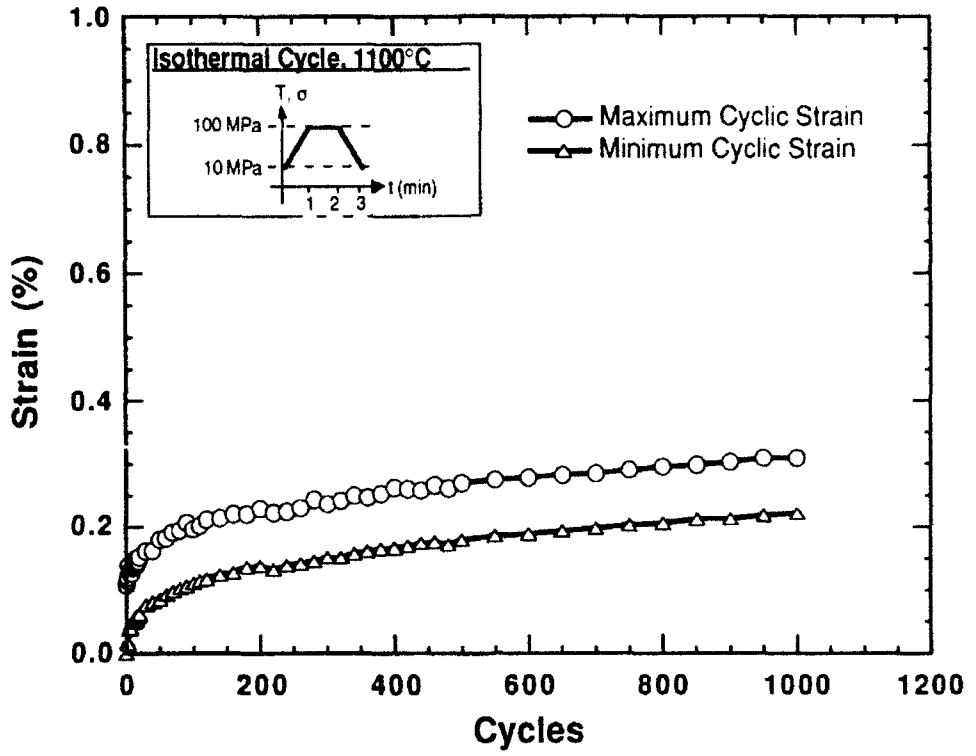


**Figure 4-4.** Cyclic strain response of $[0]_{16}$ SiC/CAS-II to an isothermal fatigue profile with a 60-sec hold at $\sigma_{max}$. $\sigma_{max}$ = 100 MPa (14.5 ksi), R = 0.1

strain of nearly 0.3 percent, but the material subjected to the profile not containing the hold time attained a maximum strain of 0.25 percent. A slight variation between the response of the composite to the two isothermal fatigue profiles may also be observed in the shape of the initial portions of the curves shown in Figures 4-3 and 4-4. The material subjected to the waveform including the 60-second hold time exhibited a more rapid increase in accumulated strain than did the material subjected to the triangular waveform. This behavior suggests an additional accumulation of creep-induced strain due to the hold time in the early phases of the isothermal fatigue tests including the hold time.

Although the hysteresis loops acquired from the isothermal tests were affected by problems which prevented the determination of exact numerical modulus values (see the section entitled **Hysteresis Loops**), no gross modulus changes were observed in these tests. Tension-tension fatigue testing performed by Prewo, *et al.*, on SiC/LAS,[23] Holmes, *et al.*, on SiC/$Si_3N_4$,[24] Zawada, *et al.*, on SiC/Aluminosilicate,[25] and Butkus, *et al.*, on SiC/CAS,[26] have all shown that material modulus is affected very little, if at all, by maximum stress values lower than the proportional limit stress presumably because of a low level of fiber damage occurring at these stress levels. (However, some recent work has observed fatigue failures occurring in CMCs at very high (~3 x $10^6$) cycle counts at low stress levels.[27]) Recalling that the maximum fatigue stress level for these tests was 100 MPa (14.5 ksi) and that the proportional limit stress is 250 MPa (36.3 ksi), the observed lack of a modulus drop is to be expected. Based on the relatively constant behavior of the modulus throughout the isothermal tests, we may attribute the strain accumulation seen in Figures 4-3 and 4-4 to the accumulation of creep strains.

## Thermomechanical Fatigue Behavior

Figures 4-5 and 4-6 illustrate the typical total cyclic strain response of the SiC/CAS-II composite to thermomechanical fatigue testing. Figure 4-5 depicts the response of the material to an in-phase triangular waveform. Figure 4-6 shows the response of the material to a waveform including a 60-second hold at $\sigma_{max}$ and $T_{max}$. Figures 4-7 and 4-8 show the same responses with the exception that the strain values have been corrected to remove thermal strains. As with the isothermal fatigue figures, strains shown in Figures 4-5 and 4-6 are expressed with respect to the initial state of the material at the beginning of each test (10 MPa at 500°C). Therefore, the

maximum strains in Figures 4-5 and 4-6 illustrate the sum of the mechanical and thermal strain response of the material. The strains in Figures 4-7 and 4-8, in contrast, show only the composite's mechanical strain response.

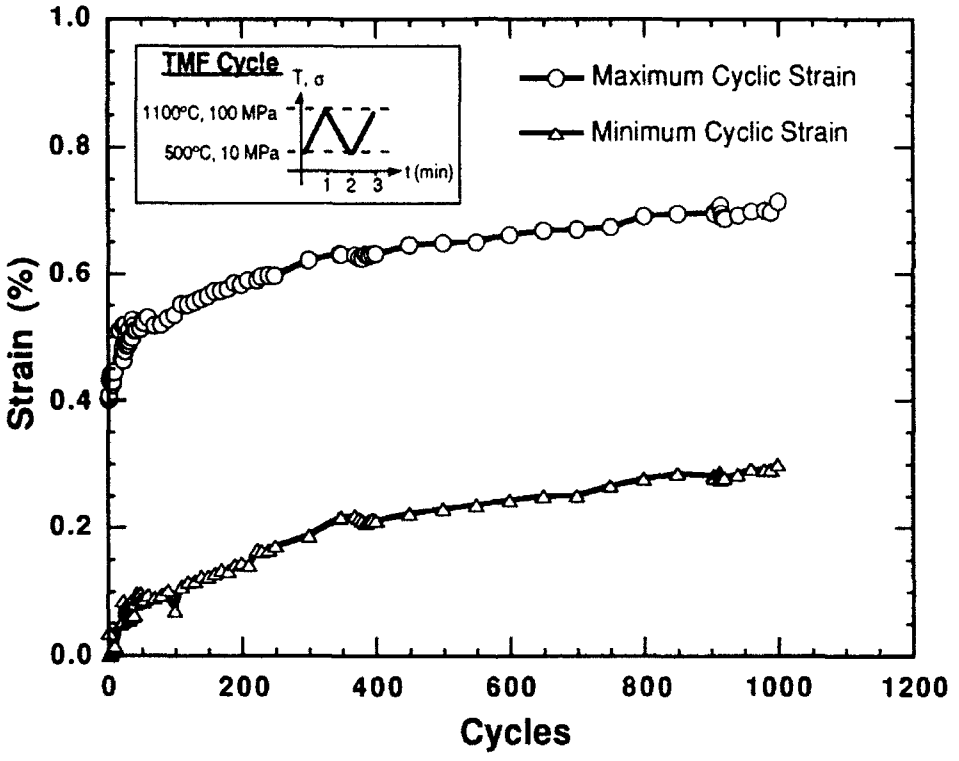


**Figure 4-5.** Cyclic strain response of $[0]_{16}$ SiC/CAS-II to a thermomechanical fatigue profile. $\sigma_{max}$ = 100 MPa (14.5 ksi), R = 0.1, $T_{range}$ = 500-1100°C.

Trends analogous to those exhibited by the isothermal fatigue response of this material are evident in the depicted responses to the two TMF profiles. Under TMF conditions, however, the effect of the superimposed hold time is much more dramatic. Initial strain accumulation in the material subjected to the hold time profile appeared to occur at a slightly faster rate than in the material subjected to the triangular TMF profile. As in the isothermal fatigue tests, the addition of a hold time to the triangular profile generated a higher level of strain

accumulation. A behavior unseen in the isothermal fatigue tests is what appears to be a saturation of strain accumulation in the response of the composite subjected to the TMF profile including the 60-second hold time. This may be caused by the load being carried primarily by the fibers. These effects may become more pronounced in tests performed with higher maximum stresses, stress ratios, and hold times.

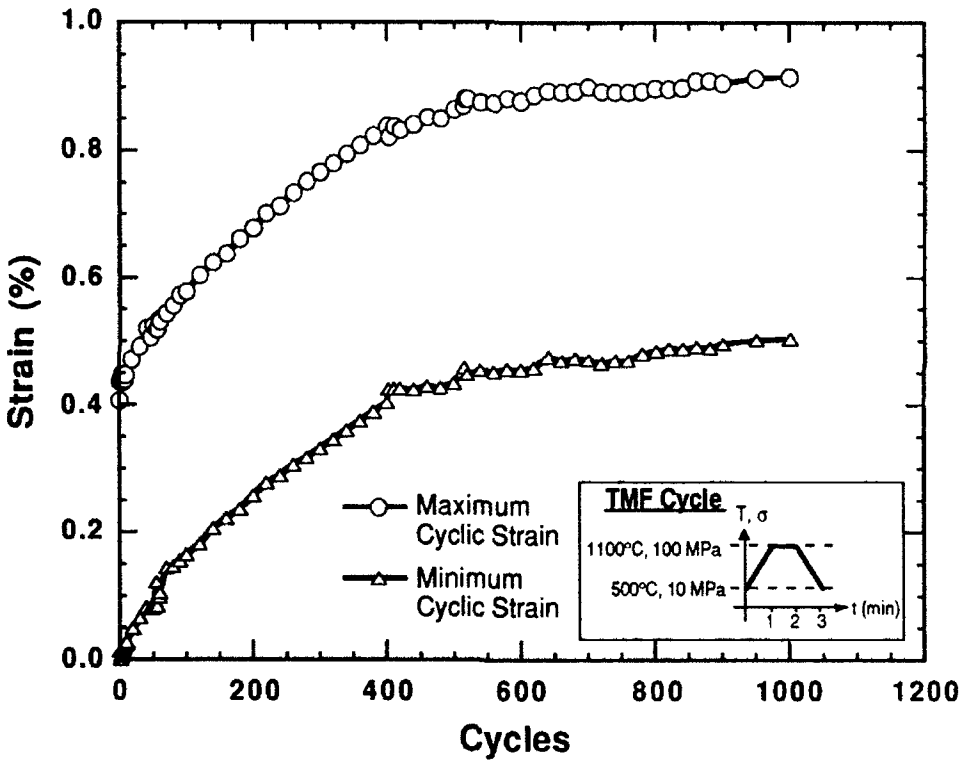


**Figure 4-6.** Cyclic strain response of $[0]_{16}$ SiC/CAS-II to a thermomechanical fatigue profile with a 60-sec hold at $\sigma_{max}$. $\sigma_{max}$ = 100 MPa (14.5 ksi), R = 0.1, $T_{range}$ = 500-1100°C.

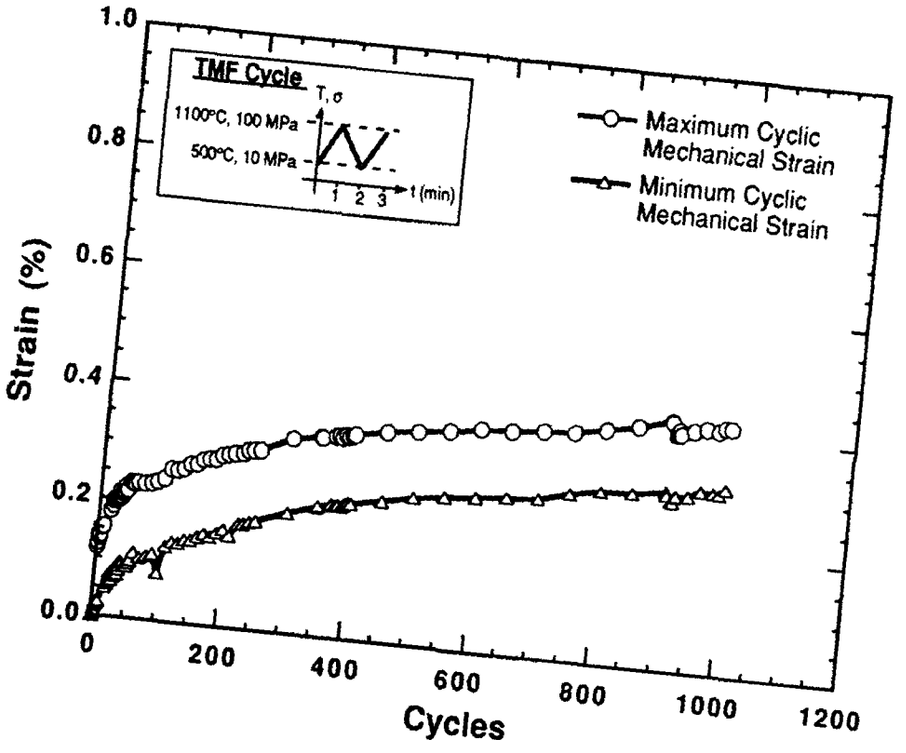


**Figure 4-7.** Cyclic mechanical strain response of $[0]_{16}$ SiC/CAS-II to the same thermomechanical fatigue profile depicted in Figure 4-5. $\sigma_{max}$ = 100 MPa (14.5 ksi), R = 0.1, $T_{range}$ = 500-1100°C.

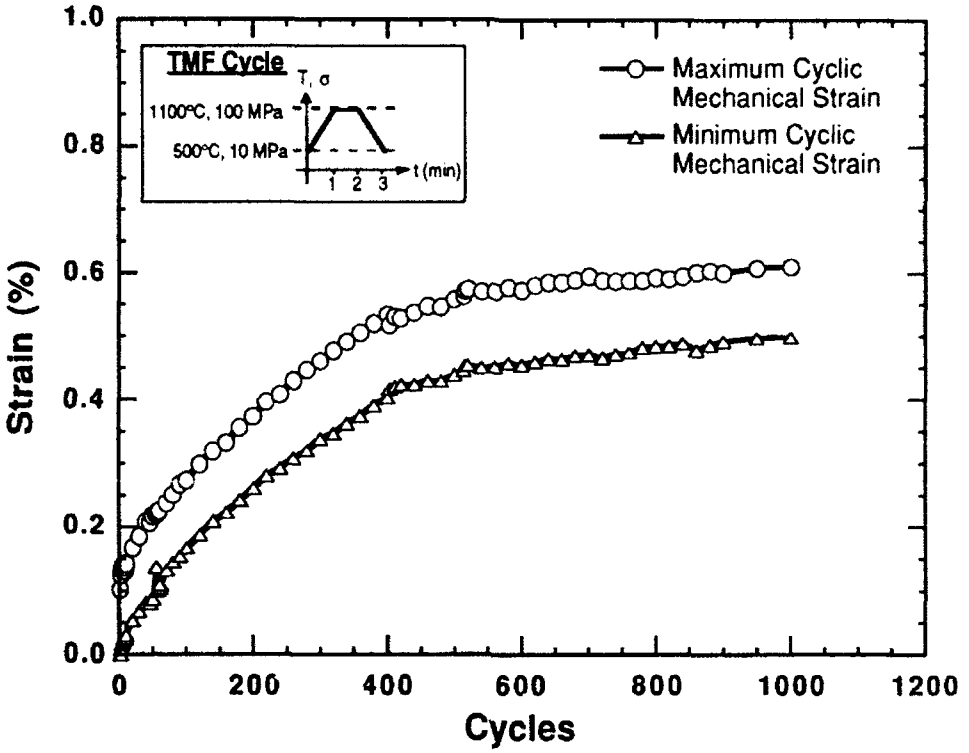


**Figure 4-8.** Cyclic mechanical strain response of $[0]_{16}$ SiC/CAS-II to the same thermomechanical fatigue profile depicted in Figure 4-6. $\sigma_{max}$ = 100 MPa (14.5 ksi), R = 0.1, $T_{range}$ = 500-1100°C, 60-sec hold at $\sigma_{max}$.

Hysteresis loops from the TMF tests were plagued by the same problems as were those from the isothermal tests (see the section entitled **Hysteresis Loops**). However, like the moduli observed in the isothermal fatigue tests, the average TMF modulus values, estimated using the minimum and maximum cyclic stresses, did not appear to change drastically during the course of a test. The increased rate and amount of strain accumulation in TMF tests including a hold time and the lack of modulus change during TMF tests suggest that strain accumulation may be used as a damage indicator for these thermomechanical tests. Also, as with the isothermal fatigue tests, matrix creep

appears to be a primary damage mechanism These premises are supported by the same factors used in analyzing the isothermal fatigue tests: the maximum axial fiber stress is lower than the creep threshold stress for Nicalon®, a low axial matrix stress, the relatively constant modulus behavior during strain accumulation, and evidence of creep in the SIC/CAS-II material at 1100°C (2012°F) and at a stress level as low as 70 MPa (10.2 ksi).

## Post-Fatigue Tensile Behavior

Immediately following the completion of 1000 cycles of isothermal or thermomechanical fatigue testing, specimens were tested in tension at 1100°C (2012°F) and 100 MPa/sec (14.5 ksi/sec) to investigate residual strength and stiffness levels. These tests were severely affected by difficulties in obtaining failures within the 25.4-mm (1.0-in.) extensometer gage section. This problem affected the acquisition of correct strains at failure, but initial modulus values and ultimate strengths were obtained.

Figures 4-9 and 4-10 show the average levels of initial modulus and ultimate strength values for all tensile tests performed as a part of this project.

Average residual modulus values for specimens tested under isothermal fatigue conditions ranged from 105 GPa (15.2 Msi) for those subjected to the triangular waveform to 112 GPa (16.2 Msi) for those subjected to the waveform including the hold time. For TMF tests, the average residual modulus values varied from 104 GPa (15.1 Msi) for material subjected to the triangular TMF profile to 112 GPa (16.2 Msi) for that subjected to the TMF profile including the hold time. These modulus values are, on the average, approximately 16 percent below modulus values obtained in room and elevated temperature tensile tests of as-received composite material. Reasons for this drop in modulus may rest on possible debonding and loss of interfacial shear strength

which occurred during fatigue testing. However, these modulus values do not appear to serve

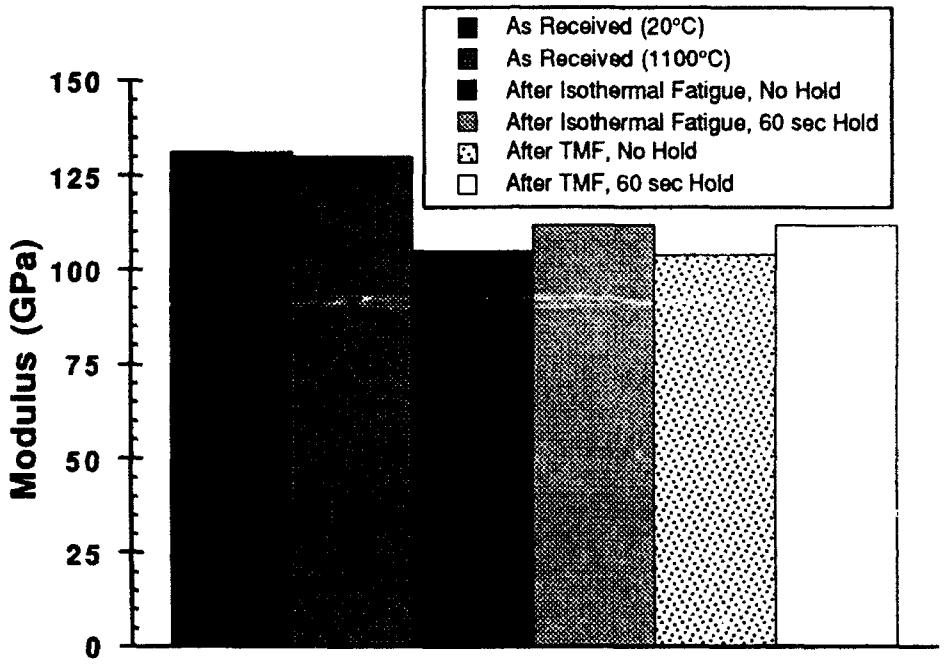


**Figure 4-9.** Residual modulus values for $[0]_{16}$ SiC/CAS-II subjected to various tensile, isothermal fatigue, and thermomechanical fatigue conditions.

as distinguishing characteristics among the final states of the material tested under the four fatigue conditions.

Average residual strengths of the composite material tested under isothermal fatigue conditions varied from 343 MPa (49.7 ksi) for material subjected to the isothermal profile without a hold time to 308 MPa (44.7 ksi) for that subjected to the isothermal waveform with a hold time. Residual tensile

tests on specimens subjected to TMF tests indicated average strengths ranging from 364 MPa (52.8 ksi) for those subjected to the no-hold profile to 319 MPa

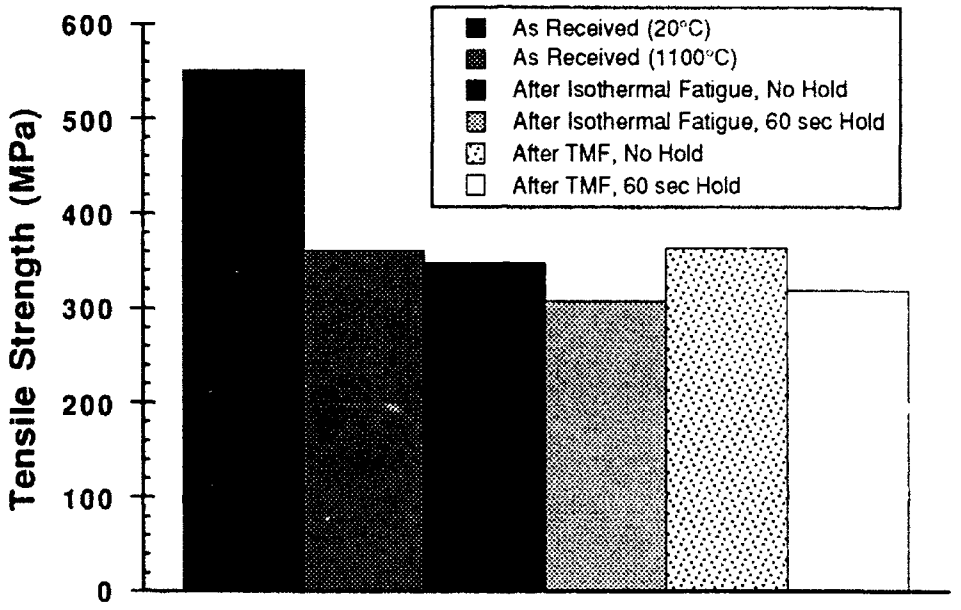


**Figure 4-10.** Residual tensile strength values for $[0]_{16}$ SiC/CAS-II subjected to various tensile, isothermal fatigue, and thermomechanical fatigue conditions.

(46.3 ksi) for those subjected to the profile including the hold time. These average residual strength values range from from 0 to 15 percent lower than 1100°C (2012°F) strength value of the SiC/CAS-II composite. This reduction in residual strength versus the room and elevated temperature tensile strengths can be attributed to the difference in the residual stress states at the beginning of each of these tests. For the room temperature tensile test, the fibers were in compression; for the elevated temperature tests, they were a

near-zero stress state, but for the residual tensile tests, the fibers were in tension. This tensile stress state in the fibers was due to the fact that during the fatigue tests, the matrix slowly shed load until it became nearly stress free. Upon unloading, the matrix was placed into compression and the fibers into tension. This residual tensile stress state in the fibers played the major role in reducing the residual tensile strength of this material. However, such a small difference in residual strength values implies that residual strength is not a sensitive indicator of accumulated fatigue damage.

## Microscopy

A limited amount of optical and SEM microscopy was performed on the tested samples. With the exception of the fiber pull-out differences mentioned in the section covering the tensile tests, no distinguishing fracture characteristics were seen in the specimens.

## Hysteresis Loops

Previous research of the fatigue of ceramic matrix composites has used hysteresis loops as a means of explaining damage accumulation during the course of a test. Fatigue of ceramic composites above the proportional limit stress is accompanied by hysteresis, an effect noted by Prewo,[28] Holmes,[29] Rousseau,[30] Shuler,[31] and others. Marshall and Oliver,[32] McMeeking and Evans,[33] and Thouless[34] have all addressed the concept of hysteresis from a material toughness and mechanics standpoint. Their approaches analyze the differences in the stress states at the fiber-matrix interface and within the fiber during a load-unload cycle of a composite.

Hysteresis loop analysis is a powerful tool for assessing the damage initiation and accumulation in a fatigued ceramic matrix composite. However,

this project will not make extensive use of such a technique. This section explains the lack of hysteresis analysis and discusses problems encountered in this project and the use of this technique in future research endeavors.

Hysteresis loops were acquired using the MATE data acquisition system. However, two problems prevented these loops from being thoroughly analyzed. First, electronic noise, as mentioned in **Chapter III: Experimental Procedure**, combined with the extreme sensitivity of the extensometer made hysteresis loops difficult to analyze. The "noisy" strain signals acquired and the small strains exhibited by the material resulted in ragged hysteresis loops, a problem especially evident for the isothermal fatigue tests (Figure 4-11). It is expected that the true stress-strain hysteresis

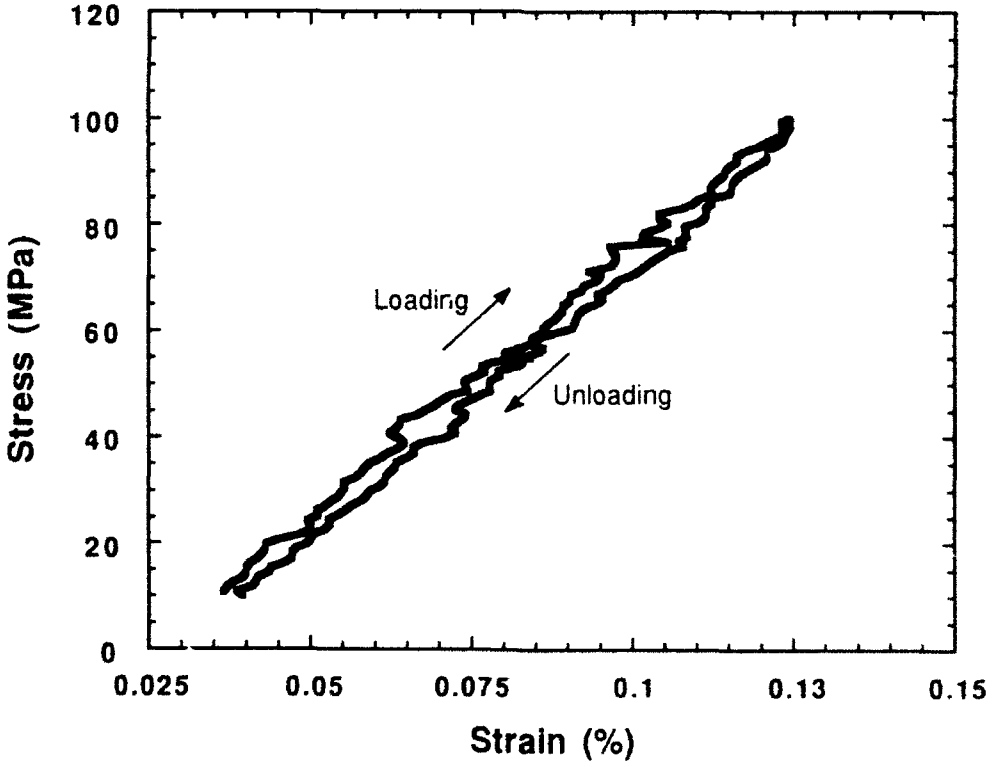


**Figure 4-11.** Typical hysteresis loop from an isothermal fatigue test.

behavior of Figure 4-11 is a closed or nearly closed, linear "loop," because the maximum fatigue stress is less than the proportional limit stress. It can also be argued that the relative differences between loops can be used to gage the effects of an increasing number of cycles on modulus and damage accumulation. However, an accurate analysis of these loops and determination of true numerical modulus values is not possible because of the acquired noise signal.

Second, one value of hysteresis loop analysis is to determine the modulus of the material at any cycle during a fatigue test. However, during a thermomechanical fatigue test, the material is subjected to a time-dependent temperature profile. If the modulus of the material is temperature-dependent, then an analysis as described above rests on the ability to draw meaningful comparisons between the moduli obtained from the hysteresis loops and the known temperature-dependent modulus of the material. Although the SiC/CAS-II material does not appear to exhibit a temperature-dependent modulus at the stress rates used in the tensile tests conducted in this project, it is postulated that the modulus is temperature-dependent at the slower loading rates used in the fatigue tests. This sensitivity to temperature may permit the effects of creep behavior to become more prevalent. Therefore, the analysis of the modulus values obtained during a thermomechanical fatigue test rests upon the knowledge of the modulus of the material at several temperatures and loading rates, knowledge which is not presently available.

A far greater problem exists with the acquired hysteresis loops from thermomechanical fatigue tests. This problem is one which can best be described by the term "reverse hysteresis" shown in Figure 4-12.

When plotted on axes having stress as the abscissa and strain as the ordinate, the unloading portion of the loop falls to the left of the loading portion,

i.e. the hysteresis loop proceeds counterclockwise during the course of a single cycle. This phenomenon is physically impossible! Reverse hysteresis implies the generation of energy and thus cannot be a function of the material but rather must be an artifact of the test procedures used. The following paragraphs offer some explanations about this observed phenomenon.

Although programmed to follow identical profiles, the load and temperature were always slightly unsynchronized during thermomechanical fatigue tests. This ever-present phase shift between the load and temperature is one reason for the observed reverse hysteresis. A temperature profile which leads the load profile slightly has a higher temperature than desired during loading and a lower temperature than desired upon unloading. This difference

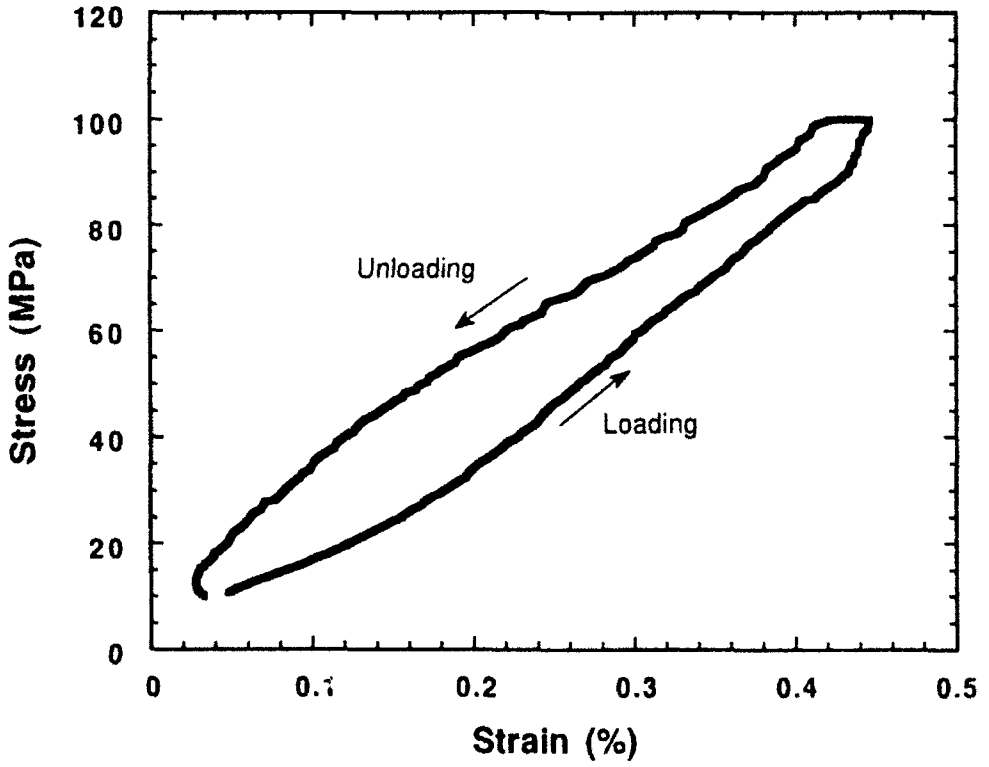


**Figure 4-12.** Typical hysteresis loop from a thermomechanical fatigue test showing "reverse hysteresis" phenomenon.

results in a higher temperature for a given load level on the loading ramp than on the unloading ramp. Since the modulus is believed to be temperature-dependent, this temperature difference results in a lower modulus on the loading ramp than on the unloading ramp at a given load level. Because of the difference in modulus at identical loading levels, a higher strain is attained at a given load level during loading than during unloading. This forces the loading leg of the hysteresis loop to be to the right of the unloading leg when plotted on a stress vs. strain set of axes, and results in reverse hysteresis.

Investigation of this proposed correlation revealed that the width of a hysteresis loop appears to increase as the phase shift between the temperature and the load becomes more positive (i.e., as the temperature "leads" the load). However, reverse hysteresis is present even with near zero and slightly negative phase shifts between the load and temperature. This behavior suggests a second contributing factor, temperature measurement. The use of ceramic cement to provide more intimate contact between thermocouples and the specimen may lead to slightly erroneous temperature readings because of the difference in the thermal conductivity and emissivity of the cement. If the cement heats slower and cools faster than the composite, the true temperature of the composite may lead the load even if the temperature acquired from the thermocouples is in-phase with the load. This explanation accounts for the presence of reverse hysteresis with a near zero or slightly negative phase-shift between the load and the temperature acquired from the thermocouple readings.

Another type of hysteresis behavior was observed when the material was subjected to a purely thermal cycle. A plot of temperature versus strain for this case also revealed reverse hysteresis. Noise in the strain signal caused by the increasing and decreasing lamp power may be the reason for this

behavior which suggests that a phase shift does not appear to be the only factor affecting the hysteresis behavior of this material.

Hysteresis analysis of future thermomechanical fatigue tests will depend on solving the problems of noise, temperature-dependent modulus, temperature measurement, and the possibility of "reverse" hysteresis. The impact of these factors complicating hysteresis analysis may be reduced if the effects of imperfect thermomechanical cycles on material behavior and the time/temperature-dependency of the material behavior can be better understood.

## States of Stress in Fiber and Matrix

Two models were employed to determine the states of stress in the fiber and matrix. The first and simplest, is a one-dimensional uniaxial model, often termed the "Rule of Mixtures" approach. The second is an elastic, axisymmetric generalized plane-strain model, often referred to as a "concentric cylinder" or "two-dimensional," model. **Appendix B: Modeling** contains a more detailed explanation of these models.

Linear elasticity was assumed in both models. Creep effects were not included. Because of this, their use is limited to determining the states of residual stress present in the composite constituent materials after processing and in estimating stress levels during testing. A further limitation of the uniaxial model is its ability to predict only axial stresses in the fiber and matrix. The axisymmetric model can be used to predict axial, radial, and circumferential stresses in the composite constituents. Both models account for applied mechanical stresses as well as thermally induced stresses. The axisymmetric model assumes a hexagonal fiber packing arrangement.

Sørensen, *et al.*, have investigated the effect of other fiber packing patterns on the residual stress state of SiC/LAS and SiC/CAS composites.[35]

Table 4-2 shows the various stress states for the fiber and matrix under specific temperature and loading conditions.

Axial stresses predicted by the models differed significantly (see Table 4-2). Axial fiber stresses predicted by the uniaxial model averaged 27 percent greater than those predicted by the axisymmetric model. Axial stresses in the matrix predicted by the uniaxial model averaged 17 percent lower than those predicted by the axisymmetric model.

As discussed previously in this chapter, the CTE mismatch between the fiber and matrix resulted in a compressive residual stress state in the fiber and a tensile residual stress state in the matrix at room temperature (Table 4-2). Furthermore, the compressive stress state in the fiber is radial and circumferential as well as axial. This suggests an increase in fiber-matrix interfacial strength with a decrease in temperature from the processing temperature.

Stresses in the fiber and matrix were also computed for the test cycles used in this project. Figures 4-13 through 4-16 show the fiber and matrix axial stress states for the isothermal and thermomechanical profiles predicted by the axisymmetric model. Note that the axial stresses are all in-phase. Because of the increase in accumulated strain and postulated creep effects over the course of the tests, the predicted stress states portrayed in Figures 4-13 through 4-16 are valid only during the initial portion of each test when linear elasticity may still be assumed to exist. Later portions of each fatigue test appear to be affected by matrix creep. Nevertheless, the models do offer valuable clues about the relative stress levels within the composite constituents.

In the isothermal tests, the fibers sustained an axial stress amplitude nearly twice as great as the matrix. Radial and circumferential stresses and stress amplitudes in the fiber and matrix were relatively lower.

The thermomechanical fatigue tests subjected the fiber to a nearly fully-reversed stress profile resulting in a stress amplitude over 750 percent greater than that sustained by the matrix. Inspection of Table 4-2 shows that the circumferential and radial stresses were greater than in the isothermal tests. In addition, the circumferential stresses on the matrix were out-of-phase with the applied stresses.

**Table 4-2. Fiber and Matrix Stress States**

| | | UNIAXIAL MODEL | | AXISYMMETRIC MODEL | | | | | |
|---|---|---|---|---|---|---|---|---|---|
| Temp. (°C) | $\sigma_{applied}$ (MPa) [ksi] | $\sigma_{fz}$ (MPa) [ksi] | $\sigma_{mz}$ (MPa) [ksi] | $\sigma_{fz}$ (MPa) [ksi] | $\sigma_{fr}$ (MPa) [ksi] | $\sigma_{f\theta}$ (MPa) [ksi] | $\sigma_{mz}$ (MPa) [ksi] | $\sigma_{mr}$ [a] (MPa) [ksi] | $\sigma_{m\theta}$ [a] (MPa) [ksi] |
| 20 | 0 | -104.0 [-15.1] | 69.6 [10.1] | -129.0 [-18.7] | -52.7 [-7.6] | -52.7 [-7.6] | 86.1 [12.5] | -52.7 [-7.6] | 123.0 [17.8] |
| 500 | 0 | -64.0 [-9.3] | 42.7 [6.2] | -79.1 [-11.5] | -32.3 [-4.68] | -32.3 [-4.68] | 52.8 [7.7] | -32.3 [-4.68] | 75.4 [10.9] |
| 500 | 10 [1.45] | -49.8 [-7.2] | 49.9 [7.2] | -65.0 [-9.4] | -32.5 [-4.7] | -32.5 [-4.7] | 60.0 [8.7] | -32.5 [-4.7] | 75.7 [11.0] |
| 1100 | 0 | -11.9 [-1.7] | 7.9 [11.5] | -14.7 [-2.1] | -6.1 [-0.9] | -6.1 [-0.9] | 9.8 [1.4] | -6.1 [-0.9] | 14.2 [2.1] |
| 1100 | 10 [1.45] | 2.0 [0.3] | 15.3 [2.2] | -0.9 [-0.13] | -6.2 [-0.9] | -6.2 [-0.9] | 17.3 [2.5] | -6.2 [-0.9] | 14.6 [2.1] |
| 1100 | 100 [14.5] | 126.8 [18.4] | 82.1 [11.9] | 123.0 [17.8] | -7.6 [-1.1] | -7.6 [-1.1] | 84.5 [12.2] | -7.6 [-1.1] | 17.8 [2.6] |

[a] measured at fiber-matrix interface

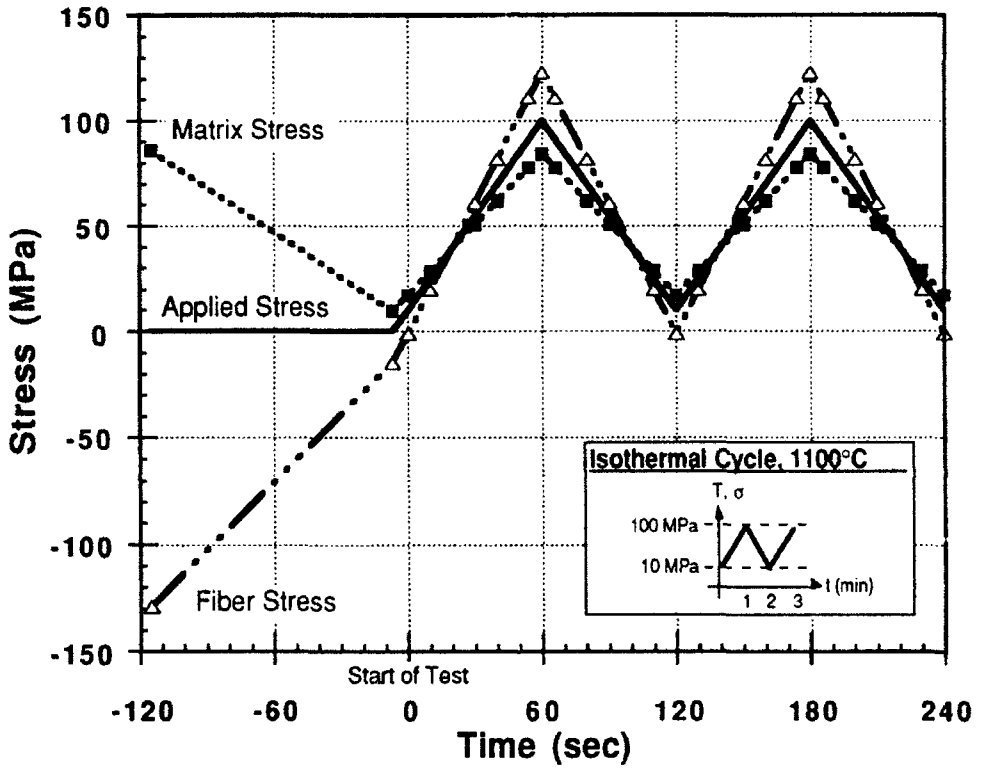


**Figure 4-13.** Axial stress states in the fiber and matrix plotted with applied stress for an isothermal fatigue cycle. $\sigma_{max}$ = 100 MPa (14.5 ksi), R = 0.1

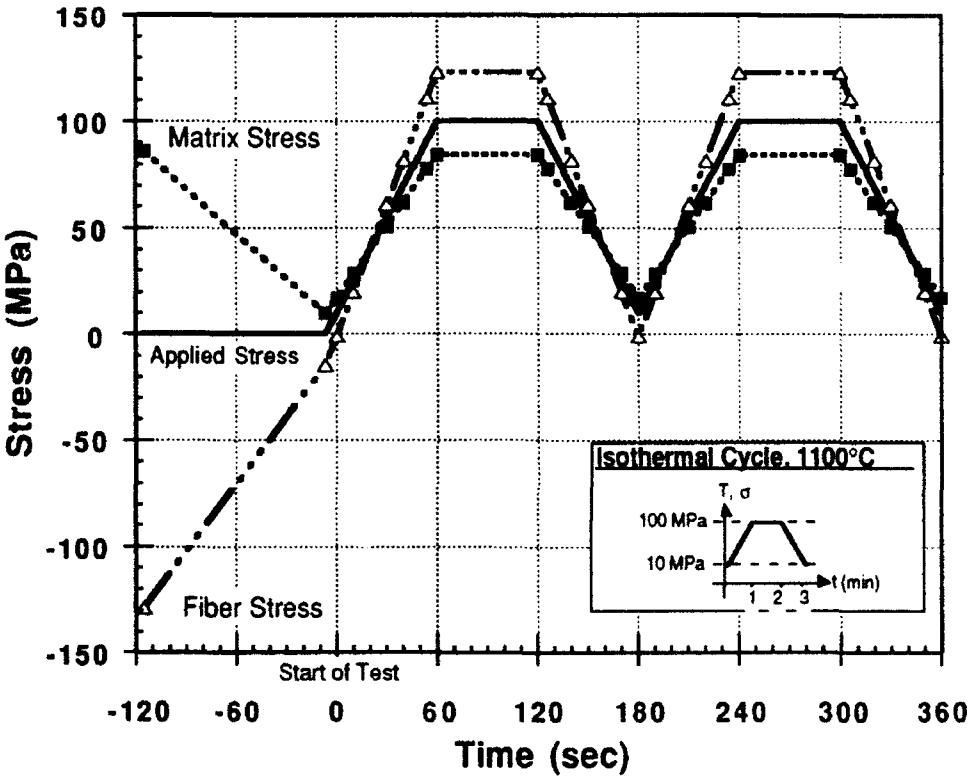


**Figure 4-14.** Axial stress states in the fiber and matrix plotted with applied stress for an isothermal fatigue cycle including a 60-sec hold at $\sigma_{max}$.
$\sigma_{max}$ = 100 MPa (14.5 ksi), R = 0.1

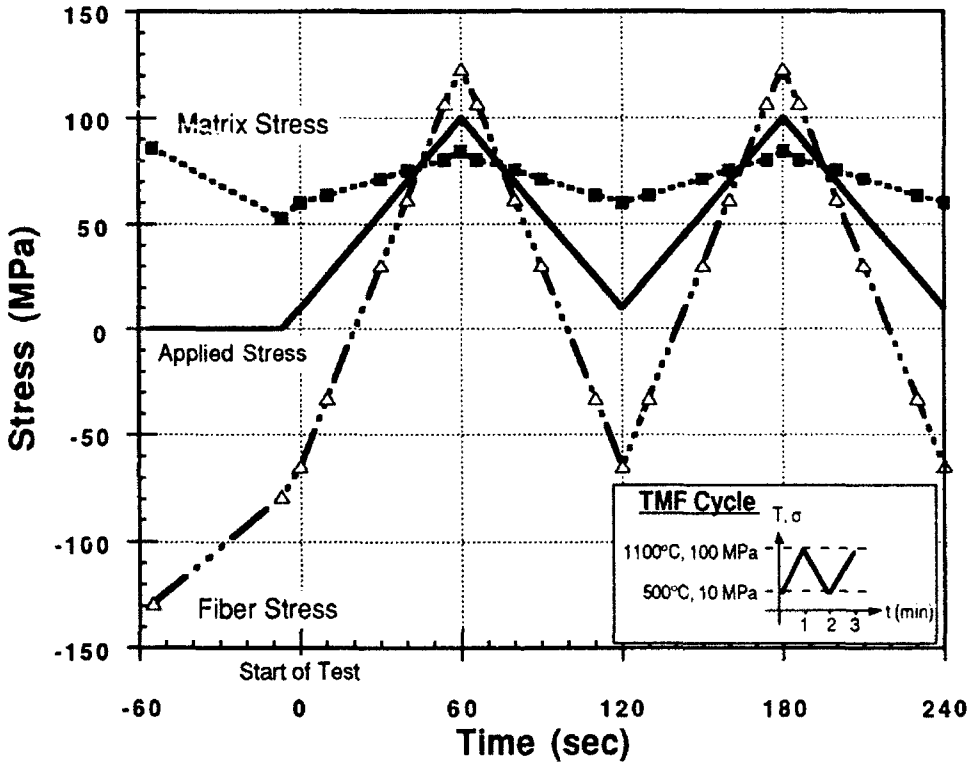


**Figure 4-15.** Axial stress states in the fiber and matrix plotted with applied stress for a thermomechanical fatigue cycle. $\sigma_{max}$ = 100 MPa (14.5 ksi), R = 0.1, $T_{range}$ = 500-1100°C.

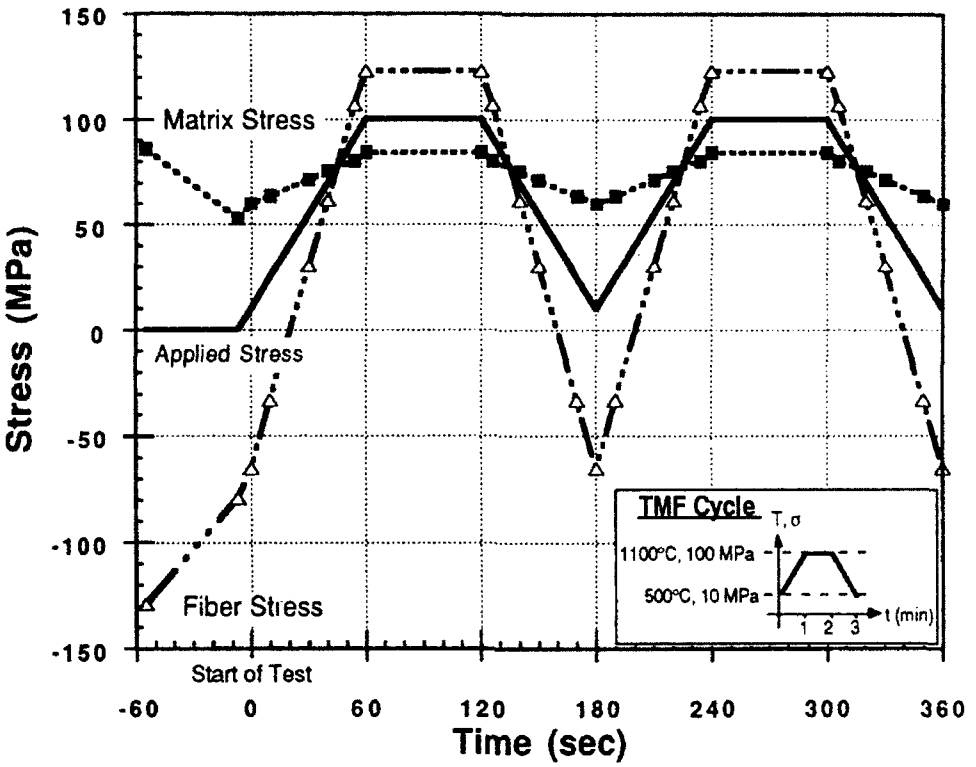


**Figure 4-16.** Axial stress states in the fiber and matrix plotted with applied stress for a thermomechanical fatigue cycle including a 60-sec hold at $\sigma_{max}$. $\sigma_{max}$ = 100 MPa (14.5 ksi), R = 0.1, $T_{range}$ = 500-1100°C.

As mentioned in the previous sections covering the isothermal and thermomechanical fatigue tests, the magnitude of the axial stresses in the fibers, though far greater than that in the matrix, was still relatively low compared to the threshold creep stress reported by Simon and Bunsell.

## Damage

Damage assessment can be defined as the observation of the degradation of a specific mechanical property of a material throughout the course of a test. For research in the field of ceramic matrix composites, such a property may be strength, strain, crack spacing, modulus, or some other

parameter. For fatigue testing, it is often beneficial to choose a property which can be analyzed during a test such as modulus or crack spacing rather than one which requires a post-fatigue evaluation such as residual strength or residual modulus. This project explored the use of modulus, residual modulus, residual strength, and accumulated strain as possible damage indicators for the tests conducted.

Original plans called for the use of acetate replicas to determine changes in crack spacing during isothermal and thermomechanical fatigue testing. However, these plans were abandoned in order to avoid numerous instances when the minimum test temperature was reduced to room temperature.

The problems relating to the use of modulus measurements acquired during the course of testing have been previously discussed in the section entitled **Hysteresis Loops**. One possible technique of using hysteresis loops to analyze real-time modulus values, regardless of the level of electronic noise or degree of "reverseness" present in the loops, is the cycle-to-cycle comparison of "effective modulus" values (Figure 4-17). Such values are simply the relative slopes of the hysteresis loops as determined from the point of minimum stress, minimum strain and the point of maximum stress, maximum strain. The use of this method with thermomechanical fatigue hysteresis loops cannot provide a modulus value comparable to one obtained during an isothermal test because of the dependence of modulus on temperature and loading rate. Nor can it be used, in the case of this project, to compare numerical modulus values from isothermal fatigue tests to those from tensile tests because of the differences in loading rates. However, this proposed technique can show the relative cyclic degradation of an "effective modulus." If the "effective modulus" is used as an indicator of damage (as modulus is used

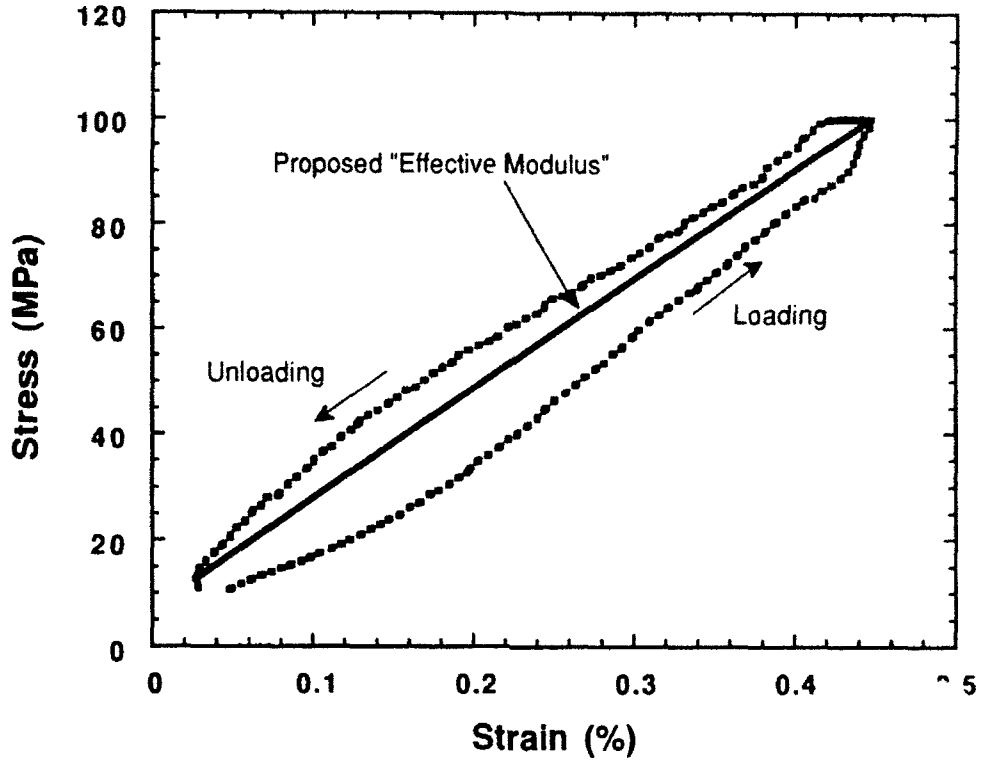


**Figure 4-17.** Diagram of proposed "Effective Modulus" method of analysis for acquired hysteresis loops.

during conventional fatigue testing), this knowledge can be used to gage the level of damage occurring within the composite during the course of an isothermal or thermomechanical fatigue test.

Use of the "effective modulus" technique on the hysteresis loops acquired during isothermal and thermomechanical fatigue tests in this project revealed no appreciable degradation during the course of the tests (i.e., no reduction in the relative slope of the stress-strain hysteresis loops was observed). The lack of an observed reduction in slope suggests that no gross changes in modulus occurred during isothermal and thermomechanical fatigue tests. This, in turn, leads to the conclusion that little or no fiber breakage

occurred and that the major contributor to the material behavior was matrix creep. A stress analysis of the fiber supports this by indicating that the maximum axial fiber stress (approximately 123 MPa [17.8 ksi]) is far below the ultimate tensile strength of the fiber at 1100°C (approximately 1400 MPa [203 ksi]).[36]

A second parameter used for evaluating the state of damage of CMCs subjected to fatigue was the residual modulus. Residual modulus values of specimens subjected to isothermal and thermomechanical fatigue were obtained during post-fatigue tensile tests and have been reported in the section entitled **Post-Fatigue Tensile Behavior**. Post-fatigue modulus values were lower than those for the unfatigued material tested in tension but did not show a clear distinguishing trend among the four types of fatigue investigated in this project.

Residual strength values suggest a different trend. The specimens tested in isothermal and thermomechanical fatigue exhibited residual strengths lower than the ultimate strengths of those subjected only to the tensile tests. Residual strengths of specimens subjected to fatigue profiles including the hold time were lower than for those subjected to the triangular isothermal and thermomechanical fatigue profiles. However, the residual strengths of the specimens subjected to TMF were slightly higher than for those subjected to isothermal fatigue.

Overall, it appears that the residual tensile tests conducted for this thesis were insensitive to the damage caused in the specimens by the particular test parameters used. A change in the test parameters such as higher stress levels, different stress ratios, or different temperatures may result in damage which residual tensile tests would more easily identify.

Accumulated strain was also investigated as a damage indicator. Accumulated strains in the TMF tests were greater than for those in the isothermal fatigue tests. Furthermore, strain accumulated slightly more rapidly in the specimens subjected to the fatigue profiles containing a hold time. The amount of strain accumulation also increased with the addition of the hold time.

With respect to all parameters discussed as possible damage indicators (modulus, residual modulus, residual strength, and accumulated strain) differences in their utility will change with changes in maximum fatigue stresses, stress ratios, loading rates, and temperatures. For example, at maximum fatigue stresses above the proportional limit modulus may be used as a damage indicator because of the expected, measurable cyclic deterioration of such a parameter. However, for the test conditions examined for this thesis, strain accumulation appears to be the parameter most applicable to indicating damage initiation and progression.

The lower values of residual strength and modulus for the specimens subjected to isothermal and thermomechanical fatigue tests indicate that damage was indeed caused by these conditions. To distinguish between the levels of damage caused by these tests, it appears better to use strain accumulation as an indicator rather than the "effective modulus" because of the relative lack of change of the latter during fatigue testing.

The increase in accumulated strain with the increased hold time at $\sigma_{max}$ suggests that creep is a dominant damage mechanism. Creep data are sparse for the composite and matrix material, but it can be postulated that the strain accumulation observed, and the damage inferred from its observation, can be attributed primarily to creep of the matrix material. Factors suggesting such speculation are outlined in the following paragraphs.

First, the maximum axial stress in the fiber is far lower than the creep threshold stress for Nicalon®. Even if the matrix carried no load, the axial fiber stress would be 250 MPa (36.3 ksi), still below the 600 MPa (87 ksi) required for fiber creep at 1100°C (2012°F).

Second, the axial matrix stress is also relatively low. If the fibers carried no load (an unlikely situation), the matrix stress would rise to only 167 MPa (24.2 ksi) at the point of maximum fatigue stress.

Third, creep has been observed in this composite at 1100°C (2012°F) at a stress as low as 70 MPa (10.2 ksi).

Fourth, the relatively constant behavior of the modulus throughout the fatigue tests suggests that the strain accumulations observed are the result of creep strains.

Finally, average creep rates for the isothermal and thermomechanical fatigue tests can be calculated by dividing the average cyclic strain accumulated in the "steady-state" region (cycles 100 to 1000) by the time occurring during these cycles (900 cycles x [120 or 180] sec/cycle = [1.08 or 1.62] x $10^5$ sec). The average creep rate is approximately 9 x $10^{-9}$/sec for the isothermal case with no hold time and 7 x $10^{-9}$/sec for the isothermal case including the hold time. The average creep rate for both forms of the the thermomechanical fatigue tests is approximately 2 x $10^{-8}$/sec. To further define the average creep rates, a time-weighted average of the fatigue stress can be calculated for both types of fatigue test profiles. For profiles including the holdtime, this time-weighted average stress is 70 MPa (10.2 ksi), and for those not including the hold time, it is 55 MPa (7.8 ksi). Though not exact, these calculated creep rates are of the same order of magnitude as those seen in actual creep tests. Apparent discrepancies between these average calculated

creep rates and those determined from actual creep tests may be attributed to cyclic effects such as matrix cracking, fiber damage, and interfacial debonding.

The use of accumulated strain as a damage indicator and the postulation that the majority of damage is caused by matrix creep agrees with an intuitive approach to expected damage levels for the four types of fatigue tests conducted. One would expect that the amount of creep experienced and resulting level of damage produced would increase with the additions of hold times and thermal cycles to an isothermal fatigue profile. Examination of the strain accumulation confirm this intuition with higher accumulated strains occurring in tests using profiles including hold times and in thermomechanical fatigue test. The relative amount of creep and damage expected (and shown if strain accumulation can be used as an indicator) increases in the following order: isothermal fatigue - no hold time; isothermal fatigue - with hold time; thermomechanical fatigue - no hold time; thermomechanical fatigue - with hold time.

## Final Condition of the Specimens

The overall surface appearance of the specimens following testing is worthy of note. The surfaces of specimens tested in tension appeared unaffected by the test temperature, even following approximately 20 minutes at temperature. However, specimens subjected to isothermal and thermomechanical fatigue experienced some localized softening and melting of the glass-ceramic surface (Figure 4-18). Evidence of matrix softening was also found upon examination by the SEM (Figure 4-19). It is believed that the long-term exposure (33.3 hours for triangular profiles, 50 hours for profiles including the 60-second hold time) is a primary cause of this effect on the composite. Specimens subjected to thermomechanical fatigue tests had an


**Figure 4-18.** *Surface of a specimen thermomechanical fatigue profile with a* 60-sec hold at $\sigma_{max}$. The bubbly appearance indicates possible localized melting. White areas are residual cement used to affix thermocouples. 12.5X


**Figure 4-19.** SEM photomicrograph showing evidence of localized softening or melting of the glass-ceramic matrix. From a specimen subjected to a thermomechanical fatigue profile including a 60-sec hold at $\sigma_{max}$. Mag: 400X

additional possible cause in the radiant energy surges of the lamps required to heat the specimens according to the rigorous temperature profiles required by these tests. No evidence was found to indicate that these areas of matrix damage were initiation sights for failure. Indeed, the majority of failures occurred away from these typically centrally located areas.

The fracture paths of the specimens can be generally described as angular. That is, a failure appeared to proceed across each specimen at an angle rather than along a plane perpendicular to the loading direction. In some instances, the fracture path ran in and out of the specimen and/or extensometer gage sections. No pattern was discernable among the failures other than this angularity and the previously mentioned fiber pull-out differences between room temperature and elevated temperature tension tests.

Finally, as stated previously, failures of the specimens within the gage section of the extensometer were uncommon. Eleven specimens were tested to failure in this project. Three experienced failures outside of the 33-mm (1.3-in.) specimen gage length. Six exhibited failures which were partially contained in the specimen gage length. Only two failed between the rods of the extensometer within its 25.4-mm (1.0-in) gage length. See **Appendix C: Summary of Test Results** for specific details.

## References — **CHAPTER IV: RESULTS AND DISCUSSION**


1 Corning Data Sheet, 1991. Note: Corning's tests were conducted in displacement-control at $8.47 \times 10^{-3}$mm/sec (0.2 in/min).

2 Wang, S-W and Parvizi-Majidi, A., "Mechanical Behavior of Nicalon Fiber Reinforced Calcium Aluminosilicate Matrix Composites," *Ceramic Engineering and Science Proceedings*, American Ceramic Society, Westerville, OH, **11**, [9-10], January 1989, pg. 1608.

3 Rigdon, M.A. and Hong, W.S., "Comparison of High-Temperature Testing Results of Ceramic Fibers," in Thermal and Mechanical Behavior of Metal Matrix and Ceramic Matrix Composites, ASTM STP 1080, Kennedy, J.M., Moeller, H.H., and Johnson, W.S., eds. American Society for Testing and Materials, Philadelphia, PA, 1990, pp. 136-151.

4 Pysher, D.J., Goretta, K.C., Hodder, R.S. Jr., and Tressler, R.E., "Strengths of Ceramic Fibers at Elevated Temperatures," *Journal of the American Ceramic Society*, American Ceramic Society, Westerville, OH, **72**, [2], 1989, pp. 284-288.

5 Personal communication with Ron Stewart, Corning Glass Works, 16 October 1991.

6 Rousseau, C.Q., "Monotonic and Cyclic Behavior of a Silicon Carbide/Calcium-Aluminosilicate Ceramic Composite," in Thermal and Mechanical Behavior of Metal Matrix and Ceramic Matrix Composites, ASTM STP 1080, Kennedy, J.M., Moeller, H.H., and Johnson, W.S., eds. American Society for Testing and Materials, Philadelphia, PA, 1990, pg. 138.

7 Rousseau, C.Q., *ibid.*, pg. 140..

8 Wang and Parvizi-Majidi, *op. cit.*

9 Rigdon and Hong, *op. cit.*

10 Pysher, *et al.*, *op. cit.*

11 "CoaxCyl5E," developed by Dr. Thomas Hahn, Naval Research Laboratory, Washington, D.C. Modified by Demirkan Coker, The University of Dayton Research Laboratory, Dayton, OH.

12 Deshmukh, U.V., Kanei, A., Freiman, S.W., and Cranmer, D.C., "Effect of Thermal Expansion Mismatch on Fiber Pull-out in Glass Matrix Composites," in High Temperature/High Performance Composites: Materials Research Society Symposium Proceedings, Vol. 120, Lemkey, F.D., Fishman, S.G., Evans, A.G., and Strife, J.R., eds., Materials Research Society, Pittsburgh, PA, 1988, pp. 253-258.

13 Thouless, M.D., Sbaizero, O., Sigl, L.S., and Evans, A.G., "Effect of Interface Mechanical Properties on Pullout in a SiC-Fiber-Reinforced Lithium Aluminum Silicate Glass-Ceramic," *Journal of the American Ceramic Society*, American Ceramic Society, Westerville, OH, **72**, [4], 1989, pp. 525-532.

14 Bischoff, E., Rühle, M., Sbaizero, O., and Evans, A.G., "Microstructural Studies of the Interfacial Zone of a SiC-Fiber-Reinforced Lithium Aluminum Silicate Glass-Ceramic," *Journal of the American Ceramic Society*, American Ceramic Society, Westerville, OH, **72**, [5], 1989, pp. 741-745.

15 Greil, P., "Thermodynamic Calculations of Si-C-O Fiber Stability in Ceramic Matrix Composites," *Journal of the European Ceramic Society*, Elsevier Science Publishers, Ltd., England, **6**, [1], 1990, pg. 56.

16 Mah, T., Mendriatta, M.G., Katz, A.P., and Mazdiyasni, K.S., "Recent Developments in Fiber-Reinforced High Temperature Ceramic Composites," *American Ceramic Society Bulletin*, American Ceramic Society, Westerville, OH, **66**, [2], 1987, pp. 304-308.

17 Luh, E.Y., and Evans, A.G., "High Temperature Failure of a SiC Fiber-Reinforced Lithium Aluminosilicate Glass Ceramic," *Ceramic Engineering and Science Proceedings*, American Ceramic Society, Westerville, OH, **6**, [7-8], 1984, pp. 608-611.

18 Luh, E.Y., and Evans, A.G., "High Temperature Properties of a Ceramic Matrix Composite," *Journal of the American Ceramic Society*, American Ceramic Society, Westerville, OH, **70**, [7], 1987, pg. 469.

19 Stewart, R.L., Chyung, K., Taylor, M.P., and Cooper, R.F., "Fracture of SiC Fiber/Glass-Ceramic Composites as a Function of Temperature," in Fracture Mechanics of Ceramics, Vol. 7: Composites, Impact Statistics and High-Temperature Phenomena, Bradt, R.C., Evans, A.G., Hasselman, D.P.H., and Lange, F.F., eds., Plenum Publishing Corp., New York, NY, 1985, pg. 41.

20 Holmes, J.W., and Jones, J.W., University of Michigan, Unpublished Data.

21 Personal communication with Ron Stewart, Corning Glass Works, 2 October 1991.

22 Simon, G. and Bunsell A.R., "Mechanical and Structural Characterization of the Nicalon Silicon Carbide Fibre," *Journal of Materials Science*, Chapman & Hall, Ltd., London, England, **19**, [11], 1984, pp. 3649-3657.

23 Prewo, K.M., Johnson, B., and Starrett, S., "Silicon Carbide Fiber-Reinforced Glass Ceramic Composite Tensile Behavior at Elevated Temperature," *Journal of Materials Science*, Chapman & Hall, Ltd., London, England, **24**, 1989, pp. 1373-1379.

24 Holmes, J.W., Kotil, T., and Foulds, W.T., "High Temperature Fatigue of SiC Fiber Reinforced Si3N4 Ceramic Composites," in Symposium on High Temperature Composites, American Society for Composites, Technomic Publishing Co., Lancaster, PA, 1989, pp. 176-186.

25 Zawada, L. P., Butkus, L.M., and Hartman, G.A., "Room Temperature Tensile and Fatigue Properties of Silicon Carbide Fiber-Reinforced Aluminosilicate Glass," *Journal of the American Ceramic Society*, American Ceramic Society, Westerville, OH, **74**, [11], 1991, pp. 2851-2858.

26 Butkus, L.M., Zawada, L.P., and Hartman, G.A., "Room Temperature Tensile and Fatigue Behavior of Silicon Carbide Fiber-Reinforced Ceramic Matrix Composites," presented at *AeroMat '90*, ASM International, Long Beach, CA, May 1990.

27 Holmes, J.W., unpublished data.

28 Prewo, Karl. M., "Fatigue and Stress Rupture of Silicon Carbide Fibre-Reinforced Glass-Ceramics," *Journal of Materials Science*, Chapman & Hall, Ltd., London, England, **22**, 1987, pp. 2695-2701.

[29] Holmes, *et al., ibid.*

[30] Rousseau, *ibid.*

[31] Shuler, S.F., "Influence of Frequency on the Room Temperature Fatigue of a Carbon-Fiber SiC Matrix Composite," Master's Thesis, University of Michigan, Ann Arbor, MI, 1991.

[32] Marshall, D.B., and Oliver, W.C., "Measurement of Interfacial Properties in Fiber-Reinforced Ceramic Composites," *The Journal of the American Ceramic Society*, American Ceramic Society, Westerville, OH, **70**, [8], 1987, pg. 524.

[33] McMeeking, R.M., and Evans, A.G., "Matrix Fatigue Cracking in Fiber Composites," *Mechanics of Materials*, Elsevier Science Publishers, New York, NY, **9**, [3], November 1990, pp. 217-277.

[34] Thouless, M.D., "A Re-Examination of the Analysis of Toughening in Brittle Matrix Composites," *Acta Metallurgica Et Materialia*, Pergamon Press, Oxford, England, **37**, [9], 1989, pp. 2297-2304

[35] Sørensen, B.F., Talreja, R., and Sørensen, O.T., "Thermomechanical Fatigue of Ceramic Matrix Composites: Analysis of Mechanisms on a Microscale." ASME Symposium on Failure Mechanisms in High Temperature Composites: 112th Annual Winter Meeting, American Society of Mechanical Engineers, New York, NY, 1991.

[36] Rigdon and Hong, *ibid.*

# V: CONCLUSIONS AND RECOMMENDATIONS

This study has shown that the equipment and ability to conduct thermomechanical fatigue tests on ceramic matrix composites now exist. Though still requiring some modifications and improvements, test procedures and hardware are available to successfully evaluate the behavior of CMC systems under conditions simulating the aircraft gas turbine engine environment.

This project examined the behavior of a 16-ply unidirectional Nicalon®-reinforced calcium aluminosilicate glass-ceramic composite (SiC/CAS-II).

Tensile tests performed at a loading rate of 100 MPa/sec (14.5 ksi/sec) at room temperature and at 1100°C (2012°F) showed no differences between initial elastic modulus values. Increased fiber pull-out observed at the higher test temperature is believed to be the result of a reduction in thermally-induced interfacial stresses which are highest at room temperature.

Specimens were subjected to isothermal and thermomechanical fatigue profiles with and without hold times at $\sigma_{max}$ and $T_{max}$. The maximum fatigue stress was 100 MPa (14.5 ksi) with an R value of 0.1. This stress level was 40 percent of the proportional limit stress determined from tensile tests conducted on the material at 1100°C (2012°F). Temperatures used were 1100°C (2012°F) for the isothermal tests and 500-1100°C (932-2012°F) for the thermomechanical fatigue tests. All fatigue tests were carried out to 1000 cycles, corresponding to 33.3 hours for the tests without the hold time and 50 hours for the tests which included the superimposed 60-second hold time.

To find a parameter which could be used as a damage indicator, residual strength, residual modulus, modulus during the fatigue tests, and strain accumulation were examined.

For specimens subjected to isothermal and thermomechanical profiles, post-fatigue residual modulus values averaged 16 percent lower than modulus values of specimens tested in tension at room temperature and at 1100°C (2012°F). Residual strength values averaged 40 percent lower than the room temperature tensile strength and 10 percent lower than the elevated temperature tensile strength. Although indicating some degree of damage compared with the as-received state of the material, the residual strength and modulus values did not suggest a distinguishing trend between isothermal and thermomechanical fatigue tests or between those profiles including a hold time and those which did not.

Electronic noise and "reverse hysteresis" prohibited the determination of numerical values for modulus during the course of the fatigue tests. However, a comparison of the slopes of the hysteresis loops acquired during the fatigue tests did not indicate any gross cyclic degradation of "effective modulus." This behavior suggests the lack of any major fiber breakage during fatigue testing at these stress levels. Stress analyses of the state of stress in the fiber support this by indicating the presence of very low fiber stresses compared with their ultimate strengths.

The greatest difference in material behavior was in strain accumulation. Initial strain accumulation rates appeared slightly higher in tests containing a hold time. Also, the amount of strain accumulation was greater in thermomechanical fatigue tests than in isothermal fatigue tests.

It is postulated that the primary cause of damage in this material under the specified conditions is matrix creep. Creep has been observed in this material at 1100°C (2012°F), and calculated average creep rates for the fatigue tests conducted for this study are of the same order of magnitude. In

addition, stress analyses of the fiber and matrix indicate that the fibers never reach a stress state above their creep threshold stress.

The performance of the $[0]_{16}$ SiC/CAS-II material under the specific conditions investigated for this thesis was very good. Further testing should be performed to determine if the saturation level exhibited by the accumulated strain is truly indicative of a steady damage state at which components made from this material can be operated safely for long lives.

Results from the testing performed for this study and experience gained during its completion suggest several areas for further exploration.

With respect to the test system:

1) Electronic noise must be minimized through the use of filters, shielding, a higher resolution data acquisition system, or an increased rate of data collection for the small-strain behavior of CMCs to be accurately analyzed in future TMF tests. The MATE system is currently undergoing such improvements.
2) The feasibility of using cooling air during a thermomechanical fatigue test to create a more uniform temperature distribution within the gage section of a specimen and to allow for improved temperature control should be investigated.
3) A method for ensuring a correct relationship betweer stress and temperature (phase shift) should be developed. Modification to the existing MATE software is needed for this purpose and is currently underway at the University of Dayton Research Institute.
4) The use of noncontact strain and temperature measurement devices such as laser extensometers and optical pyrometers would be beneficial for future TMF tests.

5) An effort should be made to optimize grip temperatures, thermal gradients, and extensometer gage lengths to maximize the likelihood of obtaining gage section failures and of obtaining accurate strain-to-failure values.

With respect to future research:

1) Future research should expand the narrow test matrix used for this thesis to include, most immediately, different fatigue stress levels and temperatures, longer test durations, and multiple specimens at each tested condition. It is expected that tests conducted at stress levels above the proportional limit will result in greater losses in modulus and residual strength and modulus. Various ramp rates, stress ratios, and hold times could also be subjects of other research projects.
2) Ultimately, some form of "spectrum" thermomechanical fatigue profile should be developed for different types of turbine engine and structural applications. This program could be similar to the FALSTAFF and MINITWIST spectrum fatigue programs which simulate fighter and transport aircraft flight profiles and would aid greatly in the assessment of the feasibility of using CMCs in specific applications. At the very least, a more accurate estimation of the temperature/stress levels and durability expected of future CMC components is needed in order to avoid testing under arbitrarily determined conditions. Every effort should be made to conduct tests that will not only fulfill the need for scientific knowledge but also the need for practical, application-related data.

3) When multiple specimens can be subjected to identical isothermal and thermomechanical fatigue profiles, the use of acetate replicas, acoustic emission, or another method of determining crack generation may help in quantifying damage initiation and accumulation. It must be understood that methods which require excursions from temperature and/or stress profiles may affect the response of the specimens to those profiles. Testing multiple specimens with and without such examination methods will allow these effects to be quantified.

4) Testing conducted for this thesis indicated that a "steady state" in strain accumulation was reached by the thermomechanical fatigue tests. Future tests carried out for longer periods may confirm the existence of such a steady state for other stress levels and temperatures.

5) Additional information about the matrix and fibers is required in order to predict and analyze material behavior. Strength and modulus values and creep rates as functions of temperature and loading rate will assist future test programs.

6) It has been shown that modulus, residual modulus, and residual strength values could not be used to distinguish among the four types of fatigue tests conducted for this thesis. Strain accumulation could distinguish among the four types of fatigue tests, and the applicability of using it as a damage indicator for TMF experiments involving small strains merits further investigation.

7) Finally, the phenomenon of "reverse hysteresis" as it applies to the thermomechanical fatigue of CMCs requires explanation and, hence, further study.

## APPENDIX A: LESSONS LEARNED

This appendix is an informal guide to those conducting future thermomechanical fatigue tests on ceramic matrix composites. Temperature control posed the greatest problems, and therefore, receives the greatest attention in this section. These notes range in specificity from those covering testing in general to those pertaining particularly to the MATE system and servohydraulic machine located at the Materials Behavior Branch, Materials Directorate (WL/MLLN, Wright-Patterson AFB, OH, 45433-6533).

### Thermocouples and Temperature Measurement

K-type thermocouples proved inadequate for isothermal fatigue tests at 1100°C (2012°F) as well as for thermomechanical fatigue tests involving thermal cycling between 500°C (932°F) and 1100°C (2012°F). Physical breakdown (oxidation) caused them to become extremely brittle and to fail during a test. Metallurgical changes caused by heat treatment of the metal resulted in time-dependent readings. For instance, when compared against a recognized standard temperature measuring device, such as temperature sensitive paint, K-type thermocouples indicated the correct temperature upon initial exposure but indicated a higher than actual temperature after approximately 15 hours of exposure. K-type thermocouples were useful, however, for short duration tests such as monotonic tension tests at elevated temperatures.

S-type thermocouples worked very well. They were accurate over the entire test time-frame and rarely failed simply because of mechanical breakdown. The disadvantage to using S-type thermocouples is their cost.

When choosing a thermocouple type for testing at elevated temperatures, consult a catalog carefully. Charts stating the maximum use temperature for a specific type of thermocouple typically state a temperature which the thermocouple made from the largest diameter wire offered can survive for an undetermined but "short" time. Catalogs also contain charts outlining the maximum long duration use temperature for specific thermocouple types. Perhaps the safest path to take would be to speak directly with a technical representative and ask what type of thermocouple is recommended for the test parameters one desires to use.

Temperature sensitive paint is an excellent way to confirm achieved temperatures. This paint is accurately formulated to melt or change colors at a specific temperature and provides a good way to check the temperature indicated by thermocouples, pyrometers, and temperature controllers.

One course of action to ensure accurate temperature readings over a given length of time is to subject a "dummy" sample, instrumented, say, with K- and S-type thermocouples, to test conditions identical those which will be used in an actual test matrix. Use the more reliable S-type thermocouples to control. Monitor both types throughout this "dummy" test and check periodically against temperature sensitive paint. Choose the thermocouple type which is most accurate over the time period you wish to run.

In this project, the thermocouples were attached using wire tie-downs which were wrapped around the specimen and one lead of the thermocouple wire. Care must be taken to avoid contacting both leads with the tie-down. This would create an effective junction at a point other than the bead and would result in erroneous temperature readings. Ceramic cement was used to protect and attach each thermocouple bead and its wire tie-down to the specimen. Application of this cement must be done with care to ensure

enough is applied to last throughout a test but to avoid "shielding" the specimen with an overly thick coating.

Optical pyrometers should be investigated. The advantage that they offer as a noncontact way of measuring temperature is valuable considering that each extra thermocouple or amount of ceramic cement added to a specimen theoretically changes its response to a given set of load or thermal inputs. The characteristics of the ceramic cement used for this thesis is suspected of contributing to the problem of reverse hysteresis.

## Cooling Air On Specimens

Some consideration was given to using air jets to induce a flow across the test specimen which, it has been speculated, may provide a more uniform temperature distribution along a specimen. Use of cooling air may also permit improved temperature control by forcing the heating lamps to draw power during cool down cycles. (In the tests for this program, the lamps often went to zero power during cool-down, forcing cooling to occur by uncontrolled conduction and convection.) However, a great disadvantage to using air cooling is the risk of generating a nonuniform airflow through the heated section which may induce cool spots and, in fact, cause a detrimental thermal gradient. Cooling air should not be required for isothermal tests. Further investigation of this issue is warranted, especially for use in thermal cycles containing rapid cooling ramps.

## Cooling Airflow Through Lamp Bodies

The flow of cooling air through the lamp bodies caused fluctuations in the way in which a specimen responded to lamp heating. This airflow was controlled by an adjustable valve which, in theory, should be able allow for

identical cooling air flows for each identical test. In fact, this was rarely possible. Cooling air required adjustment for every test and, in the event of slight fluctuations in air line pressure, even during the course of some tests.

## Bulbs

Periodic checking is important. A bulb should be replaced if the interior filament sags or if the inside of the bulb glass is hazy/smoky. This cannot totally prevent bulb failures from occurring during the course of a test, but it may help to minimize the number that do fail. Bulbs tended to last approximately 4000 cycles (500-1100°C) or 250+ hours at isothermal conditions (1100°C). Outputs sometime reached over 85 percent on the ramp to temperature.

## Temperature Ramp Rates

It is the opinion of this author that the thermomechanical fatigue cycle used in this project was very severe. Temperature ramp rates of 500 to 1100°C in 60 sec, or 10°C/sec, proved to be harsh on the material as well as on the equipment. Consideration should be given to using slower temperature ramp rates in future tests which use this test system.

Temperature ramps for the start-up portions of the tests were set to have the same ramp rate as that seen in the thermomechanical fatigue tests (10°C/sec). Loading ramps followed this same protocol.

## Control Settings on the Barber-Colman Temperature Controllers

Different settings were used on the lamp pairs ("zones") closest to the ends of the specimens (Zones 1 and 2) than were used for those which heated the middle of the specimens (Zones 3 and 4). During a test these

control settings were often adjusted slightly to improve the performance of the lamps. Only the Proportional Band and Reset settings were adjusted. Rate and Load Line settings were left as calibrated.

Some suggested settings follow:

| | | |
|---|---|---|
| **Proportional Band:** | Isothermal | - Zones 1&2: 20 |
| | | - Zones 3&4: 30 |
| | TMF | - Zones 1&2: 15 to 30 |
| | | - Zones 3&4: 30 to 75 |
| **Reset:** | Isothermal | - Zones 1&2: 1 to 2 |
| | | - Zones 3&4: 2 to 4 |
| | TMF | - Zones 1&2: 0.8 to 2 |
| | | - Zones 3&4: 2 to 8 |

## Extensometer

Because the tests in this project were run at high temperatures, care was taken to ensure that the extensometers were adjusted so that they had enough travel to accommodate the large thermal+mechanical strains. When the extensometer was set to its prescribed gage length (25.4 mm) and calibrated at room temperature, the strain output voltage was set to a negative value using the strain "Zero" adjustment on the MTS 458.20 Microconsole. This permitted the sensitivity of the extensometer to be increased (through the use of a modified ±4 percent strain range card) without allowing the extensometer output to saturate at +10 volts before reaching its physical limit of travel.

When maintenance issues (bulb replacement, etc.) required that a test be brought to room temperature during a shutdown or hold, strain readings were taken after the specimen had stabilized at room temperature. This

procedure assisted in replacing the extensometer if it was touched or moved during the required repairs of the system.

Choose or modify an extensometer to match the gage length of the spcimen being tested in order to obtain correct strain to failure values.

## Electronic Noise

Noise greatly affected the strain readings during the isothermal and thermomechanical fatigue tests. Lamp operation, particularly during thermal cycling, appeared to generate noise from the SCR rectifiers. Three suggested areas to investigate are 1) the use of an improved shielding technique for the lamp power unit such as a grounded copper mesh cage, 2) better shielding for the extensometer system (extensometer, cable, strain range card, etc.), and 3) modifications to the data acquisition system such as better filtering or increased resolution (16 bit as opposed to the present 12 bit).

## Specimen Placement

Specimens were placed in the grips with the machine in stroke control. The machine was switched to load control only after the specimen was positioned correctly instrumented with thermocouples. Even small loads caused by leaning on the load cell could cause unwanted actuator movement.

## Test Start-Up

To be safe and consistent, the author attempted to set up each test using identical procedures and placements. Key areas addressed were:

1) Lamp position - each body approximately 5mm from specimen centerline

2) Lamp air-cooling amount - set to same point for every test

3) Control settings - see section above

If better temperature control was required, incremental changes were made to avoid inducing unstable behavior.

Vigilance is important, especially during the initial cycles following any start-up or on the first of a series of tests. Incorrect control settings, temperature ramps which are too rapid, and burned out lamps can quickly cause severe temperature control problems if allowed to occur unchecked.

A scenario of the last issue follows: A test is proceeding normally. All of the control settings are working well. A bulb burns out, and subsequently, the temperature in that zone drops. After the next data acquisition cycle, the program calls for more power for the zone with the burned out bulb. More power is given to that zone resulting in the remaining bulb receiving a great amount of power. The operator realizes what has happened, shuts down the test, replaces the bulb, and starts up again. Unfortunately, the zone in which the bulb was replaced is still receiving the same amount of power called for by the last data acquisition. This situation has the potential of driving the specimen temperature over the setpoint if the problem is not corrected quickly. Some suggested courses of action: 1) use the Barber-Colman to limit the power in the zone in which the bulb was replaced; 2) readjust control settings on this zone; 3) take data immediately upon start-up to force the program to realize that there is a new bulb installed which does not require as much power; 4) most importantly, try to prevent this situation from occurring by checking the heating system often.

## The Importance of Running "Dummy" Tests

When planning to perform tests similar to those described in this thesis, conduct sample or "dummy" tests on the material of interest and at the desired test conditions. These tests will assist in determining the many idiosyncrasies of the particular test system and in discovering the correct way to proceed with a test program.

# APPENDIX B: MODELING

Many techniques may be used to determine the stresses in the fiber and matrix of a composite. For this project, particular attention was given to determining the stresses in the individual constituents as the result of cool-down from processing temperatures, and those induced by the test cycles. Residual stresses were calculated for the composite in the as-received condition. These stresses are a result of the mismatch in the coefficients of thermal expansion of the fiber and the matrix. Stresses induced by the thermal and mechanical portions of the test cycles were also determined. All analyses were conducted under assumed linear elastic conditions.

Two models were used to determine the stresses in the fibers and matrix. The first and simplest, is a one-dimensional uniaxial model, often termed the "Rule of Mixtures" approach. The second is an elastic, axisymmetric generalized plane strain model. The following paragraphs describe the characteristics of each.

Before any model can be used, the following must be defined:

| | |
|---|---|
| $V_f$ | Fiber Volume Fraction |
| $V_m$ | Matrix Volume Fraction |
| $E_f(T)$ | Fiber Elastic Modulus (temperature dependent) |
| $E_m(T)$ | Matrix Elastic Modulus (temperature dependent) |
| $\nu_f$ | Fiber Poisson's ratio |
| $\nu_m$ | Matrix Poisson's ratio |
| $\alpha_f$ | Fiber Coefficient of Thermal Expansion |
| $\alpha_m$ | Matrix Coefficient of Thermal Expansion |
| $\sigma_{applied}$ | Applied (Mechanical) Stress |
| $\Delta T$ | Temperature Difference, $\Delta T = T - T_{processing}$ (For the SiC/CAS-II, Tprocessing = 1260°C (2300°F), the "strain point" temperature. See **Chapter III. Experimental Procedure** for details.) |

## Uniaxial "Rule of Mixtures" Model

The uniaxial model used here accounts only for axial stresses in the fiber and matrix. Boundary conditions used are strain compatibility (equal strains in the matrix and fiber) and force equilibrium (forces on the matrix and fiber sum to the applied axial force). In order to determine the axial stresses in the fiber and matrix, the principle of superposition is used to determine the individual stresses and strains resulting separately from applied mechanical and thermal loads.

The model is first used to find the matrix and fiber stresses resulting from a mechanical stress applied to the composite. The boundary condition stating that the force applied to the composite must equal the sum of the forces applied to the fiber and the matrix requires,

$$P_c = \sigma_f A_f + \sigma_m A_m \tag{1}$$

Dividing both sides of (1) by the composite cross-sectional area, $A_c$, yields

$$\frac{P_c}{A_c} = \frac{\sigma_f A_f}{A_c} + \frac{\sigma_m A_m}{A_c} \tag{2}$$

For any mechanical stress applied to the composite, (2) becomes

$$\sigma_{applied} = \sigma_f V_f + \sigma_m V_m \tag{3}$$

Using the stress-strain relations,

$$\sigma_f = e_f E_f \qquad (4) \qquad \text{and} \qquad \sigma_m = e_m E_m \qquad (5)$$

we can substitute (4) and (5) into (3) to obtain

$$\sigma_{applied} = eE_fV_f + eE_mV_m \qquad (6)$$

In (6), the single symbol, e, was used to denote strain. Because of the strain compatibility boundary condition which states that the composite, fiber, and matrix strains are equal we see,

$$e = e_c = e_f = e_m \qquad (7)$$

For a mechanical stress applied to the composite, we can solve (6) for the resulting strain, $e_{mechanical}$, as

$$e_{mechanical} = \frac{\sigma_{applied}}{E_fV_f + E_mV_m} \qquad (8)$$

From (8), we can also define the modulus of the composite as

$$E_c = \frac{\sigma_{applied}}{e} = E_fV_f + E_mV_m \qquad (9)$$

Renaming the stress variables in (4) and (5) to specify the mechanically-induced stresses on the fiber and the matrix we obtain

$$\sigma_{f,\,mechanical} = e_{mechanical}E_f \qquad (10)$$

$$\sigma_{m,\,mechanical} = e_{mechanical}E_m \qquad (11)$$

For determining the stresses and strains in the constituents due solely to a thermal variation, we must first calculate the coefficient of thermal expansion of the entire composite using the relation

$$\alpha_c = \left(\frac{1}{E_c}\right)(\alpha_f E_f V_f + \alpha_m E_m V_m) \tag{12}$$

Substituting (9) into (12) for $E_c$, we obtain

$$\alpha_c = \frac{\alpha_f E_f V_f + \alpha_m E_m V_m}{E_f V_f + E_m V_m} \tag{13}$$

To determine the thermally-induced strains in the fiber and matrix, as they are in the composite, we must first consider the strains of each constituent if subjected to the same $\Delta T$ by itself (i.e., when <u>not</u> in the composite). The thermal strains for the fiber and the matrix material subjected individually to a temperature change are given by

$$e^*_{f,\,thermal} = \alpha_f \Delta T \tag{14}$$

and

$$e^*_{m,\,thermal} = \alpha_m \Delta T \tag{15}$$

Also, we must realize that the composite, as a unit, experiences a different strain when exposed to the same $\Delta T$. This strain is expressed as

$$e_{c,\,thermal} = \alpha_c \Delta T \tag{16}$$

Now, to determine the strain in the fiber and the matrix *caused by their incorporation into the composite*, we must examine the difference between

what the strains in each constituent are if exposed separately to a $\Delta T$ and what they are when incorporated into a composite. The thermal strain in each constituent *within the composite*, designated as $e_{f,\ thermal}$ and $e_{m,\ thermal}$, is the difference between the composite strain, $e_{c,\ thermal}$, and the strains computed using (14) and (15)

$$e_{f,\ thermal} = \alpha_c \Delta T - \alpha_f \Delta T = (\alpha_c - \alpha_f)\Delta T \tag{17}$$

$$e_{m,\ thermal} = \alpha_c \Delta T - \alpha_m \Delta T = (\alpha_c - \alpha_m)\Delta T \tag{18}$$

Using superposition, we see that the total strain on each constituent in the composite is simply the sum of the strain occurring from an applied mechanical stress and that occurring from a temperature change. These total strains can be expressed as

$$e_{f,\ total} = e_{mechanical} + e_{f,\ thermal} = \left(\frac{\sigma_{applied}}{E_f V_f + E_m V_m}\right) + (\alpha_c - \alpha_f)\Delta T \tag{19}$$

$$e_{m,\ total} = e_{mechanical} + e_{m,\ thermal} = \left(\frac{\sigma_{applied}}{E_f V_f + E_m V_m}\right) + (\alpha_c - \alpha_m)\Delta T \tag{20}$$

Equations (19) and (20) can be combined with the stress-strain relations for the fiber and the matrix, (4) and (5), to yield expressions for the total axial stress in the fiber and the matrix shown below.

$$\sigma_{m,\ axial} = E_m e_{m,\ total} = (E_m)\left[\left(\frac{\sigma_{applied}}{E_f V_f + E_m V_m}\right) + (\alpha_c - \alpha_m)\Delta T\right] \tag{21}$$

$$\sigma_{f,\ axial} = E_f e_{f,\ total} = (E_f)\left[\left(\frac{\sigma_{applied}}{E_f V_f + E_m V_m}\right) + (\alpha_c - \alpha_f)\Delta T\right] \tag{22}$$

Equations (21) and (22) can be combined with (13) to yield a second form of these equations

$$\sigma_{f,\,axial} = \left(\frac{V_m E_f E_m}{E_f V_f + E_m V_m}\right)\left[(\alpha_m - \alpha_f)\Delta T + \frac{\sigma_{applied}}{E_m V_m}\right] \tag{23}$$

$$\sigma_{m,\,axial} = -\left(\frac{V_f E_f E_m}{E_f V_f + E_m V_m}\right)\left[(\alpha_m - \alpha_f)\Delta T - \frac{\sigma_{applied}}{E_f V_f}\right] \tag{24}$$

Note that $\Delta T$ is computed with the processing temperature as the reference temperature. For example, in computing the thermally induced stresses resulting from the cooling of SiC/CAS-II from it's processing "strain point" temperature of 1260°C to 20°C, $\Delta T$ = -1240°C.

## Two-Dimensional Model

An elastic, axisymmetric generalized plane strain model was also used to calculate the stresses in the fiber and matrix. This model is sometimes referred to as a "concentric cylinder," "coaxial cylinder," or "two-dimensional," model. The model is based upon the solution of an axisymmetric linear elastic problem.[1,2] A computerized version of this model, *CoaxCyl5E*, was used in this project to determine the thermally induced residual stresses in the fiber and matrix following the cooling of the composite from processing to room temperature. This program was developed by Dr. Thomas Hahn (formerly of the Naval Research Laboratory, presently at Penn State University) and modified by Demirkan Coker of the University of Dayton Research Institute. The program does not incorporate applied stresses, so the stresses for the

isothermal and thermomechanical fatigue profiles were computed using the equations outlined in the following paragraphs.

This model is based upon the following assumptions:

1) Behavior of the fiber and matrix elements are axially symmetric (no shear)
2) No slip at the interface
3) Constant temperature change throughout the material
4) Linear elastic behavior
5) Isotropic properties of the constituents
6) Composite is initially stress-free (during processing)
7) Plane sections remain plane
8) Radial stress and displacement continuity at the interface
9) Fibers are arranged in a hexagonal packing pattern

The following boundary conditions apply:

1) The radial stress at the edge of the element ($r = b$) is equal to the applied radial stress ($\sigma_{r,\ applied}$)
2) Axial and radial displacements at the interface are equal for the fiber and matrix
3) Radial stresses at the interface ($r = a$) are equal for the fiber and matrix
4) The sum of the loads on the fiber and matrix is equivalent to the applied load (i.e. $\sigma_{applied} = \sigma_f V_f + \sigma_m V_m$)
5) The stresses are finite at the center of the fiber

The model uses the same variables defined at the beginning of this appendix, and is based upon the geometry shown in Figure B-1.

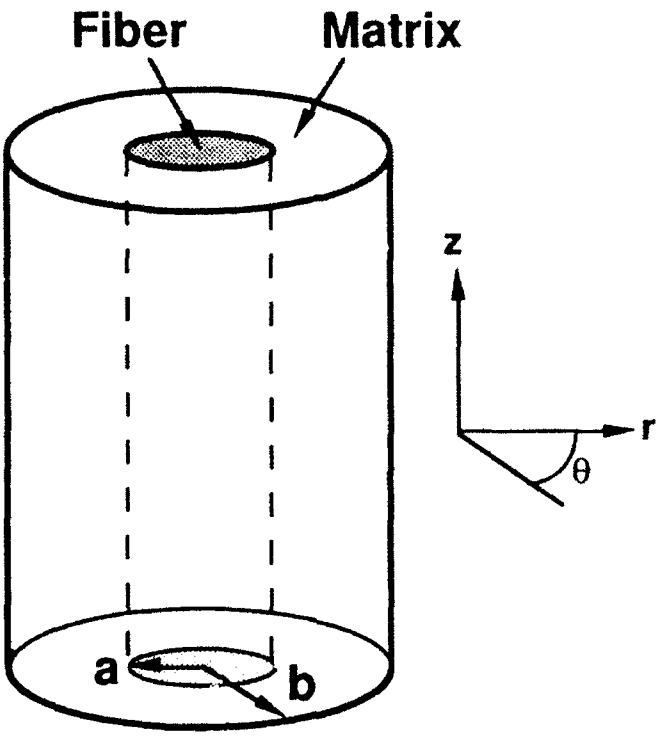


**Figure B-1.** Geometry defined for Generalized Plane-Strain Concentric Cylinder Model. Note that $r_f = a$ and $r_m = b$

Several equations can be formed using the defined variables:

$$A = \frac{n}{sm - pn}\left\{\left(\frac{b}{a}\right)^2\left[u_1 - u_2\left(\frac{m}{n}\right)\right] + (\alpha_m - \alpha_f)\Delta T\right\} \quad (25)$$

$$C = \frac{s}{sm - pn}\left\{\left(\frac{b}{a}\right)^2\left[u_1 - u_2\left(\frac{p}{s}\right)\right] + (\alpha_m - \alpha_f)\Delta T\right\} \quad (26)$$

Where

$$m = \left[1 - \left(\frac{b}{a}\right)^2\right]\left(\frac{1}{E_f}\right) - \left(\frac{1}{E_m}\right) \quad (27)$$

$$n = \left[1 - \left(\frac{b}{a}\right)^2\right]\left(\frac{1 + \nu_f}{E_f}\right) - \left(\frac{1 + \nu_m}{E_m}\right) \quad (28)$$

$$p = \left[1 - \left(\frac{b}{a}\right)^2\right]\left(\frac{2\nu_f}{E_f}\right) - \left(\frac{2\nu_m}{E_m}\right) \quad (29)$$

$$s = \left[1 - \left(\frac{b}{a}\right)^2\right]\left(\frac{1 + \nu_f}{E_f}\right) - \left[1 + \left(\frac{b}{a}\right)^2\right]\left(\frac{1 + \nu_m}{E_m}\right) \tag{30}$$

$$u_1 = \sigma_{r,\,applied}\left(\frac{2\nu_f}{E_f}\right) - \left(\frac{\sigma_{z,\,applied}}{E_f}\right) \tag{31}$$

$$u_2 = \left(\sigma_{r,\,applied} - \sigma_{z,\,applied}\right)\left(\frac{1 + \nu_f}{E_f}\right) - \sigma_{r,\,applied}\left(\frac{1 + \nu_m}{E_f}\right) \tag{32}$$

From equations (25) to (32), the matrix stresses in the axial (z), radial (r), and hoop (θ) directions for conditions of applied thermal and mechanical loads may be computed as

$$\sigma_{\theta m} = A\left[1 + \left(\frac{b}{r}\right)^2\right] - \sigma_{r,\,applied}\left(\frac{b}{r}\right)^2 \tag{33}$$

$$\sigma_{rm} = A\left[1 - \left(\frac{b}{r}\right)^2\right] + \sigma_{r,\,applied}\left(\frac{b}{r}\right)^2 \tag{34}$$

$$\sigma_{zm} = C \tag{35}$$

Similarly, for the fiber

$$\sigma_{\theta f} = \sigma_{rf} \tag{36}$$

$$\sigma_{rf} = A\left[1 - \left(\frac{b}{a}\right)^2\right] + \sigma_{r,\,applied}\left(\frac{b}{a}\right)^2 \tag{37}$$

$$\sigma_{zf} = C\left[1 - \left(\frac{b}{a}\right)^2\right] + \sigma_{z,\,applied}\left(\frac{b}{a}\right)^2 \tag{38}$$

## References — **APPENDIX B: MODELING**


1 Timoshenko, S.P., and Goodier, J.N., Theory of Elasticity, McGraw-Hill Publishing Co., New York, NY, 1970.

2 Ashbaugh, N.E., Khobaib, M., Hartman, G.A., Coker, D., Kroupa, J.L., John, R., Johnson, D.A., Goodman, R.C., Maxwell, D.A., and Muhic, L.A., Mechanical Properties of Advanced Engine Materials - 1989 Annual Report, Air Force Contract No. F33615-UDR-TR-90-85. University of Dayton Research Institute, Dayton, OH, August 1990.

## Table C-1. Summary of Test Results

| Specimen # (Plate-Specimen) | Test Type | Temp (°C) [°F] | Ramp/Profile | Max. Stress (MPa) [ksi] | Initial Modulus (MPa) [ksi] | Residual Strength (MPa) [ksi] | Residual Modulus (GPa) [Msi] | Location of Failure |
|---|---|---|---|---|---|---|---|---|
| 9032005L-07 | Tens. | 23 [73] | 100 MPa/sec | 552 [80.1] | 131 [129] | | | partially within specimen gage section |
| 9032005L-01 | Tens. | 1100 [2012] | 100 MPa/sec | 381 [55.3] | 134 [19.4] | | | partially within extensometer gage section |
| 9032006L-10 | Tens. | 1100 [2012] | 100 MPa/sec | 341 [49.5] | 129 [18.7] | | | out of gage sections (in radius) |
| 9032006L-01 | Tens. | 1100 [2012] | 100 MPa/sec | 361 [52.4] | 131 [129] | | | partially within specimen gage section |
| 9032005L-10 | ITF | 1100 [2012] | 60 sec ramp, no hold, R=0.1 | 100 [14.5] | | 343 [49.7] | 105 [15.2 | partially within extensometer gage section |
| 9032005L-09 | ITF | 1100 [2012] | 60 sec ramp, w/hold, R=0.1 | 100 [14.5] | | 339 [49.2] | 112 [16.2] | partially within specimen gage section |
| 9032005L-09 | ITF | 1100 [2012] | 60 sec ramp, w/hold, R=0.1 | 100 [14.5] | | 276 [40.0] | 112 [16.2] | partially within specimen gage section |
| 9032005L-08 | TMF | 500-1100 [932-2012] | 60 sec ramp, no hold, R=0.1 | 100 [14.5] | | 364 [52.8] | 110 [16.0] | out of gage sections (in radius) |
| 9032007L-04 | TMF | 500-1100 [932-2012] | 60 sec ramp, no hold, R=0.1 | 100 [14.5] | | 364 [52.8] | 97 [14.1] | partially within specimen gage section |
| 9032005L-06 | TMF | 500-1100 [932-2012] | 60 sec ramp, w/hold, R=0.1 | 100 [14.5] | | 341 [49.5] | 115 [16.7] | partially within specimen gage section |
| 9032006L-07 | TMF | 500-1100 [932-2012] | 60 sec ramp, w/hold, R=0.1 | 100 [14.5] | | 297 [42.2] | 110 [16.0] | out of gage sections (in radius) |

U.S. Government Printing Office:1993—750-113/80169